

**Louisiana Water Resources Research Institute  
Annual Technical Report  
FY 2010**

# Introduction

This report presents a description of the activities of the Louisiana Water Resources Research Institute for the period of March 1, 2010 to February 28, 2011 under the direction of Dr. John Pardue. The Louisiana Water Resources Research Institute (LWRRRI) is unique among academic research institutions in the state because it is federally mandated to perform a statewide function of promoting research, education and services in water resources. The federal mandate recognizes the ubiquitous involvement of water in environmental and societal issues, and the need for a focal point for coordination.

As a member of the National Institutes of Water Resources, LWRRRI is one of a network of 54 institutes nationwide initially authorized by Congress in 1964 and has been re-authorized through the Water Resources Research Act of 1984, as amended in 1996 by P.L. 104-147. Under the Act, the institutes are to:

"1) plan, conduct, or otherwise arrange for competent research that fosters, (A) the entry of new research scientists into water resources fields, (B) the training and education of future water scientists, engineers, and technicians, (C) the preliminary exploration of new ideas that address water problems or expand understanding of water and water-related phenomena, and (D) the dissemination of research results to water managers and the public.

2) cooperate closely with other colleges and universities in the State that have demonstrated capabilities for research, information dissemination and graduate training in order to develop a statewide program designed to resolve State and regional water and related land problems. Each institute shall also cooperate closely with other institutes and organizations in the region to increase the effectiveness of the institutes and for the purpose of promoting regional coordination."

The National Water Resources Institutes program establishes a broad mandate to pursue a comprehensive approach to water resource issues that are related to state and regional needs. Louisiana is the water state; no other state has so much of its cultural and economic life involved with water resource issues. The oil and gas industry, the chemical industry, port activities, tourism and fisheries are all dependent upon the existence of a deltaic landscape containing major rivers, extensive wetlands, numerous large shallow water bays, and large thick sequences of river sediments all adjacent to the Gulf of Mexico.

## History of the Institute

Louisiana has an abundance of water resources, and while reaping their benefits, also faces complex and crucial water problems. Louisiana's present water resources must be effectively managed, and the quality of these resources must be responsibly protected. A fundamental necessity is to assure continued availability and usability of the state's water supply for future generations. Specifically, Louisiana faces five major issues that threaten the quality of the state's water supply, which are also subsets of the southeastern/island region priorities:

Nonpoint sources of pollution are estimated to account for approximately one-half of Louisiana's pollution. Because of the potential impact of this pollution and the need to mitigate its effects while maintaining the state's extensive agricultural base and coastal zones, continued research is needed in the area of nonpoint issues. Louisiana's regulatory agencies are addressing non-point source problems through the development of waste load allocation models or total maximum daily load (TMDL) calculations. There are serious technical issues that still require resolution to insure that progress is made in solving the non-point source problem.

Louisiana's vast wetlands make up approximately 40% of the nation's wetlands. These areas are composed of very sensitive and often delicately balanced ecosystems which make them particularly vulnerable to

contamination or destruction resulting both from human activities and from natural occurrences. Understanding these threats and finding management alternatives for the state's unique wetland resources are priority issues needing attention.

Water resources planning and management are ever-present dilemmas for Louisiana. Severe flooding of urban and residential areas periodically causes economic loss and human suffering, yet solutions to flooding problems can be problems in themselves. Water supply issues have also recently a focus of concern. Despite the abundance of resources, several aquifers have been in perennial overdraft, including the Chicot aquifer. Louisiana passed its first legislation that restricts groundwater use in the past year. Water resources and environmental issues are intricately interconnected; therefore, changes in one aspect produce a corresponding responsive change in another. Further study is needed to understand these relationships.

Water quality protection, particularly of ground water resources, is an area of concern in Louisiana. Researchers are beginning to see contamination in drinking water supplies that was not present in the past. Delineating aquifer recharge areas, understanding the impacts of industrial activities on water resources, evaluating nonpoint sources of pollution, and exploring protection alternatives are issues at the forefront.

Wastewater management has been a long-standing issue in Louisiana. The problem of wastewater management focuses primarily on rural and agricultural wastewater and the high costs for conventional types of wastewater treatment as found in the petrochemical industry.

The Institute is administratively housed in the College of Engineering and maintains working relationships with several research and teaching units at Louisiana State University. Recent cooperative research projects have been conducted with the University of New Orleans and the EPA's Hazardous Substance Research Center- South & Southwest.

#### LWRRRI and the Deep Horizon Oil Spill

During this reporting period, Louisiana experienced impacts from the largest oil spill in U.S history. MC252 oil from the Deep Horizon leak oiled hundreds of miles of Louisiana shoreline. Prior to the spill, LWRRRI director John Pardue and other LWRRRI grantees had published and conducted research on the fate of crude oil in Louisiana's aquatic systems. As oil reached the shoreline, LWRRRI used discretionary funds to initiate time sensitive research on the fate and transport of oil in these systems. The LWRRRI director advised state and national agencies, conducted ongoing research on the fate of oil in the systems and organized and presented research results at local, regional and national meetings. Details of this activity are presented below in the "Notable Achievements" section of the report.

## Research Program Introduction

The primary goal of the Institute is to help prepare water professionals and policy makers in the State of Louisiana to meet present and future needs for reliable information concerning national, regional, and state water resources issues. The specific objectives of the Institute are to fund the development of critical water resources technology, to foster the training of students to be water resources scientists and engineers capable of solving present and future water resources problems, to disseminate research results and findings to the general public, and to provide technical assistance to governmental and industrial personnel and the citizens of Louisiana.

The priority research areas for the Institute in FY 2010 focused on selected research themes developed in conjunction with the advisory board. These themes corresponded to the major water resource areas affecting Louisiana described in the Introduction above. Projects selected were from a range of faculty with different academic backgrounds including geological scientists, environmental engineers and water resource engineers and scientists. Supporting research in these priority areas has increased the visibility of the Institute within the State.

The individual research projects designated as Projects 2010LAXXXX, are listed below.

- Project 2010LA76G, Tsai & Hanor - Hierarchical Multimodel Saltwater Intrusion Remediation and Sampling Designs:A BMA Tree Approach
- Project 2010LA71B – Tsai, “Multimodel Uncertainty Analysis for Chance-Constrained Saltwater Intrusion Management”
- Project 2010LA70B-Smith, “Wave-induced transport through coastal vegetation”
- Project 2010LA66B—DeLaune and Valsaraj, “Development of an active cap for the sequestration of mercury in contaminated lake sediments in Louisiana
- Project 2010LA73B—Deng, “Scale-dependent behavior and modeling of dissolved oxygen in coastal Louisiana rivers”

These projects include one project that focuses on water quality issues (2010LA73B), two projects that focus on groundwater flow and transport (Projects 2010LA76G and Project 2010LA71B), one Engineering project (2010LA66B) and one project that focuses on climate and hydrologic Processes (2010LA70B).

# Modeling Turbulent Enhancement of Sediment Transport

## Basic Information

<b>Title:</b>	Modeling Turbulent Enhancement of Sediment Transport
<b>Project Number:</b>	2009LA60B
<b>Start Date:</b>	3/1/2009
<b>End Date:</b>	9/30/2010
<b>Funding Source:</b>	104B
<b>Congressional District:</b>	6th
<b>Research Category:</b>	Climate and Hydrologic Processes
<b>Focus Category:</b>	Sediments, Geomorphological Processes, Water Quantity
<b>Descriptors:</b>	
<b>Principal Investigators:</b>	Heather Smith

## Publications

There are no publications.

**Project Title:** Modeling Turbulent Enhancement of Sediment Transport  
**Project Number:**  
**Start Date:** March 1, 2009  
**End Date:** February 29, 2010  
**Congressional District:** 6  
**Focus Categories:** Sediments, Geomorphological and Geochemical Processes  
**Principal Investigator:** Heather D. Smith

## Research Objectives

The State of Louisiana faces serious challenges with coastal erosion and subsidence. Restoration efforts have been focused on the ability to use sediment available from the Mississippi River to increase land building in vulnerable wetland areas. It is believed that by increasing the wetlands around the coast, storm surge can be reduced<sup>1</sup>. Additionally, increased sea level rise, combined with large recurring hurricanes will increase the potential to resuspend sediments that may have been contaminated and buried. The interactions at the interface of the sediment bed and fluid is one of the largest challenges still to be resolved in water resources. Our ability to predict sediment transport at large scales is limited by our understanding of the physics dominating sediment movement in a variety of complex forcing regimes. In addition, the characteristics of the sediment material is difficult to assess and parametrize.

The role of externally generated turbulence on local sediment transport continues to be an active area of research. Detailed laboratory experiments have been performed to investigate the effect of externally generated turbulence on bed load transport. Nelson *et al.* (1993) made detailed flow measurements around fixed two-dimensional bedforms. The authors observed that the mean bed shear stress close to the reattachment point on the lee side of a ripple continually remained below the threshold for incipient motion. Sediment motion occurs due to the presence of excess turbulence generated as a result of the flow separation. This work was further extended to the case of turbulence generated from a backward facing step. Nelson *et al.* (1995) found a strong correlation between the sediment motion and the near bed velocity fluctuations. Sumer *et al.* (2003) reported experiments performed with externally generated turbulence due to the presence of obstacles in the flow. The investigators considered the turbulence generated by large and small screens and a two-dimensional pipeline. For these experiments, the applied stress by the flow was maintained at a level low enough to produce bed load transport only without the formation of bedforms. The bed load transport rate correlated very well to the turbulent intensity. A 20% increase in local turbulence levels in the bed shear stress increased the bed load sediment transport rate by a factor of 6. The bed load transport rate was found to be insensitive to the turbulence generation mechanism (whether screens or cylinder), and only sensitive to the turbulence level. The spectrum width of the externally generated turbulence (such as the frequency of the vortex shedding) did not have a significant effect on the resulting sediment transport.

The goal of this research is to investigate the effect of turbulence on the applied shear, and thus the resulting sediment transport. The necessity to resolve the time-varying hydrody-

---

<sup>1</sup>Louisiana Coastal Protection and Restoration Draft Report - <http://lacpr.usace.army.mil>

namics and turbulence in sediment transport modeling efforts has been shown for a variety of applications, including the scour around pipelines (Sumer *et al.*, 1988; Li and Cheng, 2001), dunes (Tjerry and Fredsøe, 2005; Giri and Shimizu, 2006), and coastal bedforms (Nichols and Foster, 2007). This numerical work will consider the hydrodynamics around a bottom-mounted cylinder undergoing sinusoidal wave forcing. Three parametrization for the numerical prediction of turbulence will be investigated, the two-equation k- $\epsilon$  and two versions of the damped Smagorinsky Large Eddy Simulation (LES) closure schemes. The modeled bed stress and external flow field will be compared with a variety of available laboratory data.

## Objectives

### Objective 1: Compare the hydrodynamics around the cylinder in waves

In this objective, we will simulate the vortex generation and shedding around a bottom-mounted cylinder for three turbulence closure schemes, two surface roughness values, and two grid sizes. Predictions of the lift coefficient,  $C_l$  will be compared to available laboratory data of Sumer *et al.* (1991) and Bryndum *et al.* (1992).

### Objective 2: Compare the phase-dependent estimates of the applied bed shear

Estimates of the applied bed shear stress will be determined as a function of wave phase for the simulations of Objective 1. These predictions of the shear will be compared to the data obtained by Sumer and Fredsøe (1991). The role of the turbulent eddy viscosity in the predictions of the stress will yield important information on the appropriateness of the turbulence model as well as the spatially- and temporally-varying applied shear.

## Methodology

### Model Specifics

In this research, we utilize the three-dimensional, non-hydrostatic, commercially available model, FLOW-3D. This model utilizes a Volume of Fluid (VOF) approach to resolve fluid-fluid and fluid-boundary interfaces by tracking curvature and location of the interfaces in a cell (Richardson and Panchang, 1998; Hirt, 1993). This allows rectangular non-boundary fitted grid cells to resolve complex flow and obstacle features.

The model simultaneously solves the three-dimensional Navier-Stokes equations and the continuity equation. Pressure is calculated through the solution of the pressure Poisson equation through an iterative procedure. The contributions of the turbulence are included with the addition of a kinematic eddy viscosity,  $\mu_T$ . The turbulence models proposed in this research are the two-equation k- $\epsilon$  and the Large Eddy Simulation (LES) closure schemes. The standard k- $\epsilon$  model (Wilcox, 2002) approximates the kinematic eddy viscosity with

$$\mu_T = \frac{\rho C_\mu k^2}{\epsilon} \quad (1)$$

The closure equations for the turbulent kinetic energy,  $k$ , and the dissipation rate,  $\epsilon$  are solved with standard transport equations. The boundary conditions for  $k$  and  $\epsilon$  are given as

$$k = \frac{u_*^2}{\sqrt{C_\mu}}, \quad \epsilon = \frac{u_*^3}{\kappa y_o} \quad (2)$$

The non-transport turbulence closure scheme that will be considered is the Large Eddy Simulation (LES). The equation for the kinematic eddy viscosity,  $\mu_T$ , is given by (3)

$$\mu_T = \rho(C_{s,d}\Delta)^2 \sqrt{2e_{ij}e_{ij}} \quad (3)$$

where the strain-rate tensor  $e_{ij}$  is given by

$$e_{ij} = \left( \frac{\partial u_i}{\partial x_j} + \frac{\partial u_j}{\partial x_i} \right) \quad (4)$$

The characteristic length scale,  $\Delta$ , is

$$\Delta = (\delta x \delta y \delta z)^{1/3} \quad (5)$$

Near the wall, this length scale is modified to account for the limitations of the Smagorinsky closure scheme with a van Driest damping term,  $C_{s,d}$ , given with

$$C_{s,d} = C_s [1 - \exp(-(z_+/A_+)^n)]^m$$

where  $C_s$  is a coefficient equal to 0.1 and  $A_+$  has a value of 25. Two formulations for van Driest damping are considered here. The first is the standard form where  $n = 1$  and  $m = 1$ . A second form proposed by Guerts (2004), where  $n = 3$  and  $m = 0.5$ . In numerical models, the applied bed stress can be calculated with either a law of the wall function, or the fundamental definition of the bed shear stress, which assumes adequate resolution of the viscous sublayer. In either approach, the contribution of the turbulence closure scheme is achieved through the use of the total viscosity in the calculation. The total viscosity is defined as

$$\mu_{tot} = \mu + \mu_T \quad (6)$$

This approach will consider both formations of the bed shear stress and the sensitivity of the stress to the inclusion of the turbulent component.

### Laboratory Experiments

In this investigation, we perform model-data comparisons with laboratory data obtained by Sumer and Fredsøe (1991). In their work, the applied shear stress and the bed was measured at several streamwise locations around a 5 cm diameter cylinder with flush-mounted hot-film probes in an oscillatory U-tube. The cylinder was mounted directly onto the bed. The wave forcing had a period of 9.8 s and a maximum freestream velocity of 5.2 cm/s, yielding a Keulegan-Carpenter number of approximately 10. Values of the lift coefficient for this Keulegan-Carpenter number are based on ranges published in Sumer *et al.* (1991) and Bryndum *et al.* (1992).

For the numeric simulations, a domain size of 120 cm by 35 cm was resolved with a two different grid sizes, a variable 0.125 cm and a variable 0.0625 cm grid. The Stokes length of the wave bottom boundary layer is approximately 0.18 cm, yielding nearly 2 cells covering the boundary layer for a 0.125 cm grid and 3 cells covering the boundary layer for a 0.0625 cm grid. Both grids have a constant cell size in the vicinity of the cylinder and then the cell size expands linearly toward the domain ends (with an expansion ratio less than 1.25). Two values for obstacle and bed roughness were considered (0.008 and 0.016 cm).

## Results

### Lift Predictions

The vortex dynamics around obstacles in waves is dominated by the strength and duration of the forcing. Figure 1 presents the vortex dynamics around the cylinder as visualized with the vorticity for the LES  $n = 1$  model (left panels) and k- $\epsilon$  model (right panels). A vortex is generated in the lee of the cylinder during times with low accelerations. As the flow starts to reverse, the vortex separates from the cylinder and flips over top of the cylinder. As the flow continues in the opposite direction, the flipped vortex continues to move away from the cylinder and a new lee vortex is generated. At this point, two very distinct differences are observed with the LES  $n = 1$  and k- $\epsilon$  predictions. The LES  $n = 1$  model predicts a vortex pair that couples and sheds from the cylinder during flow reversal. This coupling is not observed with the k- $\epsilon$  model. The LES  $n = 1$  model also predicts remnants of previously flipped vortices that are still observable in the flow for several wave periods. This is consistent with other observations of the vortex dynamics around bottom-seated cylinders.

Model evaluation of both the k- $\epsilon$  and LES closure schemes of the vortex generation and shedding properties are performed with the lift coefficient. Laboratory data for the lift coefficient was obtained by both Sumer *et al.* (1991) and Bryndum *et al.* (1992). Figure 2 presents the range of parameters (grid size, roughness, damping type) for the LES models considered. Figure 3 presents the comparison of the k- $\epsilon$  and LES  $n = 1$  models. As the flow reverses, the low pressure vortex core passes over the top of the cylinder, yielding a peak in the lift coefficient. This occurs twice per wave period. The lift coefficients predicted by the LES models are lower than expected for the finer grid and are improved by increasing the grid size. Neither LES or k- $\epsilon$  coarse grid models show much sensitivity to the roughness value. The k- $\epsilon$  model does not appear to be as sensitive to grid size as the LES models. While the magnitude predictions of k- $\epsilon$  model are more consistent with the data, the LES models is able to more accurately capture the secondary lift peak associated with the shedding of the vortex pair.

### Bed Stress Predictions

The highly dynamic nature of the flow around the cylinder is expected to have a significant impact on the predictions of the bed shear stress. Figure 4 and Figure 5 present the comparisons of the predicted bed shear stress with those observed by Sumer and Fredsøe (1991). The bed stress was calculated with the formulas presented in the model section in the cell nearest to the boundary and used the total turbulent viscosity ( $\mu_{tot} = \mu + \mu_T$ ). The magnitudes of the bed stress are reasonably well predicted with the LES models. Near the cylinder, the models agree with each other fairly well, indicating that the model in the region of the cylinder is not important. The higher damping produced with the LES  $n = 3$  model provides better agreement in the far field stress predictions than that with the LES  $n = 1$  model. The interactions of the bed with remnant vortices are observed in the far-field region ( $|x/D| > 5$ ). The magnitude of the stress in these areas are not dependent on the grid size, but the spatial location of the peaks differ, indicating that the hydrodynamics may be different between models. The contributions of these large, temporally varying local bed stresses on the sediment transport would be considerable, and not considered with models unable of resolving these features.

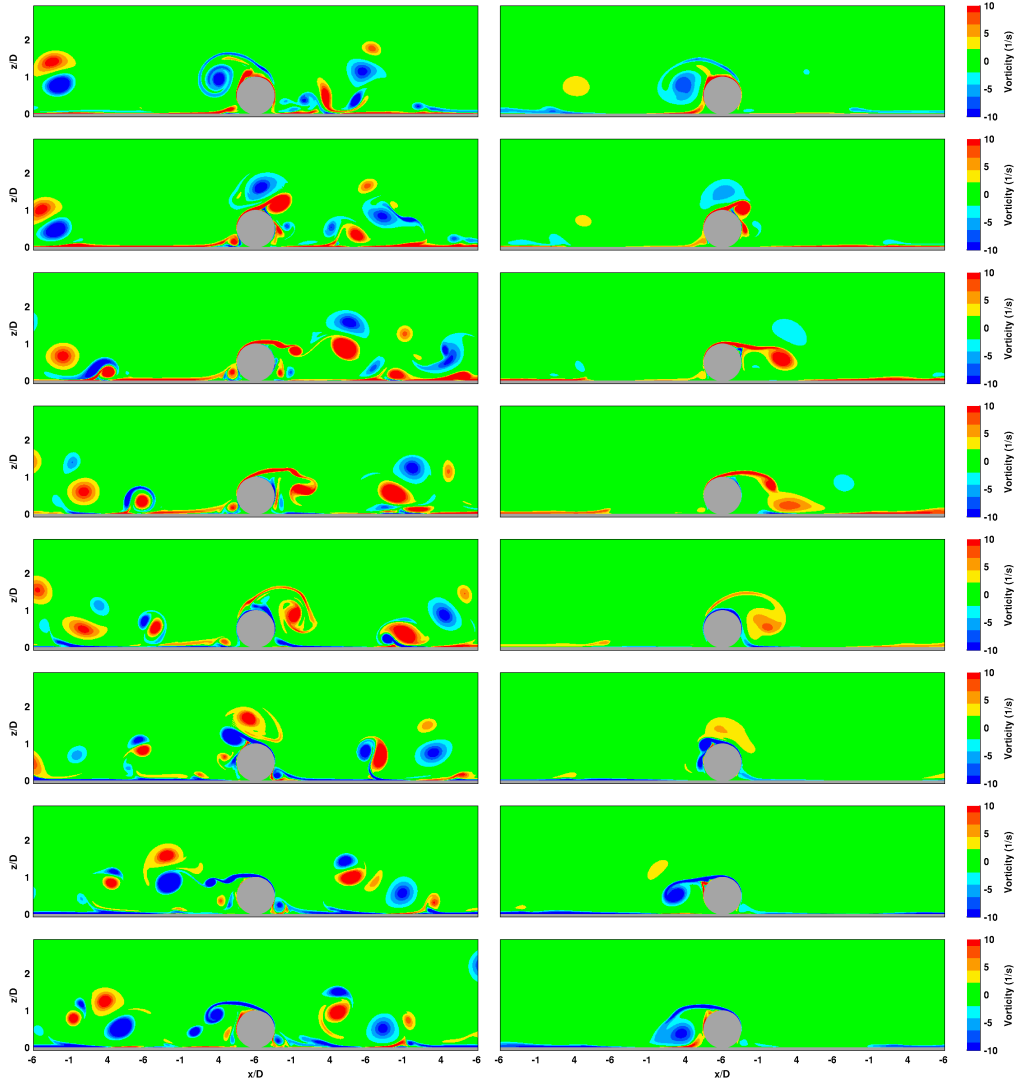


Figure 1: Modeled vorticity for the LES model ( $n = 1$ , left panels) and the  $k-\epsilon$  model (right panels) for the finer grid and a roughness of 0.008 cm. Color scaling for the vorticity is shown on the right, with red indicating clockwise rotation. The temporal location for each panel is given at the top.

Predictions of the bed shear stress when considering the  $k-\epsilon$  model are dramatically different than both those predicted with the LES closure scheme and the laboratory data (Figure 5). The predicted bed stress is several times larger than the laboratory observations. The far-field stress is well-predicted during some of the wave phases, but in general, it is over-predicted as well. The difference in the strength of the predicted vortices is also apparent. The  $k-\epsilon$  model does not show the local peaks in the bed shear stress that indicate the presence of previously shed vortices.

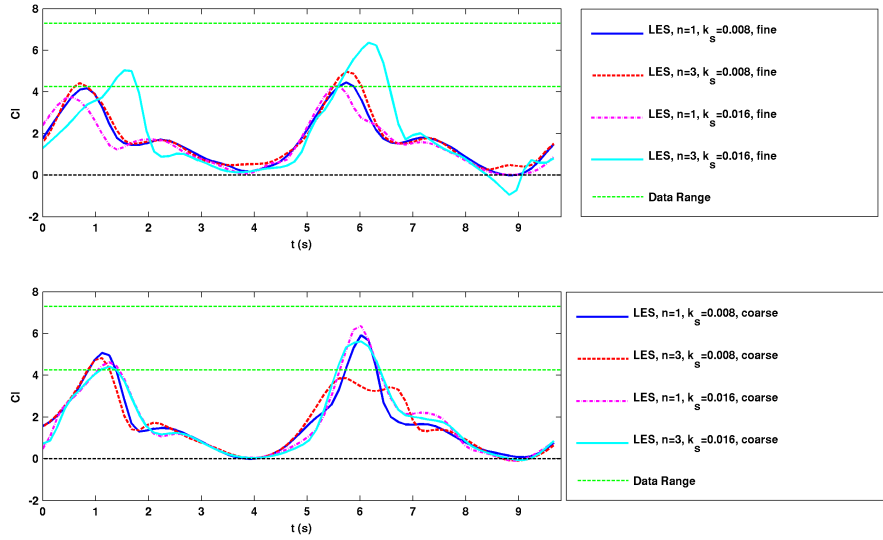


Figure 2: The modeled lift coefficient for the LES models with the fine grid (top panel) and the coarse grid (bottom panel). The legend for each panel is shown on the right of each panel. The range of available laboratory data contained within the two green lines.

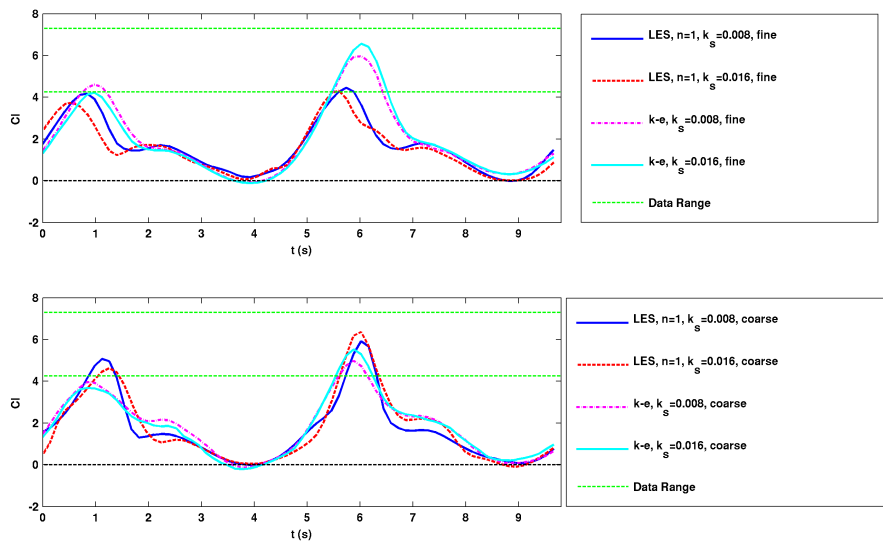


Figure 3: The modeled lift coefficient for the LES  $n = 1$  and k- $\epsilon$  models with the fine grid (top panel) and the coarse grid (bottom panel). The legend for each panel is shown on the right of each panel. The range of available laboratory data contained within the two green lines.

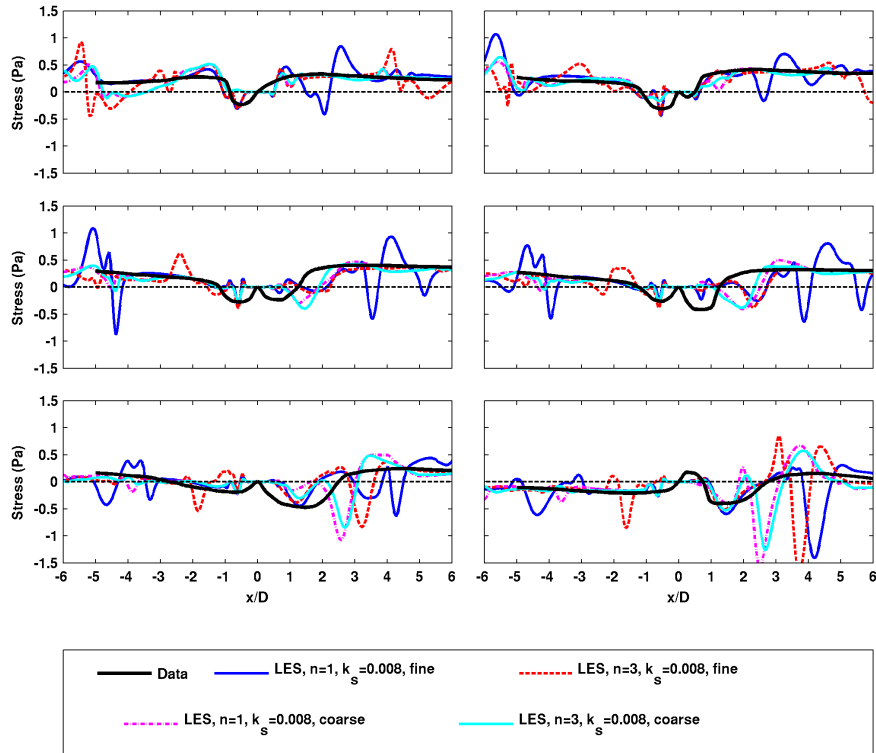


Figure 4: Comparisons of the predicted bed shear stress with the data of Sumer and Fredsøe (1991) (black line). The different LES ( $n = 1$ ,  $n = 3$ ) models and the grid sizes are presented at a roughness of 0.008 cm. The temporal location is given on the bottom right of each panel and matches the time series in Figure 1.

## Conclusions

Simulations of the turbulent flow field around a two-dimensional, bottom-seated cylinder were performed under wave forcing conditions. While the model simulations show qualitative agreement with the observations, the quantitative prediction of the vortex characteristics showed variability between closure schemes, obstacle roughness, and grid sizes. The bed stress as a function of wave phase was also examined. The predictions with the LES model were significantly improved over those predicted with the  $k-\epsilon$  model. Two different near wall van Driest type damping functions were used in the LES model. The  $n = 3$ ,  $m = 0.5$  model bed increased the accuracy of the bed stress as compared to the  $n = 1$ ,  $m = 1$  damping model.

This work was presented at the 2010 State of the Coast Conference in Baton Rouge, LA.

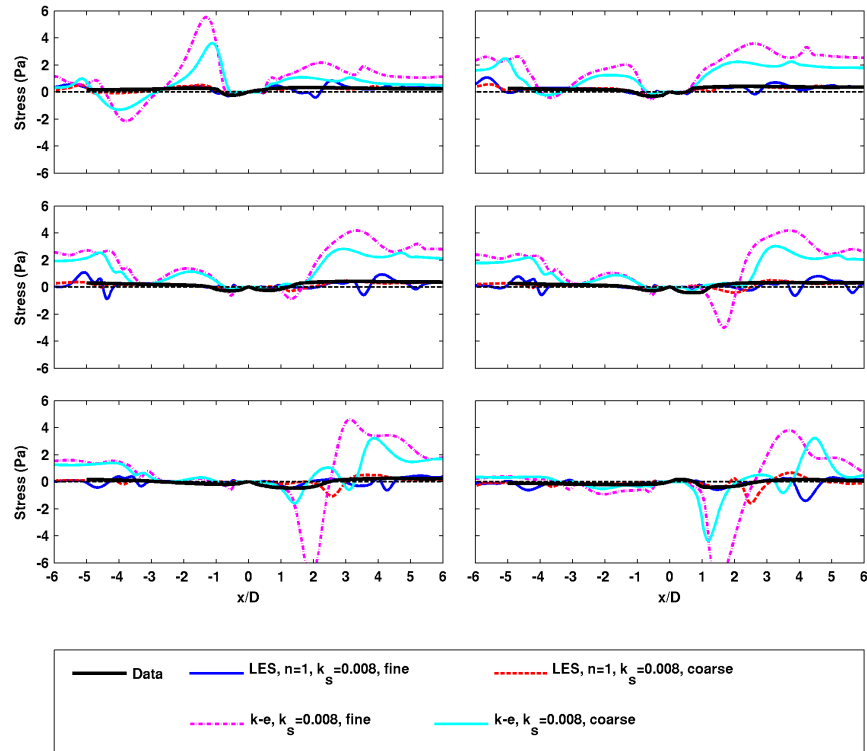


Figure 5: Comparisons of the predicted bed shear stress with the data of Sumer and Fredsøe (1991) (black line). The LES  $n = 1$  and  $k-\epsilon$  models are presented for the two grid sizes for a roughness of 0.008 cm. The temporal location is given on the bottom right of each panel and matches the time series in Figure 1.

## References

- Bryndum, M. B., Jacobsen, V., and Tsalhalis, D. T. (1992). Hydrodynamic forces on pipelines: Model tests. *J. Offshore Mech. Arct.*, 114(4):231–241.
- Giri, S. and Shimizu, Y. (2006). Numerical computation of sand dune migration with free surface flow. *Water Resour. Res.*, 42(W10422):1–19.
- Guerts, B. J. (2004). *Elements of Direct and Large-Eddy Simulation*. R. T. Edwards, Inc.
- Hirt, C. W. (1993). Volume-fraction techniques: powerful tools for wind engineering. *J. Wind Eng. Ind. Aerod.*, 46-47:327–338.
- Li, F. and Cheng, L. (2001). Prediction of lee-wake scouring of pipelines in currents. *J. Waterw., Port, Coastal, Ocean Eng., ASCE*, 127(2):106–112.
- Nelson, J. M., McLean, S. R., and Wolfe, S. R. (1993). Mean flow and turbulence fields over two-dimensional bedforms. *Water Resour. Res.*, 29(12):3,935–3,953.

- Nelson, J. M., Shreve, R. L., McLean, S. R., and Drake, T. G. (1995). Role of near-bed turbulence structure in bed load transport and bed form mechanics. *Water Resour. Res.*, 31(8):2,071–2,086.
- Nichols, C. S. and Foster, D. L. (2007). Full-scale observations of wave-induced vortex generation over a rippled bed. *J. Geophys. Res.*, 112(C10015):1–17.
- Richardson, J. E. and Panchang, V. G. (1998). Three-dimensional simulation of scour-inducing flow at bridge piers. *J. Hydraul. Eng., ASCE*, 124(5):530–540.
- Sumer, B. M., Chua, L. H. C., Cheng, N.-S., and Fredsøe, J. (2003). Influence of turbulence on bed load sediment transport. *J. Hydraul. Eng., ASCE*, 129(8):585–596.
- Sumer, B. M. and Fredsøe, J. (1991). Onset of scour below a pipeline exposed to waves. *Int. J. Offshore Polar*, 1(3):189–194.
- Sumer, B. M., Jensen, B. L., and Fredsøe, J. (1991). Effect of a plane boundary on oscillatory flow around a circular cylinder. *J. Fluid Mech.*, 225:271–300.
- Sumer, B. M., Jensen, H. R., Mao, Y., and Fredsøe, J. (1988). Effect of lee-wake on scour below pipelines in current. *J. Waterw., Port, Coastal, Ocean Eng., ASCE*, 114(5):599–614.
- Tjerry, S. and Fredsøe, F. (2005). Calculation of dune morphology. *J. Geophys. Res.*, 110(F04013):1–13.
- Wilcox, D. C. (2002). *Turbulence Modeling for CFD*. DCW Industries, second edition.

# Bayesian Model Averaging for Saltwater Intrusion Management under Model Uncertainty

## Basic Information

<b>Title:</b>	Bayesian Model Averaging for Saltwater Intrusion Management under Model Uncertainty
<b>Project Number:</b>	2009LA61B
<b>Start Date:</b>	3/1/2009
<b>End Date:</b>	7/31/2010
<b>Funding Source:</b>	104B
<b>Congressional District:</b>	6th
<b>Research Category:</b>	Ground-water Flow and Transport
<b>Focus Category:</b>	Water Supply, Water Quality, Hydrology
<b>Descriptors:</b>	
<b>Principal Investigators:</b>	Frank Tsai

## Publications

There are no publications.

## SYNOPSIS

**Title:** Bayesian Model Averaging for Saltwater Intrusion Management under Model Uncertainty

**Project Number:**

**Start Date:** 3/1/2009

**End Date:** 2/28/2010

**Funding Source:** 104B

**Congressional District:** 6

**Research Category:** Ground-water Flow and Transport

**Focus Category:** GW, M&P, MET, MOD, NPP, ST, WQL, WQN

**Descriptors:** Uncertainty, Model Averaging, Prediction, Saltwater Intrusion, Aquifer, Subsurface, Modeling, Optimization, Management

**Primary PI:** Frank T.-C. Tsai

### Problem and Research Objectives

Ground water is the primary source of drinking water for 61 percent of Louisiana's residents. Irrigation withdrawal is accounted for 37 percent of the total ground water withdrawal (Sargent, 2007). Ground water has been a significant factor to the continuation of Louisiana economic development. However, rapid growth in population and industry has increased ground water demand and resulted in saltwater intrusion to many freshwater aquifers (Tomaszewski, 1996). In addition, recent drought in Louisiana has escalated ground water withdrawal and accelerated the saltwater encroachment (Bohr, 2003). To protect the ground water, Louisiana legislature Act 446 (2001) declares: ground water resource is a matter of public interest. Ground water must be managed, protected, and regulated in the best interests of all the citizens of the state. Act 49 (2003) requires the ground water resource management program to meet the goal of long-term sustainability of the state's ground water aquifers and to sustain the economic welfare of the state's citizens.

For long-term economic growth, effective planning and management of ground water sustainability become an urgent task. Louisiana needs a scientific, systematic management plan to protect ground water from further saltwater intrusion without causing environmental detriment.

In this project, we propose a multimodel approach to study the groundwater head prediction under model uncertainty for the "1,500-foot" sand aquifer in the Baton Rouge area. The study area, shown in Figure 1, extends over about 300 km<sup>2</sup> and includes the major part of the Baton Rouge metropolitan area. Due to downthrow on the south side of the Baton Rouge Fault, the "1,500-foot" sand (north) connects to the "1,200-foot" sand (south). The fault acts as a conduit-barrier (Bense and Person, 2006) and allows ground water to cross the fault. South of the fault, the aquifer contains mostly saltwater, which comes from dissolved brine solution from two nearby salt domes, the St. Gabriel salt dome and Darrow salt dome (Bray and Hanor, 1990). North of the fault, the aquifers store excellent quality and quantity of water for the public and industry (Sargent, 2002). Heavy pumping has caused this aquifer to decline by as much as 90 m since the 1940s.

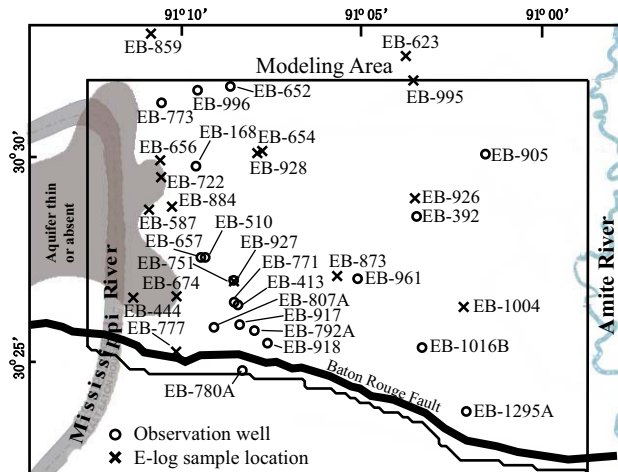


Figure 1: The “1500-foot” sand of the Baton Rouge area, Louisiana.

In the literature, the saltwater intrusion management model is commonly based on one parameterization method for distributed aquifer parameters in one simulation model. However, due to data scarcity and lack of hydrogeological information, the developed conceptual model and the chosen parameterization method are not unique. We are often overconfident in the management results from one method and one model, and neglect the impact of model uncertainty in the management decision. Detrimental results could be caused by overlooking the model uncertainty.

The goal of the project is to predict groundwater head distribution in the “1,500-foot” sand aquifer under the consideration of model uncertainty. Model uncertainty contains model structure uncertainty and model parameter uncertainty.

### **Objectives**

To achieve the project goal, we propose the following specific objectives:

#### **Objective 1 Develop a generalized parameterization method**

The project will improve the hydraulic conductivity estimation by extending the generalized parameterization (GP) method (Tsai and Yeh, 2004; Tsai, 2006) to fuse different types of data. The GP method will be able to integrate different parameterization methods under the geostatistical framework. The conditional estimate and conditional variance of the GP method will be formulated to assess the uncertainty of the hydraulic conductivity estimation.

#### **Objective 2 Develop a multimodel approach**

The project will adopt a Bayesian model averaging (BMA) method (Draper, 1995; Hoeting et al., 1999) to integrate multiple groundwater flow models and multiple parameterization methods for prediction of groundwater head. Specifically, we will consider multiple GP methods for parameterizing the hydraulic conductivity field. We will also consider the uncertainty in boundary conditions to develop a number of ground water models.

### **Methodology**

### (1) Generalized Parameterization (GP)

A generalized parameterization (GP) method is proposed to estimate hydraulic conductivity:

$$\pi_{GP}(\mathbf{x}_0 | \mathbf{x}_1, \mathbf{x}_2, \dots, \mathbf{x}_m) = \sum_{\substack{j=1 \\ j \neq k(\mathbf{x}_0)}}^m \phi_j (\pi_j - \pi_{k(\mathbf{x}_0)}) \beta_j + \pi_{k(\mathbf{x}_0)} \quad (1)$$

where  $\beta_j$  are the data weighting coefficients bounded between 0 and 1. The GP integrates an interpolation method and a zonation method honoring the sampled data. Consider that  $\pi$  is a random field in a region ( $\Omega$ ), the sampled data  $\pi_j$  are taken at locations  $\mathbf{x}_j$ ,  $j=1, 2, \dots, m$ . The sample data  $\pi_j$  can be any form of hydraulic conductivity values, e.g., logarithmic values of hydraulic conductivity. Using the GP methods in equation (1), one can obtain an estimate of a zonal structure  $\pi_{\text{Zonation}}(\mathbf{x}_0 | \mathbf{x}_k) = \{\pi_k | \mathbf{x}_0 \in \Omega_k\}$ , a smooth distribution using an interpolation method  $\pi_{\text{Interpolation}}(\mathbf{x}_0 | \mathbf{x}_1, \mathbf{x}_2, \dots, \mathbf{x}_m) = \sum_{j=1}^m \phi_j \pi_j$ , or a conditional estimate of a mixed distribution by considering different values of data weighting coefficients  $\boldsymbol{\beta}_m = \{\beta_1, \beta_2, \dots, \beta_m\}$  to the  $m$  sample sites. In this way, the GP method greatly improves parameterization flexibility.

### (2) Hydraulic Conductivity Estimation and Uncertainty using GP and Bayesian Model Averaging (BMA)

If a set of possible zonal structures  $\boldsymbol{\Omega} = \{\Omega^{(1)}, \Omega^{(2)}, \dots\}$  and a set of interpolation methods  $\mathbf{F} = \{\phi^{(1)}, \phi^{(2)}, \dots\}$  are considered for estimating hydraulic conductivity, combinations of many zonal structures and interpolation methods pose a multi-parameterization (multimethod) problem that involves many GP methods  $\boldsymbol{\Theta} = \boldsymbol{\Omega} \times \mathbf{F} = \{\theta^{(p)}; p=1, 2, \dots\}$  to describe the hydraulic conductivity for the region. To cope with the multimethod problem, a Bayesian model averaging (BMA) approach is adopted to analyze the multiple GP methods. BMA uses the Bayes rule to assess prediction uncertainty using a set of models (Draper, 1995; Hoeting et al., 1999). Let  $\Pr(\boldsymbol{\pi} | D, \boldsymbol{\Theta})$  be the conditional probability of the hydraulic conductivity given data and multiple parameterization methods. The Bayes rule (Draper, 1995) has

$$\Pr(\boldsymbol{\pi} | D, \boldsymbol{\Theta}) = \sum_p \Pr(\boldsymbol{\pi} | D, \theta^{(p)}) \Pr(\theta^{(p)} | D) \quad (2)$$

$\Pr(\boldsymbol{\pi} | D, \theta^{(p)})$  represents the conditional probability of hydraulic conductivity given data and a GP method.  $\Pr(\theta^{(p)} | D)$  is the posterior probability of a GP method. According to the Bayes rule,  $\Pr(\theta^{(p)} | D)$  is

$$\Pr(\theta^{(p)} | D) = \Pr(D | \theta^{(p)}) \Pr(\theta^{(p)}) / \sum_p \Pr(D | \theta^{(p)}) \Pr(\theta^{(p)}) \quad (3)$$

where  $\Pr(D | \theta^{(p)})$  is the likelihood probability of a GP method.  $\Pr(\theta^{(p)})$  is the prior probability of a GP method and  $\sum_p \Pr(\theta^{(p)}) = 1$ . One can evaluate estimation uncertainty by looking at the conditional expectation of the parameter heterogeneity  $(\boldsymbol{\pi} | D, \boldsymbol{\Theta})$  (Schweppe, 1973)

$$\mathbb{E}[\boldsymbol{\pi} | D, \boldsymbol{\Theta}] = \sum_p \mathbb{E}[\boldsymbol{\pi} | D, \theta^{(p)}] \Pr(\theta^{(p)} | D) \quad (4)$$

and the conditional covariance of the parameter heterogeneity  $(\boldsymbol{\pi} | D, \boldsymbol{\Theta})$

$$\begin{aligned} \text{Cov}[\boldsymbol{\pi} | D, \boldsymbol{\Theta}] &= \sum_p \text{Cov}[\boldsymbol{\pi} | D, \theta^{(p)}] \Pr(\theta^{(p)} | D) \\ &+ \sum_p \left\{ \left( \mathbb{E}[\boldsymbol{\pi} | D, \theta^{(p)}] - \mathbb{E}[\boldsymbol{\pi} | D, \boldsymbol{\Theta}] \right) \left( \mathbb{E}[\boldsymbol{\pi} | D, \theta^{(p)}] - \mathbb{E}[\boldsymbol{\pi} | D, \boldsymbol{\Theta}] \right)^T \right\} \Pr(\theta^{(p)} | D) \end{aligned} \quad (5)$$

$\mathbb{E}[\boldsymbol{\pi} | D, \theta^{(p)}]$  and  $\text{Cov}[\boldsymbol{\pi} | D, \theta^{(p)}]$  are the conditional expectation and conditional covariance of hydraulic conductivity given a GP method, respectively.

### (3) Groundwater Head Prediction and Uncertainty using GP and BMA

Similarly, one can determine a set of groundwater models  $\mathbf{M} = \{M^{(q)}; q = 1, 2, \dots\}$  (multimodel) from limited data to interpret groundwater flow process. However, each groundwater flow model embeds uncertain hydraulic conductivity estimates, which is described by multiple GP methods. The project extends the BMA to interpret the probability of groundwater head prediction,  $\Pr(\mathbf{u} | D, \boldsymbol{\Theta}, \mathbf{M})$ , with multiple simulation models and multiple GP methods:

$$\Pr(\mathbf{u} | D, \boldsymbol{\Theta}, \mathbf{M}) = \sum_q \sum_p \Pr(\mathbf{u} | D, M^{(q)}, \theta^{(p)}) \Pr(\theta^{(p)} | D, M^{(q)}) \Pr(M^{(q)} | D) \quad (6)$$

$\Pr(\mathbf{u} | D, M^{(q)}, \theta^{(p)})$  is the conditional probability of groundwater head prediction given data, a simulation model and a GP method.  $\Pr(\theta^{(p)} | D, M^{(q)})$  is the posterior model probability based on data and a model. By the Bayes theorem, we have

$$\Pr(\theta^{(p)} | D, M^{(q)}) = \Pr(D | \theta^{(p)}, M^{(q)}) \Pr(\theta^{(p)} | M^{(q)}) / \sum_q \Pr(D | \theta^{(p)}, M^{(q)}) \Pr(\theta^{(p)} | M^{(q)}) \quad (7)$$

where  $\Pr(D | \theta^{(p)}, M^{(q)})$  is the likelihood probability of a GP method given data and a simulation model.  $\Pr(\theta^{(p)} | M^{(q)})$  is the prior method probability. A prior probability subjectively depends on the modelers' belief. A method should receive higher likelihood probability  $\Pr(D | \theta^{(p)}, M^{(q)})$  if it produces better results given a simulation model.

One can obtain the conditional expectation and covariance of the model output with respect to multimodel and multimethod as follows:

$$\mathbb{E}(\mathbf{u} | D, \boldsymbol{\Theta}, \mathbf{M}) = \sum_q \sum_p \mathbb{E}(\mathbf{u} | D, M^{(q)}, \theta^{(p)}) \Pr(\theta^{(p)} | D, M^{(q)}) \Pr(M^{(q)} | \theta^{(p)}) \quad (8)$$

$$\begin{aligned} \text{Cov}(\mathbf{u} | D, \boldsymbol{\Theta}, \mathbf{M}) &= \mathbb{E}_M \left\{ \mathbb{E}_\theta \left[ \text{Cov}[\mathbf{u} | D, M^{(q)}, \theta^{(p)}] \right] + \text{Cov}_\theta \left[ \mathbb{E}[\mathbf{u} | D, M^{(q)}, \theta^{(p)}] \right] \right\} \\ &+ \text{Cov}_M \left\{ \mathbb{E}_\theta \left[ \mathbb{E}[\mathbf{u} | D, M^{(q)}, \theta^{(p)}] \right] - \mathbb{E}(\mathbf{u} | D, \boldsymbol{\Theta}, \mathbf{M}) \right\} \end{aligned} \quad (9)$$

### Principal Findings and Significance (derived from Li and Tsai, WRR, 45, W09403, 2009)

#### (1) Head Predictions in the "1,500-foot" sand of the Baton Rouge area, Louisiana

The proposed methodology was applied to predict the groundwater heads of the "1,500-foot" sand of the Baton Rouge area in Louisiana. The "1,500-foot" sand belongs to the Evangeline equivalent aquifer system, which is part of the Southern Hills aquifer system (Griffith, 2003). It is one of the ten freshwater aquifers that were originally named according to their general depth

in the Baton Rouge industrial district (Meyer and Turcan, 1955). Precipitation originated in Mississippi is the primary source of recharge of freshwater to the aquifer system.

The study area shown in Figure 1 extends about 300 km<sup>2</sup> and includes a major part of the Baton Rouge metropolitan area. Due to throw-down at the south side of the Baton Rouge fault, the “1,500-foot” sand (north) connects to the “1,200-foot” sand (south). The Baton Rouge fault restricts northward flow of groundwater from the south of the fault; 706 observed groundwater heads were obtained from 18 head boreholes, and electrical resistivity was measured at 20 electrical logs. The pumping rates from 16 pumping wells were recorded from January 1, 1990 to December 31, 2004. Previous studies reported small variation in specific storage (Huntzinger et al., 1985; Griffith, 2003). A constant specific storage,  $2.2 \times 10^{-5}$  m<sup>-1</sup> is considered for the “1,500-foot” sand. A time-varied constant head boundary condition was applied to all boundaries of the study area (Figure 1). This study adopted the groundwater model developed by Tsai and Li (2008). The head variances range between 0.2126 and 237 m<sup>2</sup>.

The Baton Rouge fault is rarely surveyed in this area and it can form pathways that connect aquifers at different depths due to the orientation and mode of fractures (Anderson and Fairley, 2008). Hydraulic anisotropy in the fault can result from a variety of mechanisms, including clay-smearing, drag of sand, grain re-orientation, and vertical segmentation of the fault plane (Bense and Person, 2006). Many studies (Chester et al., 1993; Bredehoeft, 1997; Salve and Oldenburg, 2001; Fairley et al., 2003) have been conducted to understand permeability in and near the fault zone and have shown that determination of the fault permeability still remains a formidable task. For the purpose of methodology implementation, the Baton Rouge fault is considered to be isotropic and homogeneous, where the hydraulic characteristic of the Baton Rouge fault was estimated to be  $5.19 \times 10^{-4}$ /day (Tsai and Li, 2008). Because the true HC value of the Baton Rouge fault is unknown, we consider three groundwater model structures: the impermeable-fault model M<sup>(1)</sup> with HC=0/day, the low-permeable-fault model M<sup>(2)</sup> with HC= $5.19 \times 10^{-4}$ /day, and the no-fault model M<sup>(3)</sup> with HC= $9 \times 10^5$ /day. The very high HC value ensures no influence on flows crossing the horizontal flow barriers for the no-fault model.

To estimate the hydraulic conductivity distribution from the 20 resistivity data, the Archie law (Archie 1942) was adopted to interpret the formation factor into porosity. Typically, the pore geometry coefficient varies between 0.62 and 2.45, and the value of cementation factor has a range between 1.08 and 2.15, depending on the formation. By fitting to the observation data, the pore geometry coefficient and the cementation factor for the “1,500-foot” sand were estimated at 0.8 and 2.04, respectively. The effective grain size is 0.22 mm (Meyer and Turcan, 1955) and the groundwater temperature is 30°C. The same seven grain-size based methods in Tsai and Li (2008) were used to convert porosity into hydraulic conductivity. The generalized parameterization (GP) that combines the Voronoi tessellation (VT) and the ordinary kriging (OK) was adopted to obtain the hydraulic conductivity distribution. A variance window with a scaling factor  $\alpha = 0.08$  was applied, where  $s_1 = 6$ ,  $s_2 = 2$ , and  $\sigma_D = 37.6$ .

## (2) BMA Results

The BMA was applied to each groundwater model, where the averaged head values over the seven estimation methods were obtained. The datum of the groundwater heads is NGVD 29. The

regression coefficient of the low-permeable-fault model ( $R^2=0.9033$ ) is slightly better than that of impermeable-fault model ( $R^2=0.8916$ ). The no-fault model ( $R^2=0.2038$ ) does not fit the observed data well. The no-fault model should not be considered because it cannot produce groundwater heads close to the observed heads. Using the variance window, the impermeable-fault model has a weight of 32.99% and the low-permeable-fault model has a weight of 67.01%. This indicates that the fault permeability is low. Both models favor the Kozeny-Carman method and the Sauerbrei method. The best combination is the Kozeny-Carman method with the low-permeable-fault model, which has a combined weight of 38.20%. The Kruger method and the Zunker method gain very small weights in the impermeable-fault model (1.61% and 1.51%, respectively) and slightly higher weights in the low-permeable fault model (6.29% and 7.38%, respectively). The Slichter method, the Terzaghi method, and the Zamarin method gain zero weight in both groundwater models.

Comparisons of calculated heads against the observed heads at EB-918, using the seven methods and BMA over methods in the low-permeable-fault model, are made. The Slichter method, the Terzaghi method, and the Zamarin method are far from one standard deviation from the BMA estimation. This demonstrates that the variance window is a valid model selection criterion for the purpose of BMA. Head uncertainty using the BMA is higher than individual methods for EB-918 at the observation space. This is because the BMA additionally considers the between-method variance and between-model variances. Using a single method may underestimate uncertainty. We also want to emphasize that due to intrinsic characteristics in individual methods, the best method may not necessarily have the smallest estimated head standard deviations. The Slichter method has a zero method weight, but has lower head standard deviations than the Kozeny-Carman method. Our point is that the estimated head standard deviation is a measure of uncertainty based on the selected method, but is not a measure of estimation accuracy for the method. Moreover, the head standard deviations increase over time because the parameter uncertainty propagates and accumulates to increase the head uncertainty.

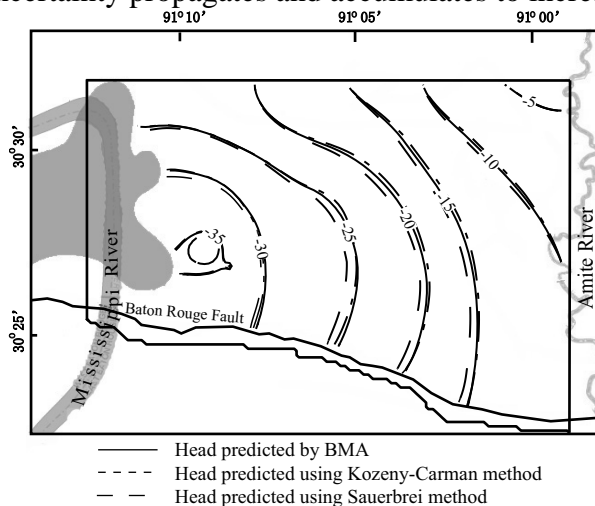


**Figure 2:** Comparisons of head prediction on 31 December 2019 by the BMA over models and methods and by the low-permeable-fault model with the Kozeny-Carman method and the Sauerbrei method.

Without the BMA analysis, one may conclude that the head uncertainty based on a wide range of methods is much larger than that from individual methods. This confirms the observation in Carrera and Neuman (1986) that the uncertainty from estimation method selection is much larger

than the uncertainty from parameter estimation. However, with the BMA analysis, the head uncertainty due to method uncertainty is similar to that of individual methods.

### (3) Head Predictions and Uncertainty with Multimodel and Multimethod

The groundwater heads for the next 15 years (from 1/1/2005 to 12/31/2019) were predicted by keeping the same head boundary conditions at the last stress period (December 2004). The time-varied monthly pumping rates were fixed to the average pumping rates of the last three years (2002-2004). Figure 2 shows the head prediction on 12/31/2019 using the BMA with the variance window against the head predictions using the low-permeable model with the Kozeny-Carman method and with the Sauerbrei method.

The BMA prediction variance of heads includes the within variance (Figure 3a), the between-method variance (Figure 3b), and the between-model variance (Figure 3c). The total BMA variance shown in Figure 3d is the sum of these three variances. Although calculated heads can be significantly different when using different simulation models and estimation methods, the between-method and between-model head prediction variances are fairly small, and the within variance dominates the total BMA prediction variance. The small between-method variance arises from the high method weight of the Kozeny-Carman method, which has a weight of 73.48% in the impermeable-fault model and 57.01% in the low-permeable-fault model. However, the low-permeable fault model, with 67.01% of the total model weight, does not dominate. Hence, the small between-model variance indicates similar head predictions by the two groundwater models.

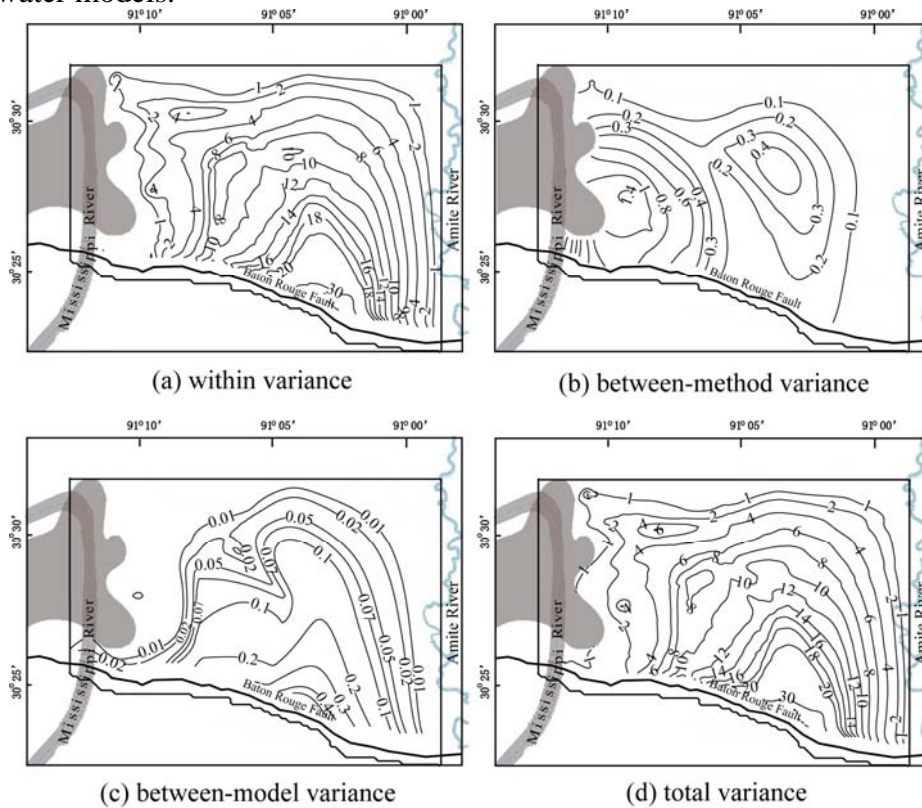


**Figure 3:** Head prediction variance ( $m^2$ ) distributions: (a) within variance, (b) between-method variance, (3) between-model variance, and (d) total variance.

We note that small between-model variance does not suggest unimportance of the hydraulic characteristic of the fault to head predictions. It cannot be used to judge the sensitivity of faults to groundwater heads. Small between-model variance simply indicates that good models produce similar predictions close to the expectation of the BMA predictions. Bad models have very little influence on the head prediction because their model weights are very small while head predictions of bad models are far from the expectation of the BMA predictions. There is no direct implication that the hydraulic characteristic of the fault is relatively unimportant to head predictions.

The within variance overwhelms the between-model and between-method variances, indicating large uncertainty propagation from hydraulic conductivity estimation to head prediction. Specially, the head prediction variance at the southeast area is large because of less hydraulic conductivity samples and head observation data. To reduce head prediction uncertainty, future sampling on hydraulic conductivity and groundwater head in these areas is necessary. Moreover, large head prediction variance near the fault indicates the need for a better understanding of the fault characteristics.

## References

- Anderson, T. R., and J. P. Fairley. (2008). Relating permeability to the structural setting of a fault-controlled hydrothermal system in southeast Oregon, USA. *Journal of Geophysical Research* 113, B05402, doi:10.1029/2007JB004962.
- Archie, G. E. (1942). "The electrical resistivity logs as an aid in determining some reservoir characteristics." *Transactions of AIME*.
- Bense, V. F., and M. A. Person. 2006. Faults as conduit-barrier systems to fluid flow in siliciclastic sedimentary aquifers. *Water Resources Research* 42, W05421.
- Bohr, G.S. 2003. Recent drought in the Southern Region: Southern Regional Climate Center, <http://www.srcc.lsu.edu/monitor/drought.html>
- Bray, R. B., and J. S. Hanor. 1990. Spatial variations in subsurface pore fluid properties in a portion of Southeast Louisiana: Implications for regional fluid flow and solute transport. *Transactions - Gulf Coast Association of Geological Societies* XL(53-64).
- Bredehoeft, J. D. (1997). Fault permeability near Yucca mountain. *Water Resources Research* 33(11), 2459–2463.
- Carrera, J., and S. P. Neuman. (1986). Estimation of aquifer parameters under transient and steady-state conditions .2. uniqueness, stability, and solution algorithms. *Water Resources Research* 22(2), 211-227.
- Chester, F. M., J. P. Evans, and R. L. Biegel. (1993). Internal structure and weakening mechanisms of the San Andreas fault. *Journal of Geophysical Research* 98(B1), 771–786.
- Draper, D. 1995. Assessment and Propagation of Model Uncertainty. *Journal of the Royal Statistical Society Series B-Methodological* 57,45-97.
- Fairley, J., J. Heffner, and J. Hinds. (2003). Geostatistical evaluation of permeability in an active fault zone. *Geophysical Research Letters* 30(18), 1962, doi:10.1029/2003GL018064.
- Griffith, J. M. (2003), Hydrogeologic framework of Southeastern Louisiana, U.S. Geological Survey, Water Resources Technical Report No. 72, Louisiana Department of Transportation and Development, Baton Rouge, Louisiana.

- Huntzinger, T.L., Whiteman, C.D., Jr., and Knochenmus, D.D. (1985). Simulation of ground-water movement in the “1,500- and 1,700-foot” aquifer of the Baton Rouge area, Louisiana. USGS, Water Resources Technical Report No. 34, LDOTD, Baton Rouge, Louisiana.
- Hoeting, J. A., D. Madigan, A. E. Raftery, and C. T. Volinsky. 1999. Bayesian model averaging: A tutorial. *Statistical Science* 14,382-401.
- Li, X., and F. T.-C. Tsai.(2009). Bayesian Model Averaging for Groundwater Head Prediction and Uncertainty Analysis Using Multimodel and Multimethod. *Water Resources Research*, 45, W09403. doi:10.1029/2008WR007488.
- Meyer, R. R., and A. N. Turcan, Jr. (1955). *Geology and Ground-Water Resources of the Baton Rouge Area Louisiana*, USGS Water-Supply Paper 1296, United States Geological Survey.
- Salve, R., and C. M. Oldenburg. (2001). Water flow within a fault in Altered Nonwelded Tuff. *Water Resources Research* 37(12), 3043–3056.
- Sargent, B. P. 2002. Water use in Louisiana, 2000. Louisiana Department of Transportation and Development Water Resources Special Report no. 15, 133p.
- Sargent, B.P. 2007. Water use in Louisiana, 2005, DOTD/USGS, Water Resources Special Report No. 16, 133p.
- Schweppe, F.C, 1973. *Uncertainty Dynamics Systems*, Prentice-Hall, New Jersey, 563pp
- Tomaszewski, D. J. 1996. Distribution and movement of saltwater in aquifers in the Baton Rouge area, Louisiana, 1990-1992. LDOTD Water Resources Technical Report No. 59, 44p.
- Tsai, F. T.-C. 2006. Enhancing Random Heterogeneity Representation by Mixing the Kriging Method with the Zonation Structure, *Water Resources Research*, 42, W08428.
- Tsai, F. T.-C., and W. W.-G. Yeh. 2004. Characterization and Identification of Aquifer Heterogeneity with Generalized Parameterization and Bayesian Estimation, *Water Resources Research*, 40, W10102.
- Tsai, F. T.-C. and X. Li. 2008 Groundwater Inverse Modeling for Hydraulic Conductivity Estimation Using Bayesian Model Averaging and Variance Window, *Water Resources Research*, 44(9), W09434, doi:10.1029/2007WR006576.

## **Publications**

### **1. Articles in Refereed Scientific Journals**

- Tubbs, K. R., and F. T.-C. Tsai. (2010). GPU Accelerated Lattice Boltzmann Model for Shallow Water Flow and Mass Transport, *International Journal for Numerical Methods in Engineering*, DOI: 10.1002/nme.3066.
- Tsai, F. T.-C. and X. Li. (2010). Reply to Comment on "Inverse Groundwater Modeling for Hydraulic Conductivity Estimation Using Bayesian Model Averaging and Variance Window" by Ye, M., D. Liu, S.P. Neuman, and P.D. Meyer, *Water Resources Research*. doi:10.1029/2009WR008591.
- Servan-Camas, B., and F. T.-C. Tsai. (2010). Two-Relaxation-Time Lattice Boltzmann Method for Anisotropic Dispersive Henry Problem. *Water Resources Research*. doi:10.1029/2009WR007837.
- Tubbs, K. R., and F. T.-C. Tsai (2009). Multilayer Shallow Water Flow using Lattice Boltzmann Model with High Performance Computing. *Advances in Water Resources*, 32(11), 1767-1776.
- Li, X., and F. T.-C. Tsai.(2009). Bayesian Model Averaging for Groundwater Head Prediction and Uncertainty Analysis Using Multimodel and Multimethod. *Water Resources Research*, 45, W09403. doi:10.1029/2008WR007488.

## **2. Book Chapter**

- Tsai, F. T.-C. and W. W-G. Yeh. (2010). Chapter 7: Model Calibration and Parameter Structure Identification in Characterization of Ground Water Systems, in Ground Water Management Manual (M. Aral and S. Taylor ed.) American Society of Civil Engineers. Accepted.

## **3. Dissertations**

- Kevin R. Tubbs, 2010, Ph.D. Dissertation “Lattice Boltzmann Modeling for Shallow Water Equations Using High Performance Computing, Engineering Science Program, College of Engineering, Louisiana State University, Baton Rouge, Louisiana, 128 pages.

## **4. Water Resources Research Institute Reports**

- Frank Tsai, 2009, Saltwater Intrusion Management with Conjunctive Use of Surface Water and Ground Water, Louisiana Water Resources Research Institute, Louisiana State University, Baton Rouge, Louisiana, 10 pages. (USGS 104G)
- Frank Tsai, 2009, Electrical Resistivity Tomography (ERT) Laboratory Experiments on Saltwater Encroachment Tracking and Modeling in Saturated Heterogeneous Sediment, Louisiana Water Resources Research Institute, Louisiana State University, Baton Rouge, Louisiana, 10 pages. (USGS 104B)

## **5. Conference Proceedings**

- Tsai, F. T.-C. (2010). A Co-Generalized Parameterization Method for Hydraulic Conductivity Estimation, World Water & Environmental Resources Congress, Providence, Rhode Island, May 16-20, 2010.
- Tsai, F. T.-C. (2010). Multimodel Approach for Groundwater Model Calibration, Prediction, and Application, World Water & Environmental Resources Congress, Providence, Rhode Island, May 16-20, 2010. (invited)

## **6. Other Publications (Abstract/Presentations)**

- Tsai, F. T.-C. (2010). Data Fusion using Co-Generalized Parameterization: Hydraulic Conductivity Estimation, 2010 Western Pacific Geophysics Meeting, 22–25 June 2010, Taipei, Taiwan
- Tsai, F. T.-C. (2010). Hierarchical Bayesian Model Averaging for Groundwater Multimodel Prediction and Management under Uncertainty, 2010 Western Pacific Geophysics Meeting, 22–25 June 2010, Taipei, Taiwan
- Tsai, F. T.-C. (2010). A Co-Generalized Parameterization Method for Hydraulic Conductivity Estimation, World Water & Environmental Resources Congress, Providence, Rhode Island, May 16-20, 2010.
- Tsai, F. T.-C. (2010). Multimodel Approach for Groundwater Model Calibration, Prediction, and Application, World Water & Environmental Resources Congress, Providence, Rhode Island, May 16-20, 2010. (invited)

## **7. Student Support**

- Kevin R. Tubbs, PhD, Spring 2010 (Graduated)

# Development of an active cap for the sequestration of mercury in contaminated lake sediments in Louisiana

## Basic Information

<b>Title:</b>	Development of an active cap for the sequestration of mercury in contaminated lake sediments in Louisiana
<b>Project Number:</b>	2010LA66B
<b>Start Date:</b>	3/1/2010
<b>End Date:</b>	2/28/2011
<b>Funding Source:</b>	104B
<b>Congressional District:</b>	Sixth
<b>Research Category:</b>	Engineering
<b>Focus Category:</b>	Sediments, Solute Transport, Treatment
<b>Descriptors:</b>	None
<b>Principal Investigators:</b>	K.T. Valsaraj, Ronald D. DeLaune

## Publications

1. MRM Chaves, KT Valsaraj, RD DeLaune, RP Gambrell, PM Buchler, "Modification of Mackinawite with L-cysteine: Synthesis, characterization, and implications to mercury immobilization in sediment" Chapter in the book "Sediment Transport", edited by Silvia Susana Ginsberg, ISBN 978-953-307-189-3, Intech Open Access Publisher, Vienna, Austria (2011).
2. M R M Chaves, K T Valsaraj, R D DeLaune, R P Gambrell, P M Buchler, "Mercury uptake by biogenic silica modified with L-Cysteine", Environmental Technology (Accepted, In Press 2011)
3. MRM Chaves, KT Valsaraj, RD DeLaune, RP Gambrell, PM Buchler, "Mercury uptake by mackinawite modified with L-Cysteine", Environmental Technology (Submitted, April 2011)
4. MRM Chaves, KT Valsaraj, JS Preston, RP Gambrell, RD DeLaune, PM Buchler, "Influence of L-methionine on the Mackinawite oxidation stability", 2010 Goldschmidt Conference in Knoxville, Tennessee on June 17th, 2010

# Development of an active cap for the sequestration of mercury in contaminated lake sediments in Louisiana

## BASIC INFORMATION

<b>Title:</b>	Development of an active cap for the sequestration of mercury in contaminated lake sediments in Louisiana
<b>Project Number:</b>	2010LA66B
<b>Start Date:</b>	3/01/2010
<b>End Date:</b>	2/28/2011
<b>Funding Source:</b>	104B
<b>Congressional District:</b>	6th
<b>Research Category:</b>	Engineering
<b>Focus Category:</b>	Sediment, Solute Transport, Treatment
<b>Descriptors:</b>	
<b>Principal Investigators:</b>	R.D. DeLaune and K.T. Valsaraj

### Publications

MRM Chaves, KT Valsaraj, RD DeLaune, RP Gambrell, PM Buchler, "Modification of Mackinawite with L-cysteine: Synthesis, characterization, and implications to mercury immobilization in sediment" Chapter in the book "Sediment Transport", edited by Silvia Susana Ginsberg, ISBN 978-953-307-189-3, Intech Open Access Publisher, Vienna, Austria (2011).

M R M Chaves, K T Valsaraj, R D DeLaune, R P Gambrell, P M Buchler, "Mercury uptake by biogenic silica modified with L-Cysteine", Environmental Technology (Accepted, In Press 2011).

MRM Chaves, KT Valsaraj, RD DeLaune, RP Gambrell, PM Buchler, "Mercury uptake by mackinawite modified with L-Cysteine", Environmental Technology (Submitted, April 2011)

MRM Chaves, KT Valsaraj, JS Preston, RP Gambrell, RD DeLaune, PM Buchler, "Influence of L-methionine on the Mackinawite oxidation stability", 2010 Goldschmidt Conference in Knoxville, Tennessee on June 17th, 2010.

## Introduction

Mercury and its compounds are considered hazardous substances, due its bioaccumulation capacity and its toxics effects on human health. The main human exposure is through the aquatic food chain. Elevated mercury concentrations in fish are the leading cause of fish advisories. In 2008, 43% of the total lake acres in the United States were under advisory for mercury (USEPA, 2009).

The Louisiana Department of Environmental Quality (LDQE) has listed in the 2000 Annual Mercury Report nineteen areas under fish consumption advisory spread along of the State. The sediment of all these areas were contaminated, but only five areas have shown sediment with mercury concentration higher than 0.200 mg/kg.

The potential sources of mercury in Louisiana are numerous, including atmospheric deposition, natural geologic deposits, industrial/municipal discharges, and previous contaminated sediments (LDQE, 2001). The industrial and municipal discharges include chlor-alkali plants, hazardous waste, municipal waste incinerators, chemical manufacturing plants, and coal-fired utilities. The Louisiana State has twenty-six facilities included in the LDQE's Toxic Emission Data Inventory (TEDI). Three facilities have reported mercury release to the surface waters of Mississippi and Calcasieu Rivers. According with LDQE (2001), the total mercury released to the environment of Louisiana from 1991 until 1999 was about 8,281 kg.

The hydrologic system of Louisiana is composed by great number of rivers, bayous and lakes. Most drainage leaves the State through the Mississippi River or flows into Lake Pontchartrain or directly into the Gulf of Mexico through smaller streams. This characteristic it seems one reason for the high mercury contamination of Gulf of Mexico coastal area in Louisiana. Thus, the remediation of sediments from lakes and rivers is important not only for the rehabilitation of the local environment, but also for the mercury transport decrease to the areas of the Gulf of Mexico.

Effective remediation of sediment contaminated with mercury is essential to minimize the contamination of fish and shellfish and, consequently, the human exposure to methyl mercury. In situ capping (ISC) is one of the remediation methods that have been shown to be effective in reducing mercury transport from contaminated sediments (Liu, Valsaraj and Delaune, 2009). In-situ capping consists in placing a layer of proper isolating material between the layers of contaminated sediment and overlying water. This method is useful in reducing the transport of the contaminant, and requires less infrastructure associated with the handling, dewatering, treatment and disposal process.

Reible (2006) discussed the sediment remediation and related that sand has been used as cap material due it being readily available, relatively inexpensive and easy to place. Sand provides many of the basic protective features of a cap; however, alternative materials could be used to improve additional effectiveness of cap. Reible is leading a demonstration of effectiveness of some materials used as capping material in field condition, in the Anacostia River - Washington DC, including coke, apatite, and aquablock<sup>®</sup>. He advised the use of coke to organic contamination, and nano sized zero valent iron where there is polychlorinated organics contamination.

As an innovative approach, Reible et al (USEPA, 2009b) are evaluating bauxite as capping material to mercury sequestration in sediment. Also, he states that cost and placement concerns normally preclude the use of conventional broadcasting techniques for these materials.

Wang et al (2004) presented a literature review of the application of sediment-capping techniques. Most of the materials presented for capping purpose were based on sand and gravels layers.

Jacobs and Forstner (1998) proposed the idea of using active barrier systems (ABS) with in situ capping (ISC). ABS usually is a reactive geochemical barrier layer that can actively block the contaminant release from the sediment entering into the overlying water, without the hydraulic contact between the sediment and the overlying water being disturbed. They used natural and modified zeolites as active material. Despite they have used to lead sorption, this feature has improved the concept of mercury sequestration using in situ capping, once mercury does not have large chemical affinity by silicate-based materials commonly used in ISC.

Sulfur, as sulfide ion, is well known to have great chemical affinity with a wide number of divalent metal ions, especially mercury. Based in this characteristic and in the chemistry of iron sulfides, Liu, Valsaraj and Delaune (2009) used mackinawite (FeS) as ABS with capping to the mercury uptake and methylation inhibition on contaminated sediment.

Liu (2008) developed her PhD works about the mercury transport through capped sediment with mackinawite. Her results have shown that mackinawite present superior efficiency on mercury immobilization (1.25 g Hg/g FeS in mercury concentration solution of 3.5mMol/l), and inhibition of mercury methylation, than sand and zeolites. However, Liu advised about the lower oxidation resistance of this material, limiting factor to use in field conditions.

We proposed the modification of mackinawite with L-cysteine, due its antioxidant property. Previous results have shown that modified mackinawite is more stable to oxidation than the unmodified mackinawite. Also, it was observed that modification process do not influence the mercury sequestration capacity, being higher than the inorganic materials (490 mg Hg/g FeS-Cys, in 10 minutes of contact). However, the effect of the mackinawite modification on the mercury sequestration in sediment was not determined.

The aim of this project was to evaluate mercury sequestration in sediments of Henderson Lake, LA, using modified mackinawite. This evaluation comprised of the following:

- a) To evaluate the mercury contamination level of sediments of a selected area;
- b) To evaluate the capping technology using modified mackinawite to prevent and minimize the transport of mercury from contaminated sediment to water column of the selected areas;
- c) To determine the efficiency of modified mackinawite to mercury sequestration in contaminated sediments, as an isolating material in capping.

The project comprised the determination of the mercury methylation inhibition capacity of modified mackinawite using contaminated sediment; and the evaluation of mackinawite as active material in in-situ capping. However, it was also needed to evaluate the mackinawite synthesis and characterization, surface modification and, the evaluation of mercury sequestration by mackinawite from aqueous solution.

## Background Research

Unmodified synthetic mackinawite has lower oxidation resistance, and it constitutes a limitation for its use, especially in capping technology. We have been working on mackinawite, in order to make this suitable to capping. We prepared pure mackinawite and mackinawite modified with L-cysteine, characterized the structure of the solids, evaluated the oxidation stability, and verified the mercury sequestration capacity in mercury spiked solution.

The following results constitute the background for the experiments of mercury sequestration from contaminated sediment in Louisiana, using in-situ capping technology.

### *Synthesis and characterization of modified and unmodified mackinawite*

The chemical composition of unmodified mackinawite was determined as  $\text{FeS}_{0.86}$ , using elemental analysis (CHNS) and ICP-OES analysis to determine iron content. Sweeney and Kaplan (1973) also found that FeS has a composition of  $\text{FeS}_{0.87-0.92}$ . For modified mackinawite, the chemical composition was determined as  $\text{FeS}_{0.735}\text{Cys}_{0.0133}$ . The results of the chemical composition characterization, supported by others analytical techniques, indicate that L-cysteine is not adsorbed on the surface of mackinawite but incorporated into the structure by replacing the sulfur. We observed by XRPD that the structure can remain stable, as mackinawite, even with a deficiency of 13% in mole of sulfur, compared to synthetic mackinawite obtained without cysteine. This feature results in layered nano-crystalline solid. XRPD and TEM analysis showed increase on (001) spacing, indicating that L-cysteine reacts with the iron, when mixed during the synthesis, and remains within the structure of mackinawite, between layers. The lattice expansion could facilitate the mercury sequestration process.

The L-cysteine affects the morphology of mackinawite clusters, being a result of its orientation and attachment during the synthesis. Cysteine takes place between the sheets of the FeS, and it forces the clusters to form plates. TEM results showed particles with average diameter of 5 nm for both modified and unmodified mackinawite. XPS and EDS analysis supported the chemical composition determination, showing the presence of  $\text{Fe}^{2+}$  and  $\text{S}^{2-}$  as the main species. Also, they indicated that modified mackinawite has higher oxidation stability than unmodified mackinawite, through the presence of oxidation products.

### *Oxidation resistance study of modified and unmodified mackinawite*

Experiments to evaluate the oxidation resistance of modified and unmodified mackinawite were performed. This evaluation was based on Eh, pH and dissolved oxygen characteristics of experiments with suspensions under magnetic stirring in more than 600 rpm, opened to the environment. Results demonstrated that FeS-Cys is more stable than the FeS, in pH range 5 to 8. In pH 4, both solids rapidly oxidize.

The most important result of the mackinawite modification with L-cysteine (FeS-Cys) is that the solid is 55% more stable to oxidation, in the experimental conditions of pH 6, temperature of 25°C, flask open to air, and mackinawite concentration of 2 g/L.

The temperature affects the mackinawite oxidation. It was observed that an increase in temperature inhibits the oxidation process. The oxidation reaction is dependent on the dissolved

oxygen in water, which decreases at higher temperatures. Even though, the Eh pattern of modified mackinawite, during the oxidation experiment, was lower than to the unmodified mackinawite in 25°C and 35°C, indicating the higher oxidation stability of modified one. In temperature of 45°C all mackinawites showed the same pattern, due the critical concentration of dissolved oxygen have limited the oxidation process.

These results were very important, and indicated that the modified mackinawite might be applied as an active insulating material in in-situ capping.

#### *Hg (II) sequestration by modified and unmodified mackinawite*

Experiments to determine the mercury sequestration capacity of the modified mackinawite was carried out, using solution of HgCl<sub>2</sub> dissolved in high pure water. Results showed that L-cysteine does not affect the mercury uptake capacity or kinetics on modified mackinawite, being capable to uptake 99.94% of mercury in solution within 10 minutes of contact. It means approximately 490 mg Hg/g FeS in media concentration of 1mmol/l Hg (II).

The pH affects Hg (II) sorption at low aqueous Hg concentrations, but that effect decreases with at high pH values. Sorption curves for Hg (II) on modified mackinawite, as function of initial concentration of Hg (II) and mackinawite, showed the same pattern as that on unmodified mackinawite, indicating no sensible difference in mackinawite adsorption capacity. The results were confirmed by XRPD and XPS. Cinnabar and metacinnabar were observed as the main product of sorption present in both modified and unmodified mackinawite.

Thus, the results established that the modification of mackinawite with L-cysteine did not affect the mercury uptake capacity, and resulted in the same products as the unmodified mackinawite. This feature is significant, making the mackinawite modification with L-cysteine as one alternative to make possible its use associated with in-situ capping.

#### *Influence of organic matter on the Hg (II) sequestration by mackinawite*

The influence of organic matter on the mercury sequestration capacity of mackinawite was evaluated. To simulate the organic matter presence, three concentrations of humic acid (Aldrich reagent) were added to solution of 1 mmol/L Hg (II). After dissolution, pH correction, and deoxygenating, each solution was put in contact with modified and unmodified mackinawite, to evaluate the mackinawite capacity of sequestration of mercury associated to organic matter. Results showed that the mercury sequestration capacity of mackinawite is strongly dependent of pH and humic acid concentration. The mercury uptake increased as pH increase in the range 3 to 5.6, then decreased until pH 8; this pattern is common for both mackinawites. This pH behavior is accentuated as higher the presence of humic acid. Considering the concentration of humic acid 1.5 g/L, and unmodified mackinawite, the mercury sequestration were about 59%, 7%, and 2%, when pH was 5.6, 7, and 8, respectively. For these pH values the Hg (II) sequestration were about 69%, 46%, and 9%, when used modified mackinawite. These results indicated that, in neutral pH and in presence of organic matter, the modified mackinawite is more efficient in Hg (II) sequestration than unmodified mackinawite.

### **Materials and methods**

The study of sequestration of mercury in contaminated sediments from Louisiana was conducted in the laboratory in in-situ capping microcosms, using modified mackinawite as an

active material for mercury immobilization. For comparison, unmodified mackinawite was prepared and studied under the same conditions.

The sediment collection and characterization, the potential of mercury methylation inhibition through sediment incubation, and the evaluation of mercury sequestration by mackinawite as a capping reactive layer are described below:

#### *Sediment collection and characterization*

To realize this study, sediment was collected from Henderson Lake, and analyzed to determine the presence of mercury (total mercury, and methyl mercury). The surface sediment (0-150mm) was collected with a Van Veen grab sampler and placed in a 5 gallon HDPE bucket. A 5 cm layer of surface water was placed over the sediment in order to maintain anaerobic conditions. These buckets were sealed, shipped to the lab and stored in a refrigerator (4°C). Prior to use, the sediment was sieved by using a steel mesh with 11mm openings to remove large debris. The sediment moisture was determined by weight change upon drying at 110°C for overnight. Organic matter content was determined as weight loss on ignition (LOI) - under temperature of 550°C during overnight - of the dried sediment samples. The pH of collected sediment was represented by the pH of the sediment slurry prepared by mixing sediment with the overlying water in a 1:1 ratio (weight), measured using an Orion ROSS pH Electrode 8156BNUWP and pH/mV meter (Oakton, pH 510 series). Sulfate in the pore water and filtrates were determined by conversion to barium sulfate, and turbidity measurement of suspension, using a 2100AN HACH turbidimeter, under EPA method 9038 (USEPA, 1986).

The total mercury content in the pore water was determined using a technique based on U.S. EPA method 7471A (USEPA, 1994), by centrifugation followed by vacuum filtration with 0.45 µm Whatmann filters. The solution was oxidized with aqua-regia and potassium permanganate (5%). Then, mercury content was determined using cold vapor absorption spectrometry (CVAAS). The total mercury content in the sediment will be determined using CVAAS of samples after acid digestion.

Methyl mercury content in sediment was determined based on the method of Alli et al. (1994), and Cai et al. (1996). The gas chromatograph separation and atomic fluorescence spectroscopy detection system will be used for quantification of Me-Hg. The integrated GC-AFS system include a Hewlett-Packard model HP 6890 Series with a gas chromatograph coupled to a PSA Merlin detector via Pyrolysis oven.

#### *Mercury methylation study through sediment incubation*

Liu (2008) have studied the mercury methylation inhibition potential of unmodified mackinawite. Thus, these experiments followed the same methodology, in an attempt to compare the results. Sediment and surface water from the site was mixed to form a slurry with a dry solid to water ratio of 1:9 (weight) placed in a 250 ml glass flask. The water content determined before the experiments was used to calculate the additional amount of surface water needed to make the slurry. Before each incubation experiment, the sediment was mechanically homogenized on a roller for 8 hours. During the incubation, the flask was sealed with a rubber stopper that had inlet and outlet holes. Ultrahigh-purity N<sub>2</sub> was purged through the flask in order to maintain anaerobic conditions, with flow rate about 1-2 bubbles per second in the gas trap. The outlet gas was connected to a sulfide trap filled with the anti-oxidation reagent (AOR) (Brouwer and Murphy, 1994). The incubation flask was wrapped with aluminum film to prevent

possible decomposition of MeHg which may be caused by exposure to light (Hammerschmidt and Fitzgerald, 2006). The experimental setup is shown in Fig. 1.

Nitrogen was purged for 30 minutes; then mackinawite (unmodified or modified) was added in one concentration of 0.05 mmol/(g-dw), 0.167 mmol/(g-dw) or 0.5 mmol/(g-dw). After 15 minutes, Hg (II) solution ( $\text{HgCl}_2$  1000  $\mu\text{g}/\text{ml}$  standard solution - SCP Science) was spiked into the slurry for a final concentration of 2  $\mu\text{g}/(\text{g-dw})$ . Experimental measurements showed that the pH of the sediment slurry decreased from 7.25 to 6.8 due to the addition of Hg (II) solution. The incubation process was about 14 days. At the end, the slurry was transferred to a HDPE flask, nitrogen was added to keep the anaerobic conditions; the flask was very tight closed and stored in the freezer until the analysis for mercury and methylmercury.

All the incubation experiments followed the same procedure except for the control experiments. The control was used to show how much MeHg was produced without addition of any potential inhibitors and thus show how effective the selected inhibitors inhibited Hg (II) methylation. For all the incubation experiments, two replicates were run simultaneously.

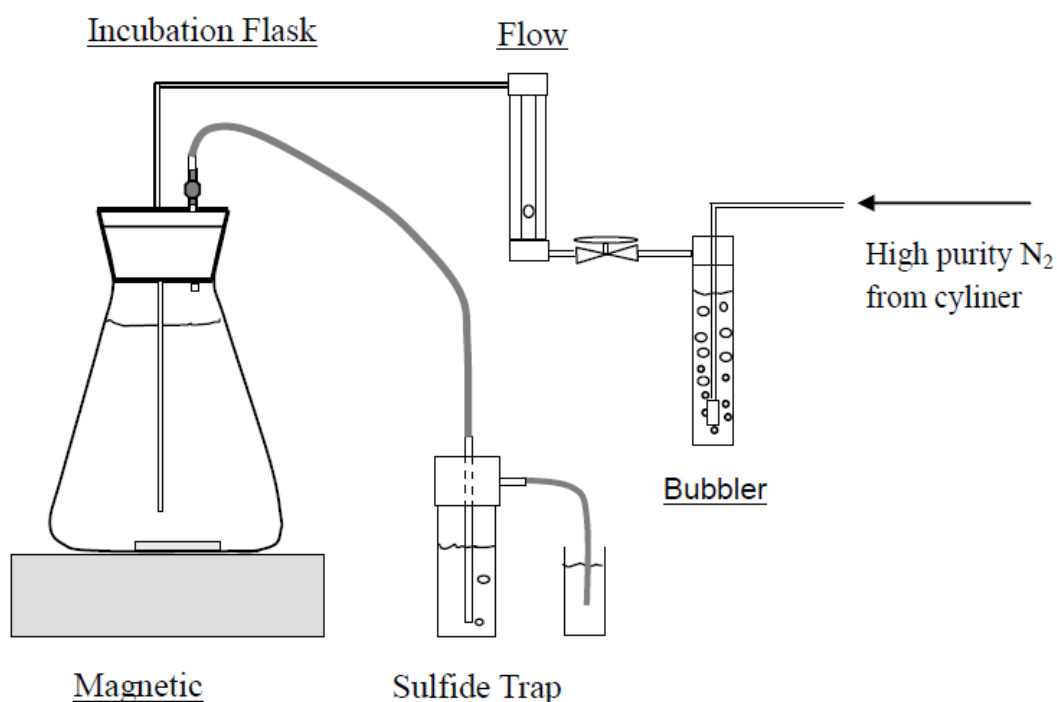


Fig. 1: Experimental setup for incubation experiments (Liu, 2008)

*Capping technology evaluation, and determination of the efficiency of modified mackinawite for mercury sequestration in contaminated sediments*

This evaluation has been carried through using acrylic capping simulator cells, to investigate the fate and transport of mercury in capped and uncapped sediments. Using the sediment collected in the area designed to this study, six cells were set up, one uncapped cell, and five capped cells with isolating material as described in the table 1.

The synthetic mackinawite (FeS) and mackinawite modified with L-cysteine (FeS-Cys) were prepared as described in Chaves et al (2011). The sand was purchase from hardware store, washed with tap water and detergent, rinsed with deionized water, and dried at 110°C before use. The sand used was the portion selected by two sieves with openings 0.125 and 0.85 mm in diameter. During the experiment, the cells were covered with aluminum foil (sides and top) to avoid direct exposure to light and avoid the potential algal growth. The top of the cells were covered with heavy metal plates to reduce possible evaporation of mercury to the air. Deionized water was passed over the sediment or cap during the experiment at a flow rate of 10 ml/hr for each cell. The depth of the overlaying water was about 12 mm. Teflon tubing was used at the outlet for water sample collection. The sediment was spiked with Hg (II) 40 µg/g-dw and homogenized during 8 hours in a roller. After this time, the sediment was transferred to the cells, and let to consolidate by 14 days.

Table 1: Design for the capping cells experiments.

Experiments	Cell 1	Cell 2	Cell 3	Cell 4	Cell 5	Cell 6
Cap layer	No	8 mm sand	8 mm FeS	8 mm FeS-Cys	3 mm Sand + 5 mm FeS	3 mm Sand + 5 mm FeS-Cys

The capping cell is illustrated in the figure 2. Its dimensions are 100 mm x 50 mm x 150 mm (L x W x H) for the part containing sediment, and 300 mm x 50 mm x 45 mm (L x W x H) for the part containing water. These cells were projected and used previously by Liu (2008), in her PhD works.

After the sediment consolidation, it was adjusted to the height with sediment, and covered with the desired capping material. Deionized water was passed over the sediment or cap during the experiment, and samples were collected to determination of mercury, and methyl mercury released to the overlying water.

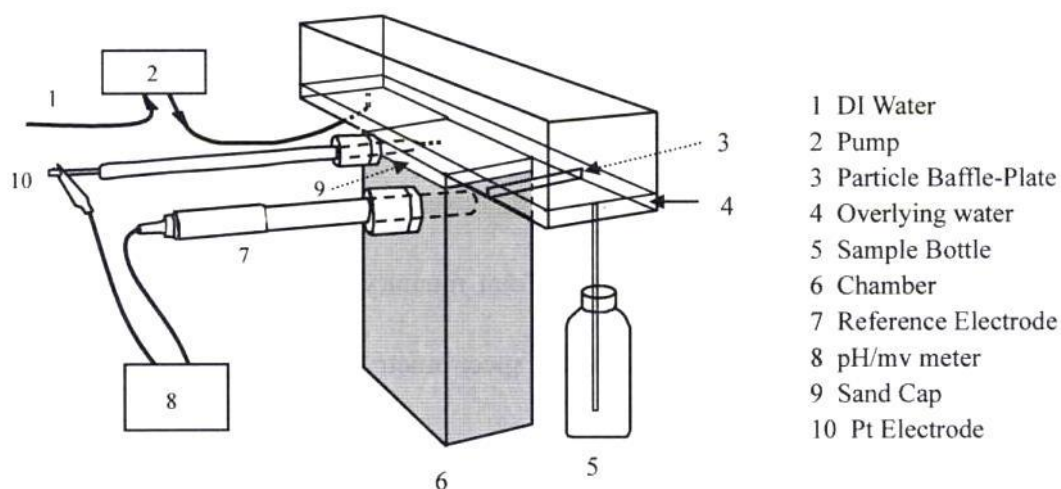


Fig. 2: Schematic of the capping cell (Liu, 2008).

The cells have been monitored to evaluate the redox conditions, and dissolved oxygen in the simulation system. The redox potential has been determined using reference electrode (Accumet, Fisher Sci.) and platinum electrodes. The platinum electrodes were made, cleaned and tested according to Patrick et al (1996).

The platinum electrodes were tested in pH 4 and pH 7 buffer solutions of quinhydrone (Alfa Aesar). The reference electrode was installed 30 mm below the water-sediment/cap interface for each cell. For uncapped cells, the platinum electrodes were installed at 30, 20, and 10 mm below the water-sediment interface. For capped cells, of 5 platinum electrodes applied, 2 were in the cap layer (at 2mm and 5 mm from water-cap interface), 1 was at the cap-sediment interface (at 10 mm from water-cap interface), and the other 2 were in the sediment (at 30 mm and 20 mm from water-cap interface). The redox potentials were measured using a pH/mV meter (Oakton, pH 510 series). At the end of the experiment, the electrodes used will be tested again to verify if they were working in the acceptable range.

The dissolved oxygen in the cell 1 and 2 was measured with a Clark-style oxygen microelectrode coupled to a 1201 chemical microsensor (Diamond General Inc.). For the cells with mackinawite, it was observed that the Clark-style oxygen microelectrode was not proper to determine DO; it was determined using a Mettler Toledo InLab<sup>®</sup> 605 sensor, with internal ATC probe, connected to Mettler Toledo SevenGo<sup>™</sup> Pro SG6 DO meter, which was calibrated following the manual instructions, using oxygen-saturated water.

The experiments were conducted over 6 months of operation. The sediments into the cells were then sliced and analyzed to determine the mercury migration on the system. The content of total mercury was determined using CVVAS, and methyl mercury will be determined using CG-AFS of digested samples for each depth. The results will allow building the profile of the mercury migration in the sediments, consequently, the fate and transport of mercury in these systems. The efficiency of FeS-Cys as an isolating material for capping will be determined by content of mercury and methyl mercury, present in sediment and water of all cells. The redox conditions, oxygen and mercury profiles, as well the sediments characteristics, will support this evaluation.

## **Results and Discussion**

Two main problems occurred during the performance of this project, and they caused delays in the project. The first one was caused by the long time required to synthesize the modified and unmodified mackinawite in large quantity. The procedure of synthesis in laboratory scale required at least 3 days (for synthesis and purification) to produce about 2.5 grams. Overall, we needed 3 months to prepare 120g of each mackinawite, resulting in delay of 6 months to the experiment start up. The second problem was that the equipment to analyze methyl mercury was under repair during August to December 2010, and no sample could be analyzed. The start up of the capping experiments was in September 2010, and it ended in April 2011. Thus, the experiments are yet to be finalized, the samples analyzed, and the results presented.

*Mercury sequestration in contaminated sediments: The efficiency of modified mackinawite, as an isolating material in capping.*

The efficiency of modified mackinawite as an isolating material in capping will be determined through the measurement of the total mercury released from sediment to overlying water, as well the methylmercury and total mercury profile in the sediment and cap layer. All the analysis for total mercury and methylmercury will be performed after the end of the experiment, and the results will be presented in the final report.

*Mercury methylation study through sediment incubation.*

The potential of mercury methylation inhibition of the modified mackinawite was performed through the sediment incubation. The samples were preserved frozen, and will be analyzed for methylmercury and total mercury; the results will be presented in the final report.

*Evaluation of the mercury contamination level in the sediment.*

The sediment collected from Henderson Lake was analyzed, regarding sulfate, AVS, pH, presence of organic matter, total mercury, and solid content. The results are summarized in table 2. It was observed that the sediment sample was in the neutral range (pore water and surface water).

The sulfate in surface water was in higher than the results reported by Liu (2008). The sulfate concentrations are higher in the winter and lower in the summer and fall (Suplee and Cotner, 2002); it can explain the observed high level of sulfate in the pore water, since the sediments were collected in March 2010, winter in Louisiana.

The AVS and total mercury concentration was lower than those observed by Liu (2008) for sediment from Henderson Lake. The sediments did not exceed the limit of 200 ng/g-dw, and showed close to the median mercury concentration (40 ng/g-dw) in sediments of Louisiana State (USEPA, 1997).

Table 2: Summary of the sediment characterization results.

<b>Solid (%)</b>	<b>Sulfate in sediment (μmol/g-dw)</b>	<b>Sulfate in surface water (μmol/L)</b>	<b>pH surface water</b>	<b>AVS (μmol/g-dw)</b>
53.3	7.53±0.48	899±4.5	7.6	6.72±0.25
<b>Organic matter (%)</b>	<b>THg sediment (ng/g-dw)</b>	<b>MeHg sediment (ng/g-dw)</b>	<b>pH pore water</b>	
2,8	45±3,6	To be determined	6.9	

*Evaluation of the capping technology using modified mackinawite.*

The capping technology evaluation using mackinawite as reactive medium has being performed through acrylic simulator cells. It was observed during the cells preparation that a minimum disturbance is enough to disperse mackinawite into the water column; once dispersed in water, is hard to mackinawite decant, due its very small size of the clusters. Thus, is not recommended to spread mackinawite in the water column, but it can be applied, for example, by slurry pumping.

The mackinawite oxidation is an important parameter to be considered, once after sorption, this process might remobilize mercury, resulting in many problems associated to its availability. The DO, pH, Eh and sulfate releasing are the parameters to monitoring the oxidation process of the species in the sediment and mackinawite cap layer, into the cells

### *Dissolved oxygen in the cells*

The cells design allowed the top part, the water column, to be in contact with air, once the cells were not hermetically closed. This feature plus the feeding water kept the water column and water/sediment-cap surface with aerobic conditions. Considering the water/sediment (or water-cap) surface as zero level, the sediment of both cells uncapped and capped with sand were anoxic in 10 mm of depth. The dissolved oxygen (DO) concentration changed as shown in the figure 3. For the sand capped cell, the DO level was higher than uncapped one, due the cap porosity allowing the oxygen diffusion.

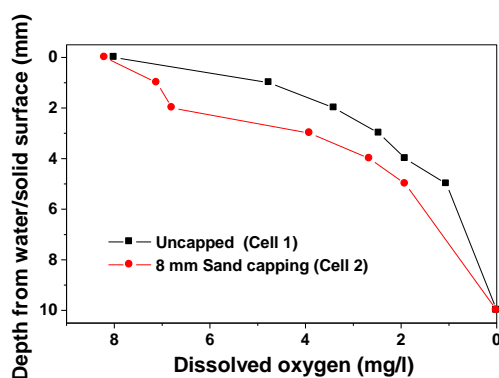


Fig. 3: The DO profile of Cells 1 and 2 after 7 days of the experiment start up.

Mackinawite in contact with water produces a fast consume of DO, resulting in strongly anoxic medium. This behavior was confirmed for the cells 3 to 6, in which the DO at zero level was 0.02 mg/L, 0.03 mg/L, 1.31 mg/L, and 1.47 mg/L for cells 3, 4, 5 and 6, respectively. After 71 days, the DO level was unchanged for cells 3 and 4; for cells 5 and 6, the DO level increased for 4,07 mg/L and 3, 67 mg/L, respectively, due the sand cap upon the mackinawite layer allow the oxygen diffusion.

### *pH and sulfate released during the capping experiments*

Mercury sorption and desorption as well mercury methylation process in sediment depend on the specific characteristics of the sediment and mercury speciation; both are directly related to the pH of the medium. Low pH is related to high mercury methylation process, as a result of several factors such as increasing in mercury desorption (Liu 2008). The pH is also important parameter to describe the reactions which take place on the sediment and water/sediment surface.

The pH of the effluent of uncapped cells, and cells capped with sand was close to the pH of the anoxic sediment after mercury amendment, around 7. It did not change during the experiment, due the absence of intense chemical reactions on the sediments.

Mackinawite is very reactive and easily oxidizes when expose to the oxygen. In the cells it occurs in the aerobic zone, above 10 mm in depth of the water/sediment surface. The oxidation process produces  $[H^+]$ ; thus, the lower pH, the higher the mackinawite oxidation. The capping layer of 8 mm in the cells 3 and 4, and 5 mm in the cells 5 and 6, had a high quantity of iron sulfide. Therefore, the oxidation process was intense enough to produce sensible pH decreasing, more than the oxidation of the sediment in direct contact with the column water (cell 1).

The pH of the effluent of the cells using unmodified mackinawite decreased below 7 in less time than the cells using modified mackinawite, confirming that the mackinawite modification with L-cysteine improves its oxidation resistance.

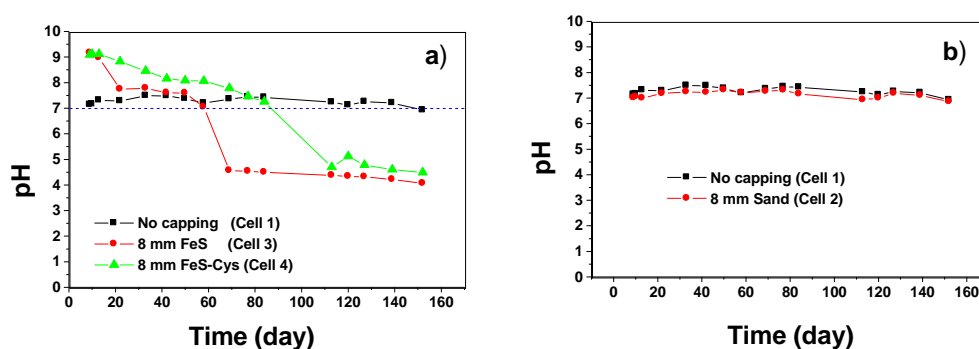


Fig 4: pH of cells uncapped and capped with sand layer.

The pH of the water effluent from cells capped with mackinawite, with and without sand layer, followed the characteristics of the used mackinawite (Fig. 5). Considering the cell 2, the 3mm sand layer is enough to reduce the DO of 8 mg/l to 4 mg/l. Thus, a sand layer reduces the DO in the cells 5 and 6, consequently, the mackinawite oxidation, making this process less intense in comparison to the cells 3 and 4. For cell 6 (Fig. 5b), the pH of the effluent was around 7 during the experiment, indicating that modified mackinawite combined with a sand layer is a good capping layer design to inhibit the mackinawite oxidation.

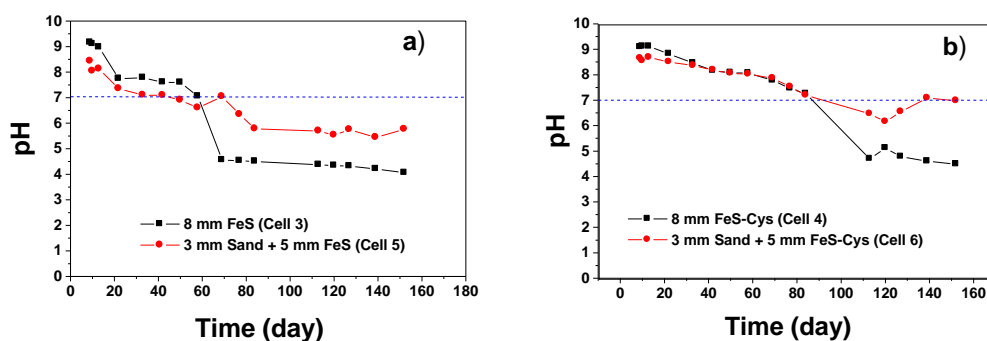
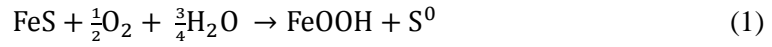


Fig. 5: pH of cells containing mackinawite during capping evaluation.

The iron sulfide (as mackinawite) is the main constituent of acid volatile sulfide (AVS) present in anoxic sediment. The mackinawite oxidation mechanism involves the oxidation of sulfide to polysulfide groups, passing through the elemental sulfur and then to sulfate (equation 1 and 2). The sulfate ions released to effluent water is related to the pH in the opposite profile.



The pH was almost constant in the cells 1 and 2 (Fig 6a, and b); consequently, the sulfate released followed the same trend. The sulfate released from the uncapped cell (cell 1) was about 70 mg/L at the experiment start up, and decreased below 40 mg/L during the experiment. Some drift occurred, but the sulfate releasing was below of the 70 mg/L over the time. The same was observed to the cell 2, capped with 8 mm of sand, where the sulfate released was below 100 mg/L; the higher sulfate releasing than the cell 1 is attributed to some sulfate adsorbed during the sand cleaning procedure with detergent.

The cells with mackinawite did not showed an aerobic zone, once all oxygen that diffuses from air to water column was continually consumed by mackinawite during its oxidation process. The sulfate released from cells 3 and 4 showed the same trend, but the quantity was lower for cell 4, due the higher oxidation resistance of modified mackinawite. During the initial 60 days, sulfate was released in very low concentration, corresponding to the oxidation inhibition phase. After them, the sulfate release has increased, due the fast oxidation of mackinawite (Fig 7c). The sulfate released from cells 5 and 6 was lower than the cells 3 and 4, confirming that the additional sand layer prevent the oxidation of mackinawite (Fig 7d).

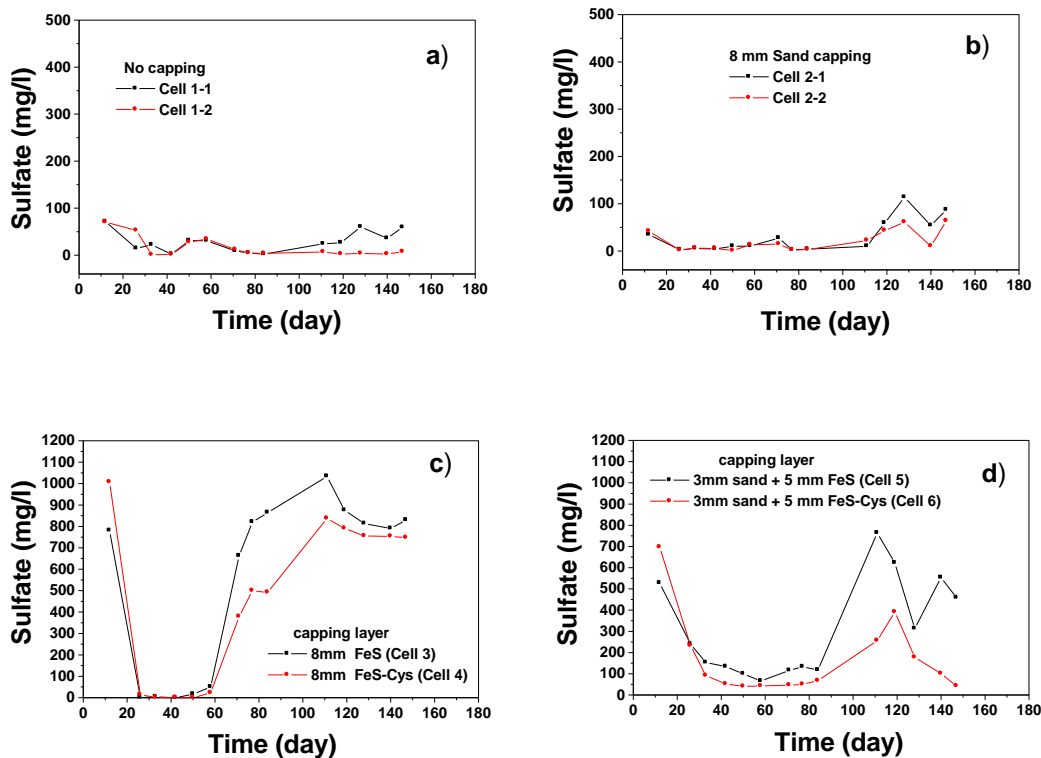


Fig. 7: Sulfate released from cells during the experiment.

Despite the experiment was not finished, the amount of sulfate released into the water until the last measurement was determined from equation 3 (Liu 2008).

$$n = \sum_i Q * C_i * \Delta t_i \quad (3)$$

Where:

n: Total sulfate released to the water;

Q: The flow rate of water (10 ml/h);

i: ith sample collected;

$C_i$ : Sulfate concentration in effluent water of sample I;

$\Delta t_i$ : Time interval between sample i and sample (i-1) were collected.

The total sulfate released from cells 1 to 6, during 147 days, is presented in the figure 8. It was observed that the modified mackinawite released about 17% (mol) less sulfate than the unmodified one. Considering the cell with unmodified mackinawite (cell 3), the sulfate released decreased about 42% when a sand layer was used (cell 5). Similarly for cell with modified mackinawite (cell 4), occurred a decreased about 62% for cell 6, and this percentage represents the contribution of the sand layer and the L-cysteine modification effect over the mackinawite oxidation in the cells.

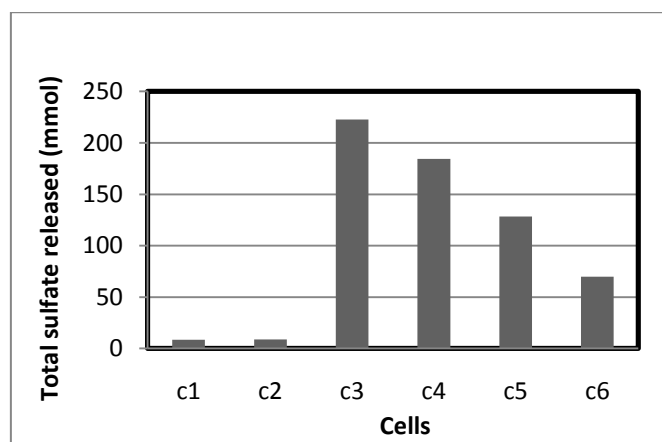


Fig. 8: Total sulfate released from cells during 147 days.

### *Redox conditions of cells*

The uncapped sediment showed the Eh typical profile for anoxic sediments (Fig. 9a). At beginning of the experiments, the Eh drifted due the electrodes stabilization process. During the experiment, the top of the sediment was oxidized, resulting in slightly increasing in Eh of the sensor at 10 mm.

The cell capped with 8 mm of sand showed the Eh profile with characteristic parts across the cells (Fig. 9b). The top part, above 2mm, the cap conditions was aerobic; therefore,

the Eh is very positive. It can be observed that the Eh of the sensors at 0 mm and 2 mm present an abrupt change after 80 days of the experiment. It was attributed to the sediment motion upward, probably due the detachment of gas bubbles from the sediment. This movement took the anoxic sediment with lower Eh to the top, exactly where the electrodes were placed, resulting in decreasing of the Eh read (Fig. 10). At the bottom part, below 10 mm of depth, the sediment was anoxic, and the Eh was similar to of same depth of the uncapped cell.

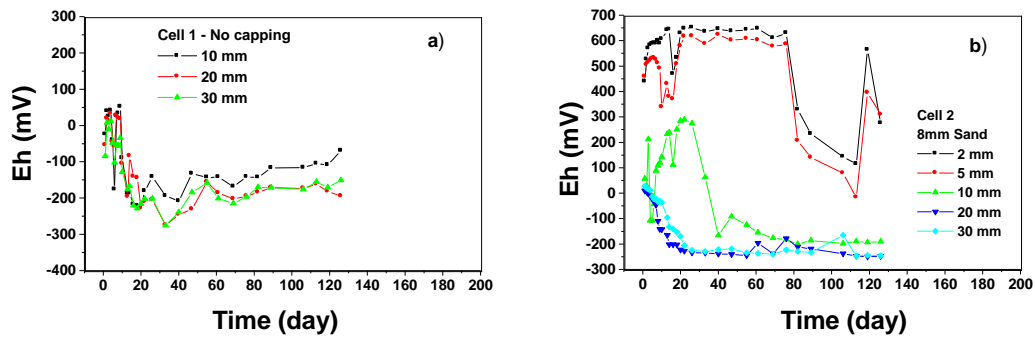


Fig. 9: The Eh in the cells 1 and 2 during the experiment.

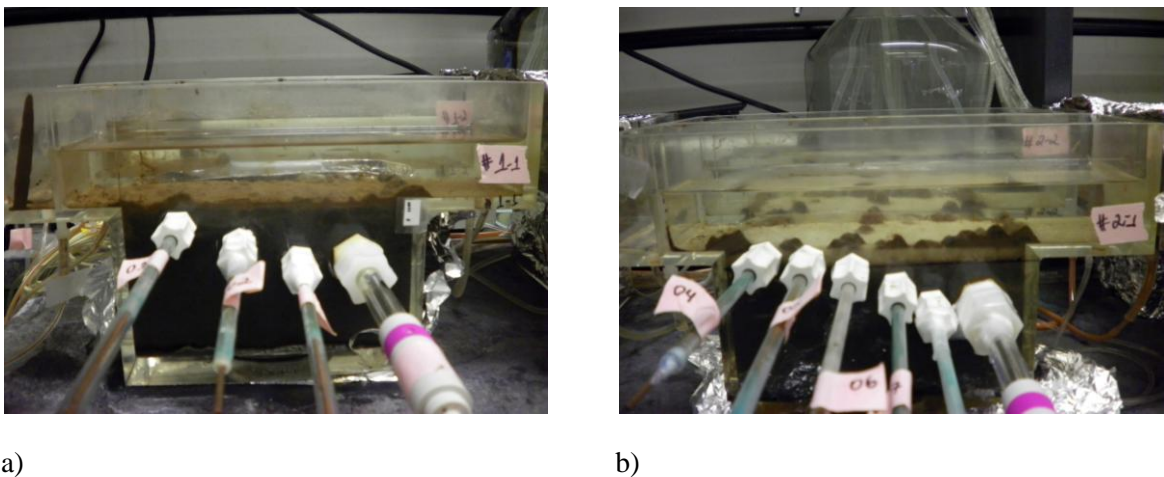


Fig. 10: The capping experiment after 60 days: a) cell 1; b) cell 2.

The potential redox in the cells capped with synthetic mackinawite describes the oxidation process of this material studied in previous works (Chaves et al, 2011). The anoxic condition of the sediment and the water/sediment surface is attributed to the oxygen consume by mackinawite.

The modified mackinawite is more reductive than unmodified mackinawite, resulting in lower Eh showed by the sensors at 10 mm and 20 mm of depth (Fig. 11b). The sensor at 30 mm showed the Eh typical of this depth for the uncapped cell. During the experiment, it was observed an increasing in the Eh of sensors at 2 mm and 5 mm of depth, due the oxidation process. The top layer partially oxidized prevents the oxidation of the bottom part, as seen for the region of the sensors at 10 mm, 20 mm and 30 mm. For the cell capped with unmodified

mackinawite, the sensors indicate that the oxidation process occurs throughout the material (Fig. 11a).

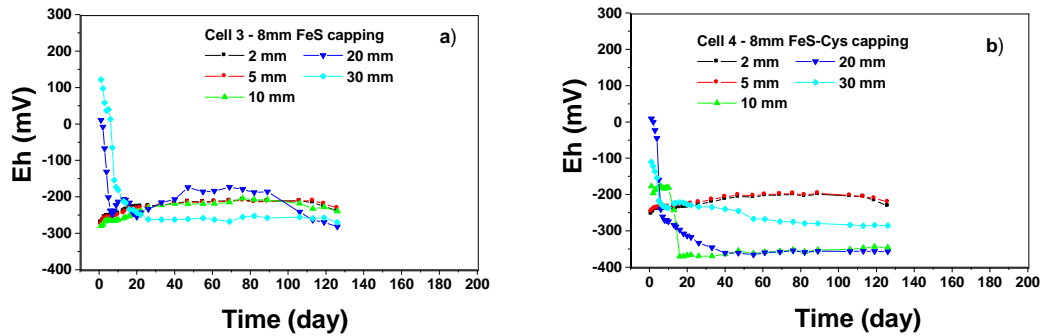


Fig. 11: Eh in the cells 3 and 4 during the experiment.

The cells with double cap layer (sand + mackinawite) showed the potential redox profile very similar than the cells with only cap layer of mackinawite for 10 mm of depth and below (Fig. 12). The top part was constituted of sand layer; the Eh is high, but not positive as cell 2, because mackinawite is very reductive, and acts surrounding areas, decreasing the Eh in the sand layer. Also, mackinawite is nano sized material and particles must have spread to the porous cap layer of sand, especially because this cell was disturbed during the start up process. This was visible in the cell 5, in which the sand layer and the water column turned black in color (Fig. 13).

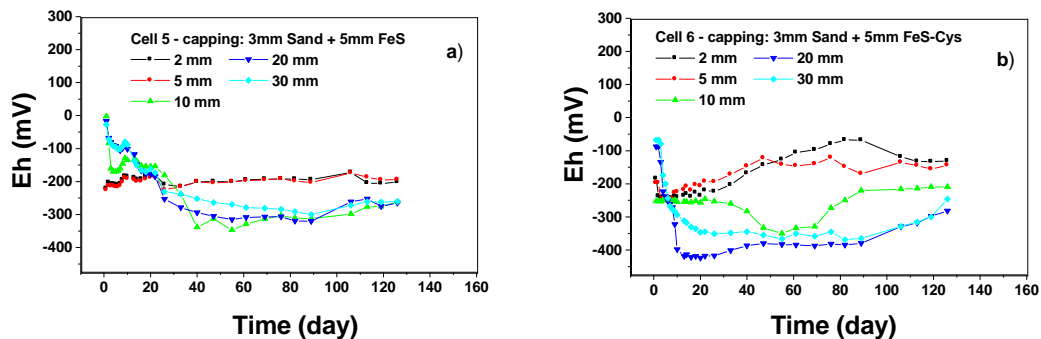
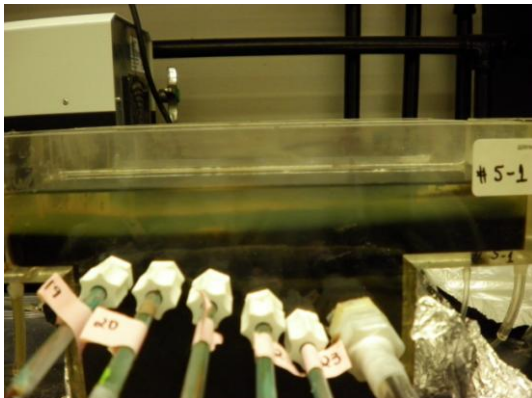
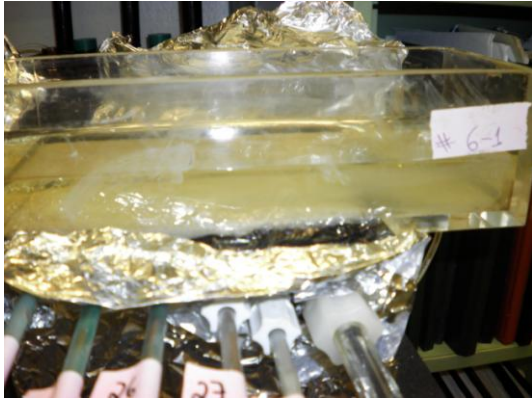


Fig. 12: The Eh in the cells 5 and 6 during the experiment.



a)



b)

Fig. 13: The capping experiment after 60 days: a) cell 5; b) cell 6.

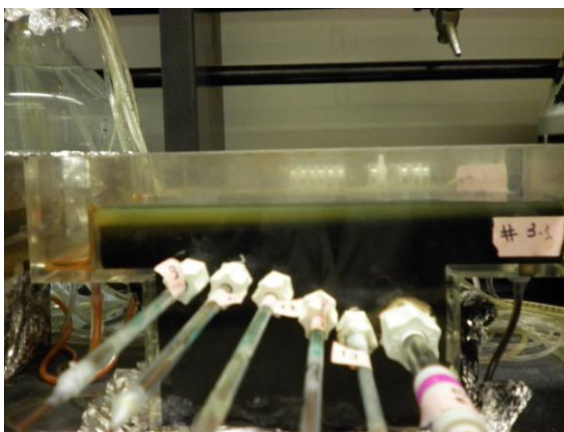
*The oxidation resistance of modified mackinawite*

The oxidation process of mackinawite in presence of oxygen presents two main phases: first occur the oxidation of the sulfide groups at the mackinawite surface, with the formation of polysulfide chains; it limits the oxygen diffusion to the bulk of the solid, working as a passivation layer. With the growth of these chains, it becomes more permeable to the oxygen diffusion, and a fast oxidation phase takes place.

Thus, to evaluate the oxidation resistance, we considered the time required to begun the fast oxidation phase. The oxidation resistance was associated to the capacity of passivation layer in prevent the oxidation of the bulk material.

Previous results showed that modified mackinawite is more resistant to oxidation than unmodified mackinawite (Chaves et al, 2011). It has being verified in the capping experiments by comparison of the results of pH, sulfate released, Eh profile in the cell, and visual inspection.

The figure 14 shows the cells 3 and 4 after 60 days of experiment. It can be observed in the cell 3 a yellowish layer of oxidized material in suspension at the top of the water column; it did not occur in the cell 4.



a)



b)

Fig. 14: The capping experiment after 60 days: a) cell 3; and b) cell 4.

Non oxidized mackinawite is black powder, which generates black dispersion. As it becomes oxidized, the black color turn progressively to red-brown, characteristic of iron (oxide) hydroxide; the degree of oxidation is related to the intensity of this color. The surface water of cell 3 showed a red-brown color, characteristic of advanced oxidation (Fig. 15). The higher oxidation resistance of modified mackinawite can be observed through the darker color of surface water that flowed from the cell 4.



Figure 15: The surface water from cell 3 and 4 after 60 days.

After 80 days, the cell 4 showed a whitish layer at the top of water column, indicating that the intense oxidation process had begun. In comparison, the same layer in the cell 3 was ochre in color (Fig. 16), corresponding to the more oxidized material.

This event can be better verified by the pH results. It was observed that the pH of cell 3 decreased below 7 about 57 days of the experiment, and it occurred for the cell 4 about 85 days. It characterizes an increase on the oxidation resistance of modified mackinawite in 50% comparing with unmodified mackinawite; it confirms the value of 55% of oxidation resistance increasing described by the previous works (Chaves et al, 2011).



Figure 16: The capping experiment after 80 days for cell 3 and 4.

### Conclusion

Preliminary results showed that the mackinawite modification with L-cysteine improves its oxidation resistance, when applied in capping cell simulators; it is very important and should allow the use of mackinawite as active material in in-situ capping technology. However, the particle size at nano scale was detected as a limitation, if applied as a powder. This will necessitate the development of a new methodology to build the capping layer under field conditions. The microcosm with modified mackinawite in a sand layer was the best design for in-situ capping experiment. It indicates that this microcosm should be useful in evaluating the mercury transport and mercury methylation through the sediment cap.

### Peer-Reviewed Publications and Presentations Resulting from the Project:

One book chapter, three publications and one presentation have resulted from this work:

MRM Chaves, KT Valsaraj, RD DeLaune, RP Gambrell, PM Buchler, “Modification of Mackinawite with L-cysteine: Synthesis, characterization, and implications to mercury immobilization in sediment” Chapter in the book “Sediment Transport”, edited by Silvia Susana Ginsberg, ISBN 978-953-307-189-3, Intech Open Access Publisher, Vienna, Austria (2011).

M R M Chaves, K T Valsaraj, R D DeLaune, R P Gambrell, P M Buchler, “Mercury uptake by biogenic silica modified with L-Cysteine”, *Environmental Technology* (Accepted, In Press 2011).

MRM Chaves, KT Valsaraj, RD DeLaune, RP Gambrell, PM Buchler, “Mercury uptake by mackinawite modified with L-Cysteine”, *Environmental Technology* (Submitted, April 2011)

MRM Chaves, KT Valsaraj, JS Preston, RP Gambrell, RD DeLaune, PM Buchler, “Influence of L-methionine on the Mackinawite oxidation stability”, 2010 Goldschmidt Conference in Knoxville, Tennessee on June 17<sup>th</sup>, 2010.

## References

- Alli, A. et al. (1994). Analysis of organomercury compounds in sediments by capillary GC with atomic fluorescence detection. *Hrc-Journal of High resolution Chromatography*, v.17, p. 745-748.
- Brouwer, H. and Murphy, T. P. (1994). Diffusion Method for the Determination of Acid-Volatile Sulfides (AVS) in Sediment. *Environmental Toxicology and Chemistry*, 13(8), 1273-1275.
- Cai, Y. et al. (1996). Determination of organomercury compounds in aqueous samples by capillary gas chromatography atomic fluorescence spectrometry following solid-phase extraction. *Analytica Chimica Acta*, v. 334, p. 251-259.
- Chaves, M. R. M. et al (2011), *Modification of Mackinawite with L-Cysteine: Synthesis, Characterization, and Implications to Mercury Immobilization in Sediment*, Chapter in "Sediment Transport", ISBN 978-953-7619-X-X (in press), InTech Open Publishers, Vienne, Austria.
- Hammerschmidt, C. R. and Fitzgerald, W. F. (2006). Photodecomposition of Methylmercury in an Arctic Alaskan Lake. *Environmental Science & Technology*, 40(4), 1212-1216.
- Jacobs, P.H., Fostener, U. (1998). Concept of subaqueous capping of contaminated sediments with active barrier systems (ABS) using natural and modified zeolites. *Wat. Res.* v.33, p. 2083-2087.
- Liu, J. (2008) Mercury transport through a capped sediment. 164 p., Thesis, Louisiana State University, Baton Rouge, LA, USA.
- Liu, J., Valsaraj, K. T., Delaune, R. D. (2009). Inhibition of Mercury Methylation by Iron Sulfides in an anoxic Sediment. *Environ. Eng. Sci.*, v. 26, p. 833-840.
- Louisiana Departmento of Environmental Quality (2001). 2000 Annual mercury report – mercury contaminant levels in Louisiana biota, sediments and surface waters. Baton Rouge, LA.
- Patrick, W. H. et al (1996). Redox measurement of soils, method of soil analysis, part 3. Chemical methods, p. 1255-1273. Soil Science Society of America, Madison.
- Reible, D.D. et al. (2006). Active Capping Demonstration in the Anacostia River, Washington, DC, Remediation: The Journal of Environmental Cleanup Costs, Technologies and Techniques, 17, 1, Winter (2006).
- Suplee, M. W. and Cotner, J. B. (2002). An Evaluation of the Importance of Sulfate Reduction and Temperature to P Fluxes from Aerobic-Surfaced, Lacustrine Sediments. *Biogeochemistry*, 61(2), 199-228.
- Sweeney, R. E., and Kaplan, I. R. (1973) Pyrite framboid formation, laboratory synthesis and marine sediments, *Econ. Geol.*, v. 68, p. 618-634.

- U. S. Protection Environmental Agency – USEPA (2009). The National Study of Chemical Residues in Lake Fish Tissue. EPA-823-R-09-006. U.S. Environmental Protection Agency, Office of Water, Washington, DC.
- U. S. Protection Environmental Agency – USEPA (2009b). Available at: [http://epa.gov/ord/npd/pdfs/lrp-factsheet\\_capping.pdf](http://epa.gov/ord/npd/pdfs/lrp-factsheet_capping.pdf). Accessed 12/07/2009
- U. S. Protection Environmental Agency – USEPA (1997). Mercury study report to Congress. Available at: <http://www.epa.gov/ttn/atw/112nmerc/volume3.pdf>.
- U. S. Protection Environmental Agency – USEPA (1994), *Method 7470 - Mercury in liquid waste (Manual Cold Vapour Technique)*. Washington, D.C. Available at: <http://www.epa.gov/osw/hazard/testmethods/sw846/pdfs/7470a.pdf>.
- U. S. Protection Environmental Agency – USEPA (1986), *Method 9038 - Sulfate (turbidimetric)*. Washington, D.C., Available at: <http://www.epa.gov/osw/hazard/testmethods/sw846/pdfs/9038.pdf>.
- Wang, Q. et al. (2004). Sources and remediation for mercury contamination in aquatic systems - a literature review. *Environ. Pollution* v.131, p.323-336.

# Wave-induced transport through coastal vegetation

## Basic Information

<b>Title:</b>	Wave-induced transport through coastal vegetation
<b>Project Number:</b>	2010LA70B
<b>Start Date:</b>	3/1/2010
<b>End Date:</b>	2/28/2011
<b>Funding Source:</b>	104B
<b>Congressional District:</b>	6th
<b>Research Category:</b>	Climate and Hydrologic Processes
<b>Focus Category:</b>	Sediments, Geomorphological Processes, Wetlands
<b>Descriptors:</b>	None
<b>Principal Investigators:</b>	Heather Smith

## Publication

1. Agnimitro Chakrabarti, Heather D. Smith, Dan Cox, Denny A. Albert. Investigation of Turbulent Structures in Emergent Vegetation under Wave Forcing. Presented at Coastal Sediments 2011 in Miami Florida

## Problem Description and Research Objectives

The State of Louisiana is facing serious challenges in dealing with coastal erosion and subsidence. The Mississippi River has been hydraulically engineered since the last four decades to suit navigational and economic requirements of the country and this in turn has resulted in massive shortage of sediment supply to Louisiana's wetlands. Further, wave erosion at wetland fringes coupled with a sediment supply rate that is considerably lower than that needed to offset the subsidence along with a massive sea-level rise in the recent years has resulted in the loss of nearly 4900 km<sup>2</sup> of wetlands (Day *et al.*, 2007). Globally, the steady occurrence of natural disasters like the 2004 Indian Ocean Tsunami, Hurricane Katrina, and others have only bolstered the dire need for an ecologically sustainable, cost effective, natural alternative to shoreline protection. Coastal vegetation comes up as an excellent candidate for this purpose (Danielsen *et al.*, 2005, Kathiresan & Rajendran, 2005, Barbier *et al.*, 2008). Vegetation aids in the reduction of energy of incoming waves by turbulent dissipation, commonly called damping. The efficiency of the wave attenuation is significantly more as dissipation occurs not only at the bottom but throughout the entire vegetation height as eddies are generated and shed along the entire stalk. In their field experiment with *Spartina anglica* salt marshes in eastern England, Neumeier and Amos (2006) found that in wave dominated environments, significant attenuation of wave orbital velocity occurring in the denser part of the salt marsh canopy resulting in an effective reduction of 20-35% of the turbulent kinetic energy. The resulting turbulence in the water column is found to control the settling rate of sediments and through a reduction in the bed shear stress limits the bed erosion rate. The vortices generated by the turbulence act as vehicles of exchange for nutrients and manifests biological processes such as dispersion of fish larva. While a considerable number of researchers have worked to quantify the influence of canopy structure in mono-directional current flows in field environments (Leonard and Luther, 1995 and Leonard and Reed, 2002) and in the laboratory with artificial vegetation (Nepf, 1999 and Nepf and Vivioni, 2000), studies in exclusively wave-dominated environments are limited. Koch and Gust (1999) noticed for sea-grass in the field that the vegetation flaps with the wave forcing, producing barriers between the flow and the lower part of the vegetation over part of the wave cycle and an open structure as the wave reverses. This open structure is thought to be an avenue of sediment exchange, but the exact mechanism is unknown. The uncertainty is primarily due to the increased difficulty in getting accurate field measurements of wave forcing within the canopy and also in part due to the difficulty in reproducing a natural canopy in the laboratory flume. Existent work using artificial flexible and rigid vegetation (Augustin *et al.*, 2009) in waves is a first attempt to understand the mechanism. However only a study of a fully natural vegetation canopy can possibly encompass the effects of the structural variety offered by a natural system and can attempt to properly simulate the complex flapping mechanism which plays significant role in turbulent dissipation. The present work is a significant step in this direction as natural vegetation beds of *Schoenoplectus pungens* (bulrush) were used for the present laboratory flume experiments.

The purpose of this project is to quantify the wave-damping capacity of bulrush and to analyze the vertical variation of TKE in order to gain insights into the turbulent structures in play in the water column. In particular the reduction of the observed wave orbital velocities will be studied by comparing with the theoretical LWT values obtained using the wave height data. Energy density spectra for the horizontal and vertical orbital velocities are presented and spectral energies corresponding to the wave component and the turbulent component calculated and their vertical variation within the water column is analyzed.

## **Objectives**

To achieve the project goal, we propose the following specific objectives:

### **Objective 1: Quantify Wave Damping by Emergent Vegetation**

The project will seek to quantify the wave height attenuation over a given distance of vegetation bed. Wave height data collected from wave gauges placed at a given distance apart will be used to calculate the wave height attenuation factor. Both vegetation and vegetation-less channel data will be presented to study the effect of vegetation on the wave field.

### **Objective 2: Compare Wave orbital velocities in both horizontal and vertical directions at different heights from the bed with the corresponding Linear Wave Theory predicted values obtained from the wave height data**

Velocity measurements from Acoustic Doppler Velocity signals at various heights above the bed in the water column will be collected. Linear Wave Theory will be used to calculate the velocities at the same heights from the wave height data collected in Objective 1. A comparison of these values will give an idea of the variation of the orbital velocities due to the effect of the vegetation.

### **Objective 3: Conduct an analysis of the spectrum of velocity signals to separate the wave component from the turbulent component and calculate the energy corresponding to the wave portion and the turbulent portion**

Spectral energy density plots will be obtained from the ADV measurements of velocities at various depths and the dominant frequency corresponding to the wave component will be isolated to separate the turbulence signal. The area under the turbulent energy spectrum will quantify the turbulence intensities at various depths.

### **Objective 4: Compare Root Mean Square (RMS) velocities of turbulent and wave components of the orbital velocities at various depths and verify the findings of Objective 3**

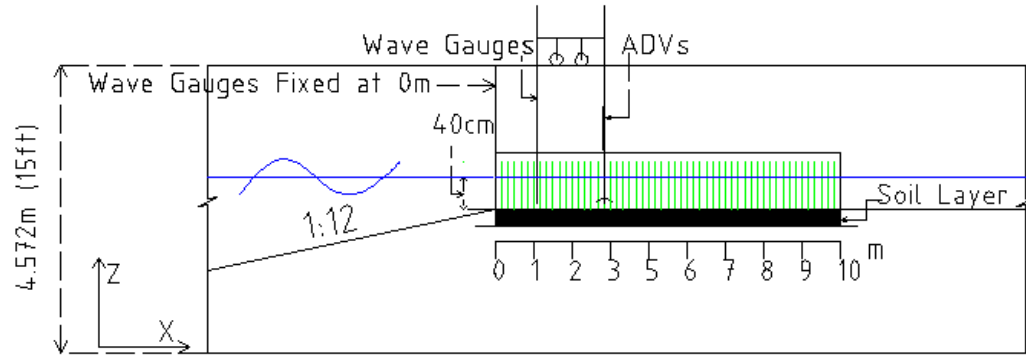
As a final task of the project, a comparison of the root mean square of orbital velocities at various depths will be made in both vegetation and vegetation-less channels to verify the trend in turbulence intensities as observed in Objective 3.

### **Experimental Description**

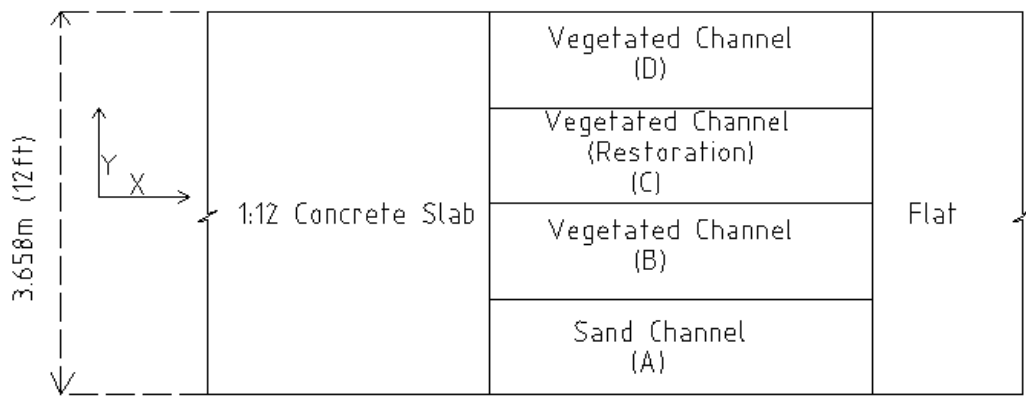
The species *Schoenoplectus pungens* or bulrush is a fairly common species of wetland vegetation growing throughout the United States. It is a perennial species with the stem having a triangular cross-section for most of the upper part with a circular cross-section at the base. The vegetation used in the experiment were harvested from young natural bulrush beds in the Tillamook Bay of Oregon in the late spring of 2009. The bulrush stems with their root system still intact were cut out in blocks from the inner estuarine regions experiencing low to moderate wave forcing similar to what was simulated in the laboratory. These were then placed in the specially constructed channel boxes and careful preparation was undertaken to sustain their growth throughout the winter of 2009 in the laboratory, under Dr. Albert's supervision and expertise. The purpose of this exercise was to mimic the field conditions in the best possible way.

The wave experiments were performed at the Oregon State University O. H. Hindsdale Wave Research Laboratory in the large-scale wave flume in the summer of 2010. The wave flume is 104 m long, 3.7 m wide and 4.6 m deep. An upgraded programmable hydraulic ram wave-maker capable of generating regular and random waves was used for generating the waves in this experiment.

Wave gauges placed at the wave maker ram location ensured quality control of these offshore parameters throughout the experiment. Four partitioned channels (A, B, C and D in plan view Fig. 1) each measuring 10 m in length and 63.5 cm in width were constructed parallel to each other and extending in the shoreward direction with channel A being the sand channel, channel B and D being vegetation channels with similar vegetation densities (approximately 1200 stems/m<sup>2</sup>) and channel C, the restoration channel, having significantly lesser vegetation density. The vegetation heights in channel D ranged mostly between 50-70 cm with approximately 66% of the stems having heights within this height range. The water depth was 40 cm and thus predominantly emergent conditions prevailed. The waves originated at a distance of 57.94 m offshore from the point where the beds started. A series of wave gauges one in each channel were placed at the beginning of each channel (position marked as 0 m in elevation view of Fig. 1). A movable wheel-mounted platform had wave gauges attached to its offshore end and Acoustic Doppler Velocimeters (ADV, model Nortek) attached to its onshore end (elevation view Fig. 1). Both regular and random waves were considered, with input wave heights ( $H_s$ ) of 5 cm to 15 cm and wave periods ( $T_p$ ) of 1.5 to 3 seconds.



ELEVATION



PLAN

Fig. 1: Experimental setup in the Large Wave Flume. Figure is not to scale.

For the data presented in this report, wave gauges were positioned at  $x=1.1$  m and the ADVs were placed at  $x=2.9$  m in channels A and D (Fig. 2) as these were considered representative for comparing the wave attenuation and resulting turbulence effects in a vegetated channel with a control channel where there is no vegetation. The particular regular wave case presented in this report had  $H_s = 15$  cm and  $T_p = 1.5$  seconds. Wave trains were run in bursts of 120 seconds (2 minutes) and it took on an average 66 seconds for the first wave to reach the 0 m mark while the signal after 105 seconds had effects of the end waves and were often inconsistent. The wave signal between 75 seconds to 102 seconds (18 waves) was found to be completely devoid of any initial and end effects and therefore this

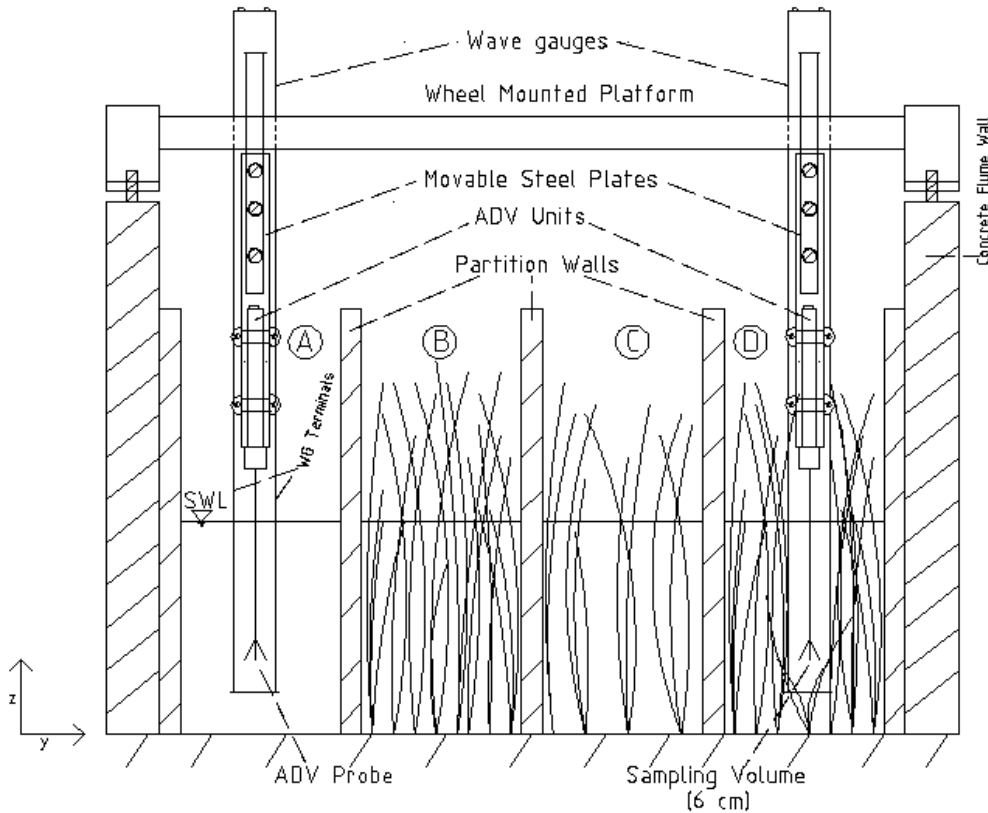


Fig. 2: Cross-sectional view of channels with ADVs and Wave Gauges deployed.

interval has been chosen as the representative interval for all the data presented here. The wave heights, both at 0 m and 1.1 m were computed using a zero crossing method (Tucker and Pitt, 2001) from the wave gauge data. Though precautions were taken to create identical incident wave conditions at the beginning of the channels, post processing of the measured data revealed that the incident wave height at 0 m differed 10-12% from trial to trial for channels A and D and as such it was thought best to acknowledge this experimental variation and present the incident wave height data separately for the two channels. The incident wave heights at 0 m for the two channels were found to be 9.28 cm for the sand channel (A) and 11.41cm for the vegetation channel (D). The wave period was found to remain constant at 1.5 seconds at both  $x=0$  m and  $x=1.1$  m locations implying no significant frequency shift in the waves. The depths of the channels were noted as 42.5 cm for the sand channel and 36.3 cm for the vegetation channel at the ADV location of  $x=2.9$  m. Based on these estimates the incident waves can be considered to be weakly non-linear and use of linear wave theory in estimating the orbital velocities at the study point is not expected to introduce significant errors. A study of the wave transmission coefficients at different points in the vegetated channel from a previous experiment revealed that the variation of wave heights between 1.1 m and 2.9 m was less than 15%. Therefore the use of  $x=1.1$  m wave gauge data to calculate wave orbital velocity values using linear wave theory at  $x=2.9$  m is considered acceptable as a first attempt. The vertical locations of the ADV were

varied from -12.4 cm to -40.4 cm for the sand channel and -12.4 cm to -34.4 cm for the vegetation channel, with the vertical heights being measured from the still water surface at 2 cm increments.

**Methodology**

Free surface water level elevations were calculated using wave gauges placed in the vegetated and sand channel. The wave heights are computed using the zero crossing method (Tucker and Pitt, 2001) from the elevations data for both the locations in the two channels. Wave height decay is quantified using the wave transmission coefficient  $K(x)$  which is defined as a function of wave height  $H(x)$  (Dalrymple *et al.*, 1984) as

$$K(x) = \frac{H(x)}{H_0} \dots\dots\dots (1)$$

where  $H_0$  is the incident wave height and  $x$  is the shoreward distance from the incident wave height location.

In order to compare the measured wave orbital velocity data with that predicted by linear wave theory, the theoretical horizontal ( $u$ ) and vertical ( $w$ ) velocities were computed using the observed free surface elevation from the wave gauges at as follows,

$$u(t) = \eta(t) \frac{\cosh k(z + d)}{\sinh(kd)} \dots\dots\dots (2)$$

$$w(t) = \eta(t) \frac{\sinh k(z + d)}{\sinh(kd)} \dots\dots\dots (3)$$

where  $\eta(t)$  is the water surface elevation time series obtained from the wave gauge readings at  $x=1.1$  m;  $d$ =the water depth;  $k=2\pi/L$ =wave number where  $L$ =wavelength calculated iteratively using the dispersion relationship  $L=L_0 \tanh(kd)$  where  $L_0=gT^2/2\pi$ =deepwater wavelength,  $T$  being the wave period.

The observed velocities were obtained by de-spiking the ADV data using the method of Mori *et. al* (2007). The missing data points in the de-spiked data set were then obtained using linear interpolation from the nearest neighbor data points. The velocity time series was time synchronized for all the trials using a cross-correlation technique so as to represent the same time window for every trial.

The spectral density (S) was computed with a Fast Fourier Transform algorithm using two ensemble averages and one band average with four degrees of freedom. The spectral energies corresponding to the wave component ( $E_u$  or  $E_w$ ) and the

turbulent component ( $E_{u_t}$  or  $E_{w_t}$ ) were separated using these cutoff frequencies, and the spectral energies are defined as,

$$Eu = \frac{1}{2} \rho \int_{f_1}^{f_2} S_u(f) df \dots\dots\dots (4)$$

$$Eu_t = \frac{1}{2} \rho \int_{f_2}^{f_n} S_{u_t}(f) df \dots\dots\dots (5)$$

where,  $\rho$  = density of water ( $10^3$  Kg/cu.m),  $f_n$  = Nyquist frequency, with  $S_u$  and  $S_{u_t}$  being the spectral densities for the wave component and the turbulent component respectively.

### Results and Discussions

The variation of the free surface elevation with time at the initial position ( $x=0$  m) and at the  $x=1.1$  m wave gauge location for both the sand (channel A, top panel) and vegetation (channel D, bottom panel) channels are shown in Fig. 3. Both the sand and the vegetated channels show attenuation of the incoming wave height with the attenuation in the vegetation channel being significantly higher.

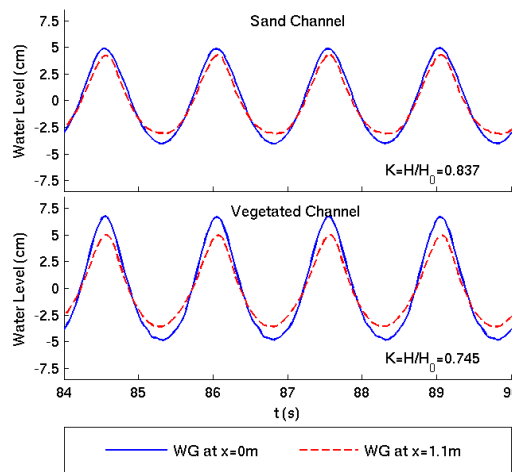


Fig. 3: Wave attenuation by vegetation. The sand channel (channel A) is shown in the top panel, and the vegetated channel (channel D) is shown in the bottom panel. The solid blue line is the incoming wave and the dashed red line is the wave observed 1.1 m into the channel. The wave transmission coefficient is shown for each case.

Using Eqn. (1) the wave transmission coefficients are calculated for each channel, with a wave transmission coefficient of 0.837 for the sand channel and 0.745 for the vegetated channel. The lower value of  $K(x)$  in the vegetated channel shows a greater attenuation of the incident waves by the vegetation and yields an increase of 11% in the reduction of the incoming wave over just 1 m of vegetation.

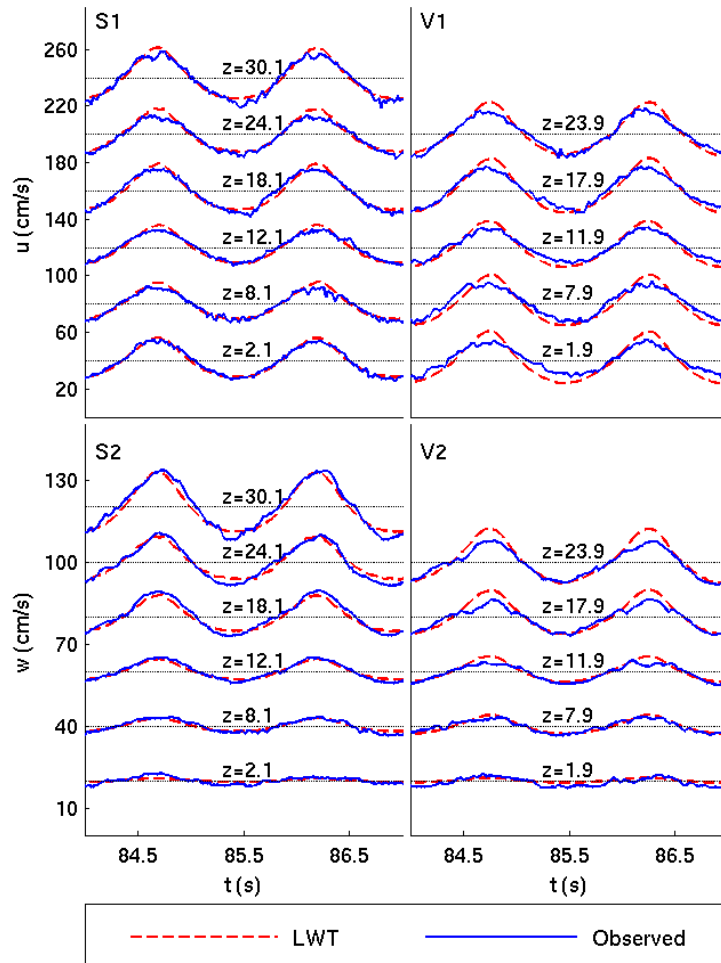


Fig. 4: Comparison of horizontal ( $u$ ) and vertical ( $w$ ) components of the wave orbital velocities (solid blue line) in the sand channel (panels S1 and S2) and the vegetation channel (panels V1 and V2) with those predicted by Linear Wave Theory (LWT, dashed red line) calculated from the wave gauge data. Here  $z$  represents height in cm from the bed and each elevation is offset by 40 cm/s for panels S1 and V1 and 20 cm/s for panels S2 and V2.

Fig. 4 presents the comparison of the orbital velocity components in both channels with those predicted by LWT at different heights from the bed. It is seen that the observed orbital velocity signatures follow more or less the LWT profiles for the sand channel, while those in the vegetation channel show pronounced variation from the LWT profiles. The deviation is particularly prominent at lower depths for the horizontal component with the linear wave theory predicting higher values. For the vertical component however the variation is more discernible in the upper part of the water column, where the vertical velocities are larger.

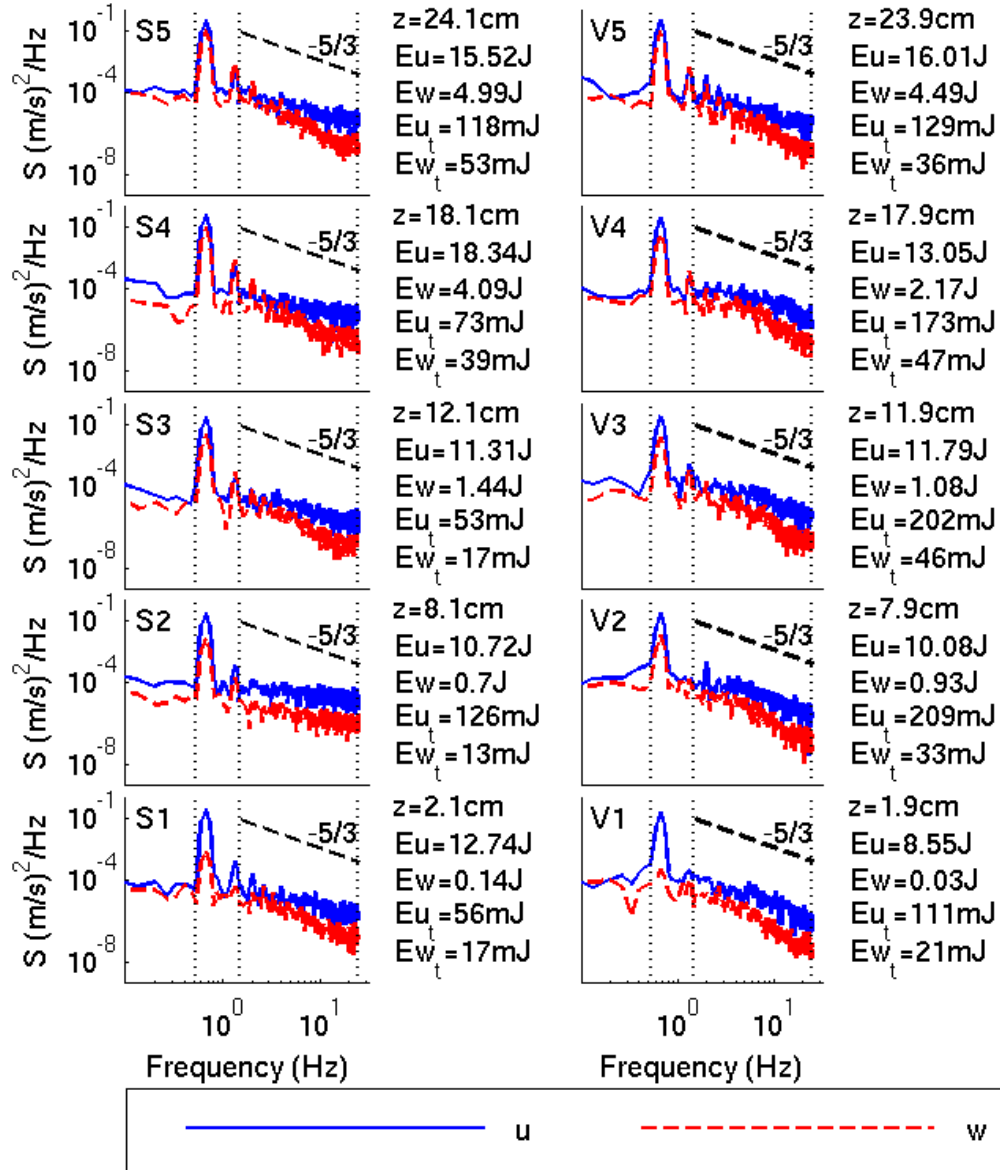


Fig. 5: Power spectra of the horizontal (u, blue solid line) and vertical (w, red dashed line) orbital velocity obtained from the ADV data at different heights (z) above the bed. Eu and Ew are the spectral energies for the wave component while Eu<sub>t</sub> and Ew<sub>t</sub> are the spectral energies for the turbulent component. S is the spectral density. The vertical dotted lines correspond to the lower and higher cutoff frequencies for the wave component and the Nyquist frequency.

Fig. 5 shows the distribution of the spectral density for the horizontal and vertical velocity components of the observed wave orbital velocity at different elevations above the bed for both sand and vegetated channels. Power spectra plots for all the vertical positions were investigated and the average lower (f<sub>1</sub>) and higher (f<sub>2</sub>) cutoff frequencies for the wave component of the velocity were found to be 0.531 Hz and 1.492 Hz, respectively as shown with the dotted lines on Fig. 5. Small variations of these frequencies were not found to have any significant effect on the

results. The inertial sub range denoted by the dashed line approximates the slope of the  $-5/3$  line in the log-log scale (Soulsby, 1983) for the vegetation channel. The spectral energies for the wave component ( $E_u$  and  $E_w$ ) decrease with depth for the vegetation channel with the vertical component almost vanishing near the bed, while for the sand channel the  $E_u$  value remains fairly invariant while the  $E_w$  value decreases with depth indicating the characteristic reduction of the vertical component of the orbital velocity. The turbulent spectral energies are significantly higher for both the velocity components in the vegetation channel than those in the sand channel. Vertical variations reveal that  $E_{u_t}$  and  $E_{w_t}$  show a steady decline with depth from the free surface for the sand channel except for an outlier value of  $E_{u_t}$  (possibly due to imperfections in the ADV measurement) at the  $z=8.1$  cm location from bed. On the other hand, for the vegetation channel,  $E_{u_t}$  increases with depth from the free surface up to about the  $z=6$  cm location from the bed.  $E_{w_t}$  also shows a somewhat similar trend except the decrease appears at a shallower depth of about  $z=8$  cm from the bed. From these spectral energy plots we may say that the maximum reduction of the orbital velocity occurs between 8 to 24 cm that is approximately between the one-fourth to two-third part of the depth, possibly due to increased above ground biomass content within this region.

The vertical distribution of the root-mean-squared (RMS) velocities for the total, wave, and turbulent components are presented in Fig. 6. Panels S1 and V1 show the RMS velocities for the total velocity ( $u_{rms}$  and  $w_{rms}$ ) for the sand and vegetated channels, respectively. The total wave orbital velocity component is defined as  $u = u_w + u_t$ , where  $u_w$  = frequency filtered component containing the effect of the mean wave action only and  $u_t$  = turbulent component corresponding to the inertial sub-range of the frequency spectrum. For the sand channel, it is seen that the horizontal component almost matches the linear wave theory value consistent with the velocities shown in Fig. 4. However, the vertical component is higher throughout the depth, and may be attributed to the sensitivity of the vertical velocity to the differences in the actual wave height occurring at the  $x=2.9$  m position with the measured values at  $x=1.1$  m from which the LWT velocities are calculated. For the vegetated channel, it is observed that the vertical velocity component remains generally lower than the LWT estimate in the upper two-third portion of the water column implying greater turbulence reduction. No such consistent profile is however observed for the horizontal component.

Panels S2 and V2 in Fig. 6 present the RMS velocities of wave component ( $u_{w,rms}$ ,  $w_{w,rms}$ ). While the general trends of the vertical profile follow a similar nature for both sand and vegetated beds, the vegetated channel velocities shows an appreciable decrease in the vertical orbital velocity due to dissipation. Consistent with the spectral energies calculated in Fig. 5, most of the total energy is contained in the mean wave energy. The vertical distribution of the RMS of the turbulent component of the orbital velocities ( $u_{t,rms}$  and  $w_{t,rms}$ ) are shown in panels S3 and V3. Both the horizontal and vertical components of the RMS values of the turbulent components in the vegetated channel exhibit a decrease with height from the bed, while the observations in the sand channel do not. At lower elevations, the

turbulent components of the horizontal velocities are much higher than those observed in the sand channel, indicating increased turbulence generation at higher vegetation density (increased vertical biomass). This is consistent with the previous observations from the spectral energy values in Fig. 5. The spike in turbulence at approximately  $z=15$  to  $20$  cm is likely due to a local change in the vertical distribution of the biomass and needs to be further looked into in correlation with vertical biomass distributions in future publications. This is

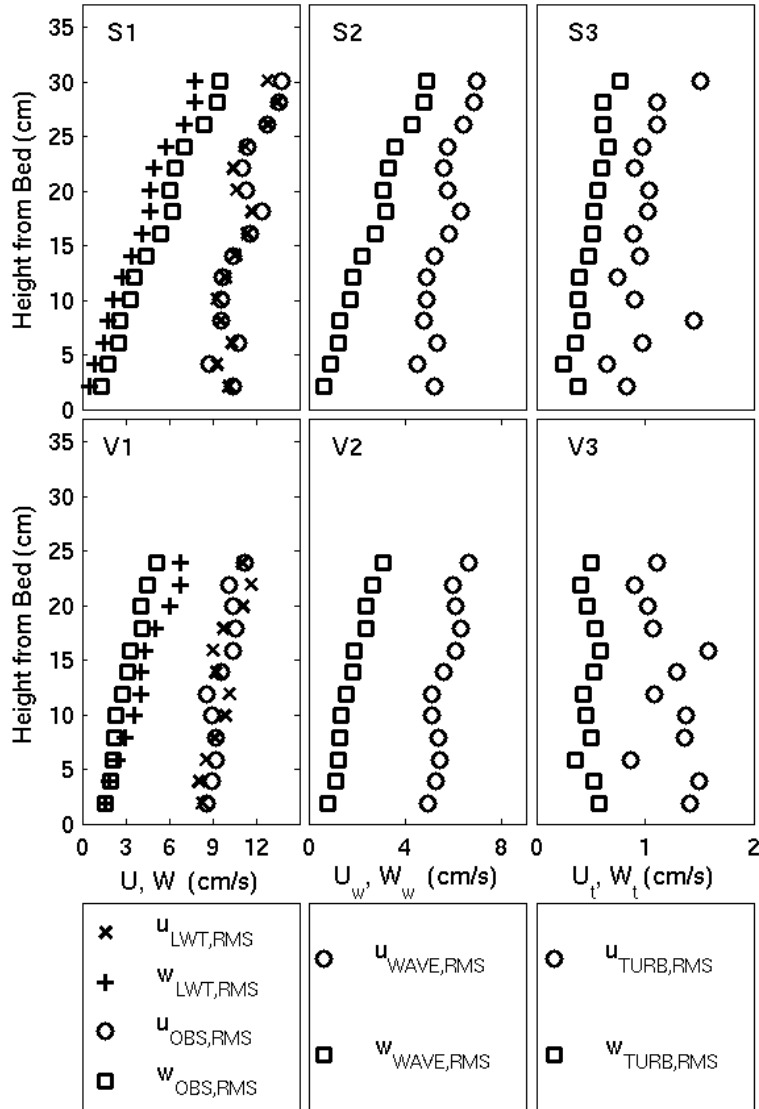


Fig. 6: Comparison of root-mean-squared (RMS) velocities with depth. Panels S1 and V1 present the RMS of the total velocity, panels S2 and V2 present the RMS of the wave velocity and panels S3 and V3 present the RMS of the turbulent velocities. Top panels (S1, S2, S3) are distributions for the sand channel and bottom panels (V1, V2, V3) for the vegetated channel. Please note the velocity scale difference in these panels.

consistent with the observations of Neumeier and Amos (2006) who found a spike in observed three-dimensional Reynold's stresses between this range for fully submerged *Spartina* canopies. The turbulent vertical velocity magnitudes are similar between the vegetated and sand channels. Though the relative scatter in these figures are higher than the previous ones, still it gives an understanding into the dynamics of turbulence distribution within the canopy.

### **Conclusions**

Regular wave cases with significant wave heights and wave periods typical of estuarine conditions were run over two parallel beds, one containing only sand and the other a particular species of bulrush under emergent conditions in the Large Wave Flume at Oregon State University. Wave attenuation effects of the vegetation channel was found to be superior, the wave transmission coefficient for the vegetated channel being 11% lower than that of the sand channel over just the first 1 m of vegetation alone. ADV measurements were obtained and the de-spiked wave orbital velocities after proper time synchronization between the trials were compared to the linear wave theory predicted values, obtained from water surface elevation data from wave gauges at a nearby point. The vertical component of the velocity in the vegetation channel showed greater agreement at the lower water depths with those predicted by LWT, while the horizontal profiles matched the LWT trends in the upper part of the water column. The observed velocity profiles showed close agreement with the LWT profiles for the sand channel.

The power spectra for the orbital velocity components suggests the horizontal and vertical turbulent spectral energies in the vegetation canopy are higher between 10 to 24 cm from the bed with the values decreasing with height from the bed. However no such general trend is observed in the sand channel indicating this is a property of the above ground biomass distribution. As a future scope for work, the correlation of this distribution of the turbulent kinetic energy with the above ground biomass distribution will be studied. The vertical variation of root-mean-squared (RMS) velocities show that for the vegetated channel, the upper half of the water depth exhibits marked reduction in turbulence thereby confirming the earlier finding from the spectral energy values. The turbulence signal for the horizontal velocity component in the vegetated channel is higher than that for the sand channel, yielding increased wave dissipation, but also may affect the dynamics of suspended sediment in the layer. It is worthwhile to point out that during the course of these experiments no discernible sediment movement was observed on the bed, except the formation of minor dunes and troughs.

This work was presented at the 2011 Coastal Sediments Conference in Miami, Florida in May of 2011. One graduate student, Agnimitro Chakrabarti, was supported under this work.

## References

- Augustin, L.N., Irish, J.L., and Lynnet, P. (2009). "Laboratory and numerical studies of wave damping by emergent and near-emergent wetland vegetation," *Coast. Eng.*, 56(3):332-340.
- Barbier, E., Koch, E., Silliman, B., Hacker, S., Wolanski, E., Primavera, J., Granek, E., Polasky, S., Aswani, S., Cramer, L., Storms, D., Kennedy, C., Bael, D., Kappel, C., Perillo, G., and Reed, D. (2008.) "Coastal ecosystem-based management with nonlinear ecological functions and values," *Science* 319:5861.
- Dalrymple, R.A., Kirby, J.T., Hwang, P.A. (1984). "Wave refraction due to areas of energy dissipation," *J. Waterw., Port Coast. Ocean Eng.* 110(1):67-69.
- Danielsen F., Sorensesn, M.K., Olwig, M.F., Selvam, V., Parish, F., Burgess, N.D., Hiraishi, T., Karunagaran, V.M., Rasmussen, M.S., Hansen, L.B., and Suryadiputra, N. (2005). "The Asian Tsunami: A protective role for coastal vegetation," *Science* 310:643.
- Day, J.W., Boesch, D.F., Clairain, E.J., Kemp, P., Laska, S.B., Mitsch, W.J., Orth, K., Mashriqui, H., Reed, D. J., Shabman, L., Simenstad, C.A., Streever, B.J., Twilley, R.R., Watson, C.C., Wells, J.T., and Whigham, D.F. (2007). "Restoration of the Mississippi delta: Lessons from Hurricanes Katrina and Rita," *Science*, 315:1,679-1,684.
- Kathiresan, K., and Rajendran, N. (2005). "Coastal mangrove forests mitigated tsunami," *Estuar Coast Shelf Sci* 65:601-606.
- Koch, E. and Gust, G. (1999). "Water flow in tide- and wave-dominated beds of seagrass thalassia testudinum," *Mar. Ecol.*, 184:63-72.
- Leonard, L.A. and Luther, M.E. (1995). "Flow hydrodynamics in tidal marsh canopies," *Lim. Ocean.*, 40:1474-1484.
- Leonard, L.A. and Reed, D.J. (2002). "Hydrodynamics and sediment transport through tidal marsh canopies," *J.Coast. Res.*, SI 36:459-469.
- Mori, N., Suzuki, T., Kakuno, S. (2007). "Noise of acoustic doppler velocimeter data in bubbly flows," *J. Eng. Mech.*, 133(1):122-125.
- Nepf, H.M. (1999). "Drag, turbulence, and diffusion in flow through emergent vegetation," *Water Res. Res.*, 35(2):479-489.
- Nepf, H.M. and Vivoni, E.R. (2000). "Flow structure in depth limited, vegetated flow," *J. Geophys. Res.*, 105(C12): 28547-28557.
- Neumeier, U. and Amos, C.L. (2006). "Turbulence reduction by the canopy of coastal spartina salt marshes," *J. Coast. Res.*, SI 39:433-439.

Soulsby, R.L. (1983). "The bottom boundary layer of shelf seas," John, B. (ed), *Physical oceanography of coastal and shelf seas, Elsevier Ocean. Series*: 189-266.

Tucker, M.J. and Pitt, E.G. (2001). "Waves in ocean engineering," Amsterdam, Elsevier, 521 p.

# Multimodel uncertainty analysis for chance-constrained saltwater intrusion management

## Basic Information

<b>Title:</b>	Multimodel uncertainty analysis for chance-constrained saltwater intrusion management
<b>Project Number:</b>	2010LA71B
<b>Start Date:</b>	3/1/2010
<b>End Date:</b>	2/28/2011
<b>Funding Source:</b>	104B
<b>Congressional District:</b>	6th
<b>Research Category:</b>	Ground-water Flow and Transport
<b>Focus Category:</b>	Groundwater, Solute Transport, Management and Planning
<b>Descriptors:</b>	None
<b>Principal Investigators:</b>	Frank Tsai

## Publications

1. Tubbs, K. R., and F. T.-C. Tsai. (2010). GPU Accelerated Lattice Boltzmann Model for Shallow Water Flow and Mass Transport, International Journal for Numerical Methods in Engineering, DOI: 10.1002/nme.3066.
2. Tubbs, K. R., and F. T.-C. Tsai. (2010). GPU Accelerated Lattice Boltzmann Model for Shallow Water Flow and Mass Transport, International Journal for Numerical Methods in Engineering, DOI: 10.1002/nme.3066.
3. Servan-Camas, B., and F. T.-C. Tsai. (2010). Two-Relaxation-Time Lattice Boltzmann Method for Anisotropic Dispersive Henry Problem. Water Resources Research. doi:10.1029/2009WR007837.
4. Tubbs, K. R., and F. T.-C. Tsai (2009). Multilayer Shallow Water Flow using Lattice Boltzmann Model with High Performance Computing. Advances in Water Resources, 32(11), 1767-1776.
5. Li, X., and F. T.-C. Tsai.(2009). Bayesian Model Averaging for Groundwater Head Prediction and Uncertainty Analysis Using Multimodel and Multimethod. Water Resources Research, 45, W09403. doi:10.1029/2008WR007488.
6. Tsai, F. T.-C., Bayesian Model Averaging Assessment on Groundwater Management under Model Structure Uncertainty, Stochastic Environmental Research and Risk Assessment, 24(6), 845-861, 2010.
7. Tsai, F. T.-C. and W. W-G. Yeh. (2010). Chapter 7: Model Calibration and Parameter Structure Identification in Characterization of Ground Water Systems, in Ground Water Management Manual (M. Aral and S. Taylor ed.) American Society of Civil Engineers. Accepted.
8. Kevin R. Tubbs, 2010, Ph.D. Dissertation "Lattice Boltzmann Modeling for Shallow Water Equations Using High Performance Computing, Engineering Science Program, College of Engineering, Louisiana State University, Baton Rouge, Louisiana, 128 pages.
9. Tsai, F. T.-C. (2010). A Co-Generalized Parameterization Method for Hydraulic Conductivity Estimation, World Water & Environmental Resources Congress, Providence, Rhode Island, May 16-20, 2010.
10. Tsai, F. T.-C. (2010). Multimodel Approach for Groundwater Model Calibration, Prediction, and Application, World Water & Environmental Resources Congress, Providence, Rhode Island, May 16-20, 2010. (invited)

## Multimodel uncertainty analysis for chance-constrained saltwater intrusion management

11. Tsai, F. T.-C. (2010). Data Fusion using Co-Generalized Parameterization: Hydraulic Conductivity Estimation, 2010 Western Pacific Geophysics Meeting, 22–25 June 2010, Taipei, Taiwan
12. Tsai, F. T.-C. (2010). Hierarchical Bayesian Model Averaging for Groundwater Multimodel Prediction and Management under Uncertainty, 2010 Western Pacific Geophysics Meeting, 22– 25 June 2010, Taipei, Taiwan
13. Tsai, F. T.-C. (2010). A Co-Generalized Parameterization Method for Hydraulic Conductivity Estimation, World Water & Environmental Resources Congress, Providence, Rhode Island, May 16-20, 2010.
14. Tsai, F. T.-C. (2010). Multimodel Approach for Groundwater Model Calibration, Prediction, and Application, World Water & Environmental Resources Congress, Providence, Rhode Island, May 16-20, 2010. (invited)

## SYNOPSIS

**Title:** Multimodel Uncertainty Analysis for Chance-Constrained Saltwater Intrusion Management

**Project Number:**

**Start Date:** 3/1/2010

**End Date:** 2/28/2011

**Funding Source:** 104B

**Congressional District:** Louisiana

**Research Category:** Ground-water Flow and Transport

**Focus Category:** Ground Water, Solute Transport, Management & Planning

**Descriptors:** Uncertainty, Chance Constraint, Model Averaging, Prediction, Saltwater Intrusion, Aquifer, Subsurface, Modeling, Optimization, Management

**Primary PI:** Frank T.-C. Tsai

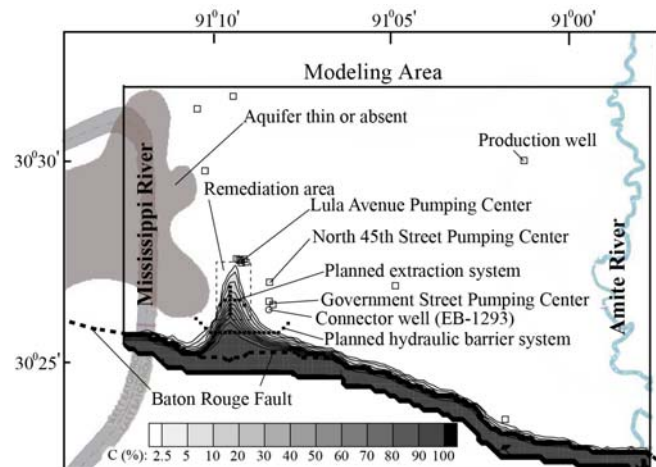
### Problem and Research Objectives

The Baton Rouge aquifer system located at south central Louisiana is a major source of drinking and industrial water. The aquifer has a fault running east-west located at the southern part near the coastline of the region. The fault cuts the aquifer system into two parts: the up-thrown north side and the down-thrown south side. The fault was considered to act as an impermeable barrier to groundwater movement across it. A recent study suggests the Baton Rouge Fault as a conduit-barrier fault (Bense and Person 2006). Predominantly, the region south of the aquifer contains saltwater and north of the aquifer contains fresh water. However, by 1990, the water quality data at the existing wells to the north of the fault indicated that increasing water withdrawn in the region was resulting in saltwater intrusion to the north and a decrease in water quality within the aquifer system (Tomaszewski 1996). The sources of the saltwater are nearby the St. Gabriel salt dome and Darrow salt dome (Bray and Hanor 1990). The project focuses on mitigating saltwater intrusion in the “1,500-foot” sand aquifer.

**Figure 1:** The study area of the “1,500-foot” sand aquifer in the Baton Rouge area, Louisiana. The contour lines represent the saltwater concentration (%) distribution at the beginning of 2005.

The study area shown in Figure 1 is the “1,500-foot” sand aquifer, where the extent of the saltwater intrusion was predicted at the beginning of year 2005. There are three major groundwater production centers in this area, which have developed a large depression cone and caused saltwater intrusion from south of the Baton Rouge fault. Recent study of

groundwater modeling in this area indicated that the groundwater heads are continuously decreasing (Tsai and Li 2008a, Li and Tsai 2009, Tsai 2010), which could result in undesired chloride concentration at production wells in the future.



The objective of the study is to develop a management model using an injection-extraction approach to protect the production wells from saltwater intrusion. The idea has been actually implemented for hydraulic control to the West Coast Basin of coastal Los Angeles, California (Reichard and Johnson 2005) and was considered in Spain (Abarca et al. 2006). This study considers the joint operations of the hydraulic barrier system and the extraction system shown in Figure 1 to (i) intercept the incoming saltwater plume toward the production wells and (ii) reduce brackish water north of the fault. The injection wells align to form a hydraulic barrier to reduce saltwater movement towards the production wells. The pumping wells are placed at the pathway of the brackish water in order to remove the brackish water from the aquifer and prevent northward movement of the brackish water pushed by the hydraulic barrier system. The locations of these well pumps are fixed in this study.

## Methodology

### (1) Genetic Algorithm for Injection-Extraction Management Model

The overriding objective of the management model is to minimize the total amount of injected and extracted water as follows

$$\min_{\substack{z_{i,n}^R \in \{0,1\}, q^R \\ z_{j,n}^P \in \{0,1\}, q^P}} \sum_i \sum_n z_{i,n}^R q^R \Delta t_n + \sum_j \sum_n z_{j,n}^P q^P \Delta t_n, \quad (1)$$

The range of injection and extraction rates is constrained by

$$\begin{aligned} 0 &\leq q^R \leq q_{\max}^R \\ 0 &\leq q^P \leq q_{\max}^P \end{aligned}, \quad (2)$$

where  $q^R$  and  $q^P$  are the injection rate and the extraction rate, respectively.  $q_{\max}^R$  and  $q_{\max}^P$  are the maximum injection rate and extraction rate, respectively.  $z_{i,n}^R$  and  $z_{j,n}^P$  are the scheduling binary variables for spatial and temporal allocation of the pump rates at injection site  $i$ , pumping site  $j$ , at time period  $n$ .  $\Delta t_n$  is the time interval for the period  $n$ . To reduce operation complexity, this study searches for optimal constant injection rate and constant extraction rate and optimal operation schedule to determine well pump activities.

The concentration at the Lula Avenue pumping center (see Lula wells in Figure 1) is constrained by the maximum permissible level (MPL):

$$C(\mathbf{x} = \mathbf{x}_{Lula}, t \in [t_0, t_T]; z_{i,n}^R, q^R, z_{j,n}^P, q^P) \leq C_{MPL}, \quad (3)$$

where  $C$  is the predicted concentration by the simulation models,  $C^{tar}$  is the maximum permissible level (MPL) of concentration,  $\mathbf{x}_{Lula}$  is the location of Lula wells,  $t_0$  is the starting time of remediation horizon, and  $t_T$  is the ending time of the remediation horizon. The concentration in the remediation area is also constrained by the MPL:

$$C(\mathbf{x} \in \Omega_R, t = t_T; z_{i,n}^R, q^R, z_{j,n}^P, q^P) \leq C_{MPL}, \quad (4)$$

where  $\Omega_R$  is the domain of remediation area (see Figure 1). The joint operations of hydraulic barrier and extraction systems present a mixed integer nonlinear programming (MINLP) problem, which involves the ground water model and transport model. This study employs a genetic algorithm (GA) with binary chromosomes to search for optimal pump rates as well as optimal binary values of scheduling variables. Using the GA, the constraints are moved as the penalty terms to the objective function. Then, a multiobjective function is formulated:

$$\begin{aligned}
& \min_{\substack{z_{i,n}^R \in \{0,1\}, q^R \\ z_{j,n}^P \in \{0,1\}, q^P}} w_1 \left( \sum_i \sum_n z_{i,n}^R q^R \Delta t_n + \sum_j \sum_n z_{j,n}^P q^P \Delta t_n \right) + \\
& w_2 \int_{t_0}^{t_T} \max \left[ C(\mathbf{x} = \mathbf{x}_{Lula}, t; z_{i,n}^R, q^R, z_{j,n}^P, q^P) - C_{MPL}, 0 \right] dt +, \\
& w_3 \int_{\Omega_R} \max \left[ C(\mathbf{x}, t = t_T; z_{i,n}^R, q^R, z_{j,n}^P, q^P) - C_{MPL}, 0 \right] d\mathbf{x}
\end{aligned} \tag{5}$$

where  $w_1$ ,  $w_2$ ,  $w_3$  are the weights to reflect the priorities, which in this study are in order of minimizing the concentration violation at Lula wells, minimizing the concentration violation in the remediation area, and minimizing the total amount of water injected and extracted.

## (2) Concentration Prediction using Bayesian Model Averaging under Uncertainty of Head Boundary Values and Variograms for Hydraulic Conductivity

The optimized joint operations are subject to the uncertainty of model structure that can cause large constraint violations. To assess the robustness of the optimized operations, this study introduces the Bayesian model averaging (BMA) (Hoeting et al. 1999) to obtain the predicted concentrations to evaluate the violations at Lula wells and in the remediation area.

Let  $\mathbf{M} = \{\mathbf{M}^{(p)}; p = 1, 2, \dots\}$  be a set of saltwater intrusion simulation models based on different boundary values of ground water heads. Each simulation model may have different variogram models to estimate hydraulic conductivity, which is denoted as  $\boldsymbol{\theta} = \{\boldsymbol{\theta}_q^{(p)}; q = 1, 2, \dots\}$ . Given data  $\mathbf{D}$ , the expectation and covariance of chloride concentrations using multiple models can be obtained as follows:

$$E(\mathbf{C} | \mathbf{D}) = \sum_p \sum_q E(\mathbf{C} | \mathbf{M}^{(p)}, \boldsymbol{\theta}_q^{(p)}, \mathbf{D}) \Pr(\boldsymbol{\theta}_q^{(p)} | \mathbf{M}^{(p)}, \mathbf{D}) \Pr(\mathbf{M}^{(p)} | \mathbf{D}), \tag{6}$$

$$\begin{aligned}
\text{Cov}(\mathbf{C} | \mathbf{D}) = & E_M E_\theta \left[ \text{Cov}[\mathbf{C} | \mathbf{M}^{(p)}, \boldsymbol{\theta}_q^{(p)}, \mathbf{D}] \right] + E_M \text{Cov}_\theta \left[ E[\mathbf{C} | \mathbf{M}^{(p)}, \boldsymbol{\theta}_q^{(p)}, \mathbf{D}] \right] \\
& + \text{Cov}_M E_\theta \left[ E[\mathbf{C} | \mathbf{M}^{(p)}, \boldsymbol{\theta}_q^{(p)}, \mathbf{D}] \right],
\end{aligned} \tag{7}$$

where  $E_M E_\theta \left[ \text{Cov}[\mathbf{C} | \mathbf{M}^{(p)}, \boldsymbol{\theta}_q^{(p)}, \mathbf{D}] \right]$  is the within-covariance of concentration,  $E_M \text{Cov}_\theta \left[ E[\mathbf{C} | \mathbf{M}^{(p)}, \boldsymbol{\theta}_q^{(p)}, \mathbf{D}] \right]$  is the covariance of concentration due to different variogram models in simulation models, and  $\text{Cov}_M E_\theta \left[ E[\mathbf{C} | \mathbf{M}^{(p)}, \boldsymbol{\theta}_q^{(p)}, \mathbf{D}] \right]$  is the covariance of concentration due to different simulation models.  $\Pr(\mathbf{M}^{(p)} | \mathbf{D})$  is the posterior probability of simulation model  $p$  and  $\Pr(\boldsymbol{\theta}_q^{(p)} | \mathbf{M}^{(p)}, \mathbf{D})$  is the posterior probability of variogram model  $q$  used in simulation model  $p$ .

The likelihood value,  $\Pr(\mathbf{D} | \mathbf{M}^{(p)}, \boldsymbol{\theta}_q^{(p)})$ , is needed in order to calculate the posterior model probabilities and is approximated using the Bayesian information criterion (BIC) (Raftery 1995; Madigan et al. 1996):  $\Pr(\mathbf{D} | \mathbf{M}^{(p)}, \boldsymbol{\theta}_q^{(p)}) \approx \exp\left(-\frac{1}{2} \text{BIC}_q^{(p)}\right)$ , where the BIC is

$$\text{BIC}_q^{(p)} = -2 \ln \Pr(\mathbf{D} | \mathbf{M}^{(p)}, \boldsymbol{\theta}_q^{(p)}, \hat{\boldsymbol{\beta}}_q^{(p)}) + m_q^{(p)} \ln L. \tag{8}$$

where  $\hat{\boldsymbol{\beta}}_q^{(p)}$  is the maximum-likelihood estimated unknown parameters,  $m_q^{(p)}$  is the dimension of  $\hat{\boldsymbol{\beta}}_q^{(p)}$ , and  $L$  is the size of the data  $\mathbf{D}$ . In this study,  $\boldsymbol{\beta}_q^{(p)}$  refers to the data weighting coefficients in the GP methods used to estimate hydraulic conductivity (Tsai 2006).

Therefore, one can assess the constraint violations by using the BMA expectation for concentration prediction as follows

$$\begin{aligned} \min_{\substack{z_{i,n}^R \in \{0,1\}, q^R \\ z_{j,n}^P \in \{0,1\}, q^P}} \quad & w_1 \left( \sum_i \sum_n z_{i,n}^R q^R \Delta t_n + \sum_j \sum_n z_{j,n}^P q^P \Delta t_n \right) + \\ & w_2 \int_{t_0}^{t_T} \max \left[ C_{BMA}(\mathbf{x} = \mathbf{x}_{Lula}, t; z_{i,n}^R, q^R, z_{j,n}^P, q^P) - C_{MPL}, 0 \right] dt +, \\ & w_3 \int_{\Omega_r} \max \left[ C_{BMA}(\mathbf{x}, t = t_T; z_{i,n}^R, q^R, z_{j,n}^P, q^P) - C_{MPL}, 0 \right] d\mathbf{x} \end{aligned} \quad (9)$$

where  $C_{BMA}$  is obtained by Eq. (6) using the variance window (Tsai and Li 2008a,b), which is

$$C_{BMA} = \frac{\sum_p \sum_q E(C | M^{(p)}, \theta_q^{(p)}, \mathbf{D}) \exp\left(-\frac{1}{2} \alpha \Delta \text{BIC}_q^{(p)}\right)}{\sum_p \sum_q \exp\left(-\frac{1}{2} \alpha \Delta \text{BIC}_q^{(p)}\right)}. \quad (10)$$

This optimization problem is very time-consuming because it involves many simulation models and variogram models in the management model.

## Principal Findings and Significance

### (1) Model Uncertainty

To assess the robustness of the optimized joint operations under this uncertainty, five groundwater flow models are created, which have 0%,  $\pm 10\%$ , and  $\pm 20\%$  changes of the predetermined head boundary values over the entire boundary. Moreover, the uncertainty in experimental variograms for hydraulic conductivity is also considered. Three variogram models (exponential (EXP), spherical (SPH) and Gaussian (Gau) models) are used. A total of 15 simulation models are developed. Detail information can be found in Tsai (2010).

### (2) No-Action Scenario

Without the hydraulic barrier and extraction systems (no-action scenario), the chloride concentration is slowly moving northward toward the Lula wells. The concentration distributions predicted by the best model (Gau+0%) and the BMA are similar. Both confirm that the 2.5% isochlor does not reach the Lula wells within the management period. The variances of the predicted chloride concentrations due to different variogram models in individual simulation models are much smaller than the variances due to different simulation models. Given the similar weights of the variogram models in the best and second best simulation models, this indicates similar concentration predictions made by different variogram models within a simulation model. However, different simulation models due to head boundary uncertainty exhibit relatively large differences in concentration predictions.

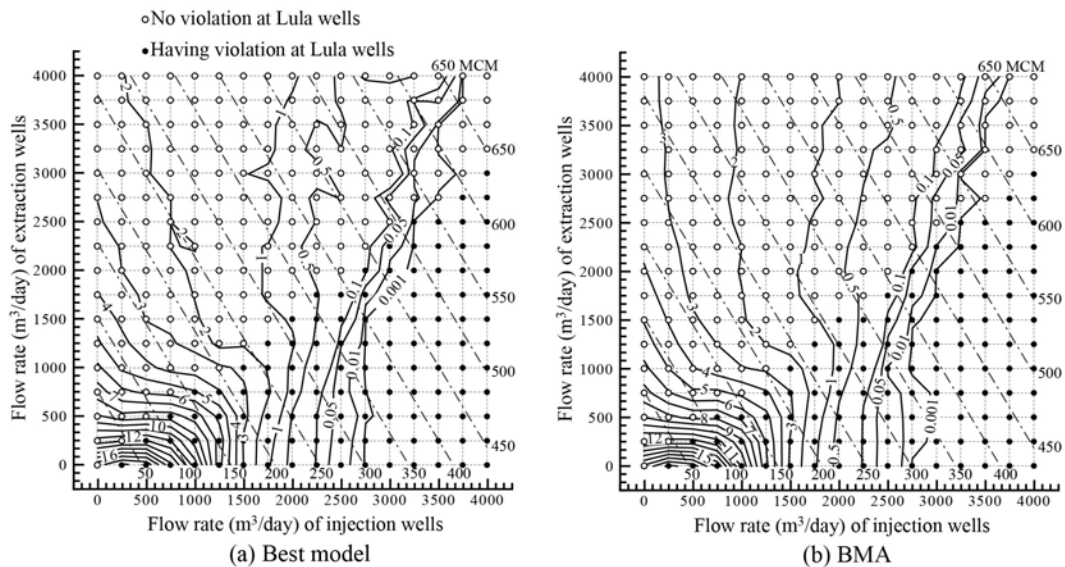
### (3) Joint Operations with Well Pumps Active All Time

By considering the well pumps of the hydraulic barrier and extraction systems active all the time, the injection rates and extraction rates are increased systematically from the no-action scenario to illustrate the impact of the systems on the saltwater intrusion. A viable remedial action is defined for the case where the sum of violations (the second term in Eq. (5)) at the Lula wells is zero during the management period. Otherwise, the remedial action is not acceptable. For example, the no-action scenario is a viable scenario. A viable remediation scenario

represents the minimum requirement for an operation action because any actions that cause the Lula wells to be contaminated are not acceptable. Moreover, optimized operations would become very expensive if one was restricted to zero violation in the remediation area at the end of the management period. This study relaxes this restriction for practical purposes and considers a remedial action acceptable with a violation of less than 0.001 for the third term in Eq. (5). The threshold for this small acceptable violation is subjective and depends on decision makers.

Figure 2 shows the matrix of scenarios without violation (open circles) and with violation (filled circles) at Lula wells, created by enumerating the combinations of different injection rates and extraction rates using the best model (Gau+0) and the BMA. The injection and extraction rates are operated full time for 15 years. The total amount of pumped and injected water in million cubic meters (MCM) is plotted in Figure 2, which is the potential (maximum) amount of water the systems need to deal with. For example, an injection rate of 3250 m<sup>3</sup>/day and extraction rate of 2750 m<sup>3</sup>/day operate a potential amount of water of 537 MCM. Figure 2 also shows the contour lines of the sum of violations in the remediation area at the end of the 15-year management period. Based on the information in Figure 2, one can draw the following observations: (1) Actions with low injection rates with low extraction rates are unacceptable because they cannot cleanup the remediation area even though they are viable actions to the Lula wells. (2) High injection rates with low extraction rates are unacceptable because the hydraulic barrier system pushes northward and end up brackish water in the Lula wells. This can result in zero violation in the remediation area at the end of the management period. (3) Low injection rates with high extraction rates are generally not acceptable remedial actions. While no violation occurs in the Lula wells, the extraction system enlarges and deepens the depression core, induces more saltwater intrusion northward, and causes high violations in the remediation area. (4) Using higher injection rates and higher extraction rates is likely to achieve the goal of cleaning the brackish water in the remediation area without jeopardizing the Lula wells.

Figure 2: Matrix of actions with different injection and extraction rates using (a) the best model and (b) the BMA with the variance window. Open circle represents a viable action. Filled circle represents an unacceptable action. Solid line represents the sum of violations in the remediation area. The dotted-dashed line represents the total amount water injected and pumped in million cubic meters (MCM).



#### (4) Joint Operation Optimization

To reduce the complexity of the management model and increase the efficiency of searching for the optimal operation, the operation considers all injection wells and all pumping wells are active or inactive on a monthly basis for 15 years. Therefore, there are 180 scheduling variables for the injection wells and 180 scheduling variables for the pumping wells. A micro-GA solver (Carroll 1996) is used to minimize the objective function. The population in the micro-GA is five, the uniform crossover probability is 0.5, and the mutation probability is 0.02. The tournament selection strategy is used. The maximum number of generations for each GA run is 200. These GA parameters are suggested in the solver (Carroll 1996). The maximum injection rate ( $q_{\max}^R$ ) and extraction rate ( $q_{\max}^P$ ) in the GA are set to  $4,000 \text{ m}^3/\text{day}$ . The injection rate and extraction rate are given the same length of 12 bits in the binary chromosomes. To prioritize the multiple objections, it sets  $w_1 = 10^{-11}$ ,  $w_2 = 100$ ,  $w_3 = 1.0$  for the objective function. The length of a binary chromosome is 384 bits. To obtain the fitness of each chromosome (one possible operation solution), the 12 simulation models are executed together to calculate the BMA concentrations. The computation is extremely extensive.

Again, the author recognizes the possibility of considering individual operations of the well pumps on the monthly basis. This will reduce operation costs by increasing flexibility in well operations in the management model. However, this will result in 3,600 scheduling variables for the injection wells and 2,160 scheduling variables for the pumping wells. This complicated optimization problem is avoided in this study.

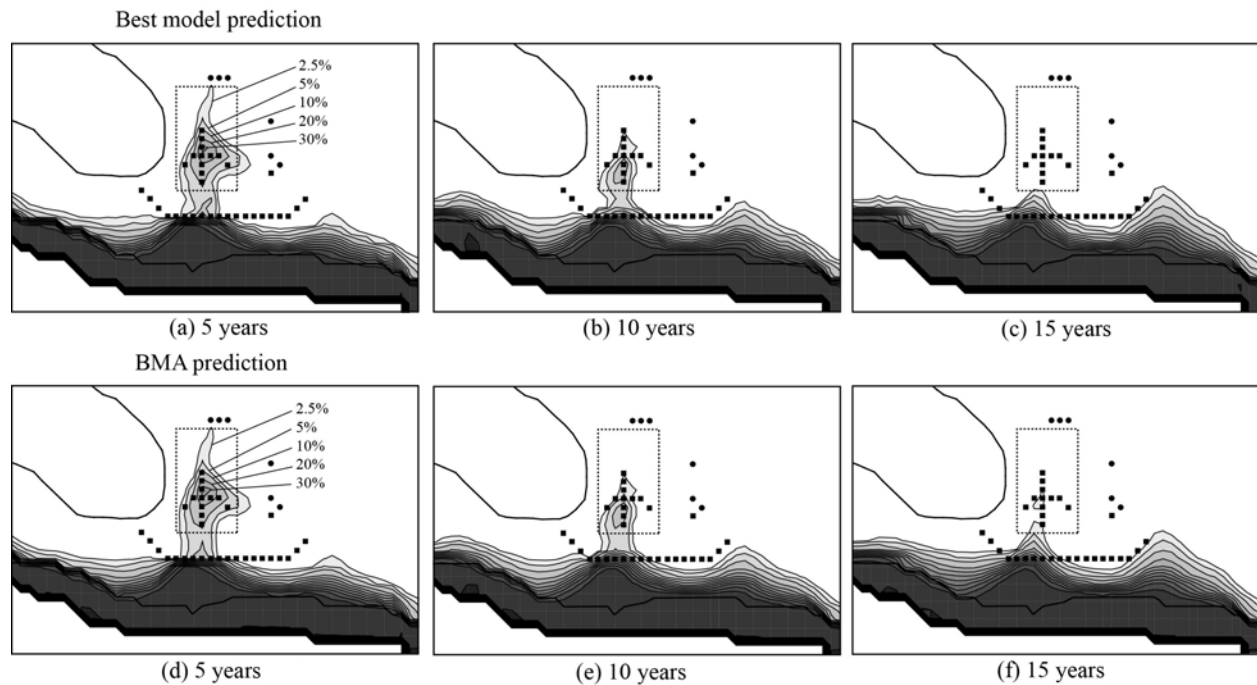
Two management models are compared to show the difference if model uncertainty is not considered. The first management model only considers the best model (Gau+0%). The second management model uses the BMA to predict concentration based on the 12 simulation models. Again, for the no-action scenario, two management models show no violation at Lula wells. However, the sum of violations in the remediation area is very high. If considering the best model only in the management model, the GA obtains the optimal injection rate to be  $3,217 \text{ m}^3/\text{day}$  and the optimal extraction rate to be  $2,448 \text{ m}^3/\text{day}$ . No violation occurs at the Lula wells and in the remediation area at the end of the management period. The total amount of water injected and pumped is 331 MCM. Comparing to the same injection and extraction rates in Figure 2, the management model significantly reduces concentration violations and the amount of water to deal with compared to pumping all wells all 15 years. Figure 3(a)-(c) shows the chloride concentration predictions at 5-years, 10-years, and 15-years. However, if model uncertainty is considered, one can test if the optimal operation from the best model is acceptable by re-evaluating the sum of violations using the BMA concentrations. This optimal solution produces noticeable violation in the remediation area at the end of the management period. The violation can be seen in Figure 3(f) at the end of the 15 years based on the BMA prediction. The violation is expected because the optimal operation from the best model neglects other good models and gives a biased solution.

Using the BMA to predict chloride concentration in the management model, the GA increases the optimal injection rate to  $3,729 \text{ m}^3/\text{day}$  and increases the optimal extraction rate to  $3,012 \text{ m}^3/\text{day}$  in order to reduce the violations from other models. The increased injection and extracting rates due to considering model uncertainty reflect the need of “overdesigning” the strategy to insure reliability (Wagner and Gorelick 1987). The optimal operation using the BMA presents an acceptable solution because no violation occurs at the Lula wells and the sum of violations in the remediation area is less than 0.001. The total amount of water injected and

pumped is 371 MCM. The optimal operation using BMA is also tested if it is an acceptable solution for the best model. After re-evaluating the sum of violations, the optimal operation using the BMA also works for the best model. The variances of chloride concentration at the end of 15 years due to different variogram models in individual simulation models are much smaller than the variances due to different simulation models.

Using the BMA prediction in the management model does not prevent other models from violation. An exhaustive management model can consider the constraints that include concentration predictions from individual models, but this would result in a very expensive management policy in terms of the total amount of injected and pumped water in order to satisfy all models. Moreover, this way would exaggerate the influence from insignificant models. With BMA, one can avoid this problem while considering the model uncertainty.

Figure 3: Isochlors predicted by the best model (Gau+0%) at (a) 5 years, (b) 10 years, and (c) 15 years, and by the BMA with the variance window at (d) 5 years, (e) 10 years, and (f) 15 years, given the optimal joint operation, injection rate = 3,217 m<sup>3</sup>/day and extraction rate = 2,448 m<sup>3</sup>/day, from the best model.



## Conclusions

[1] Groundwater management is far more difficult and complex because of model structure uncertainty. Uncertain model structure often results in multiple possible simulation models. Management plans under the consideration of a single simulation model tend to bias optimized operations. To alleviate the biasedness, a reliable groundwater management model should take into account the predictions from multiple simulation models.

[2] Bayesian model averaging (BMA) has been shown to be capable of integrating multiple models for prediction in the management model. Optimized operations based on the BMA predictions show more reliable management outcomes than those from one simulation model. However, the optimized operation is more expensive in order to reduce constraint violations elevated by considering many models.

[3] The study has demonstrated the importance of considering the model structure uncertainty in a real-world case study. Using the best model underestimates the optimized injection rate and extraction rate for the hydraulic barrier and extraction systems. Using the BMA prediction for chloride concentration, the optimized injection and extraction rates increase to reduce the concentration violation in the remediation area.

[4] The study also demonstrates the importance of using the variance window for uncertainty analysis in the management model. Using Occam's window literally accepts only the best model and neglects model uncertainty. However, the incorporation of more simulation models in the management model, as suggested by the variance window, could result in more expensive operations in order to reduce additional constraint violations created by the additional simulation models. A further investigation should be conducted to understand the impact of the size of the variance window with respect to Occam's window.

## References

- Abarca, E., E. Vazquez-Sune, J. Carrera, B. Capino, D. Gamez, and F. Batlle. (2006). Optimal design of measures to correct seawater intrusion. *Water Resources Research* 42(9), W09415, doi:10.1029/2005WR004524.
- Bense, V. F., and M. A. Person. (2006). Faults as conduit-barrier systems to fluid flow in siliciclastic sedimentary aquifers. *Water Resources Research* 42(5), W05421, doi:10.1029/2005WR004480.
- Bray, R. B., and J. S. Hanor. (1990). Spatial variations in subsurface pore fluid properties in a portion of Southeast Louisiana: Implications for regional fluid flow and solute transport. *Transactions - Gulf Coast Association of Geological Societies* XL(53-64).
- Carroll, D. L. (1996). Chemical laser modeling with genetic algorithms. *AIAA Journal* 34(2), 338-346.
- Hoeting, J. A., D. Madigan, A. E. Raftery, and C. T. Volinsky. (1999). Bayesian model averaging: A tutorial. *Statistical Science* 14(4), 382-401.
- Li, X., and F. T.-C. Tsai. (2009). Bayesian model averaging for groundwater head prediction and uncertainty analysis using multimodel and multimethod. *Water Resources Research*, 45, W09403, doi:10.1029/2008WR007488.
- Madigan, D., S. A. Andersson, M. D. Perlman, and C. T. Volinsky. (1996). Bayesian model averaging and model selection for Markov equivalence classes of acyclic digraphs. *Communications in Statistics-Theory and Methods* 25(11), 2493-2519.
- Raftery, A. E. (1995). Bayesian model selection in social research. *Sociological Methodology* 25, 111-163.
- Reichard, E. G., and T. A. Johnson. (2005). Assessment of regional management strategies for controlling seawater intrusion. *Journal of Water Resources Planning and Management-ASCE* 131(4), 280-291.
- Tomaszewski, D. J. (1996). Distribution and movement of saltwater in aquifers in the Baton Rouge area, Louisiana, 1990-1992. Louisiana Department of Transportation and Development Water Resources Technical Report No. 59.
- Tsai, F. T.-C. (2006). Enhancing random heterogeneity representation by mixing the kriging method with the zonation structure. *Water Resources Research* 42(8), W08428, doi:08410.01029/02005WR004111.

- Tsai, F. T.-C., Bayesian Model Averaging Assessment on Groundwater Management under Model Structure Uncertainty, *Stochastic Environmental Research and Risk Assessment*, 24(6), 845-861, 2010.
- Tsai, F. T.-C., and X. Li. (2008a). Inverse groundwater modeling for hydraulic conductivity estimation using Bayesian model averaging and variance window. *Water Resources Research* 44(9), W09434, doi:10.1029/2007WR006576.
- Tsai, F. T.-C., and X. Li. (2008b). Multiple parameterization for hydraulic conductivity identification. *Ground Water* 46(6), 851-864.
- Wagner, B. J., and S. M. Gorelick. (1987). Optimal groundwater quality management under parameter uncertainty. *Water Resources Research* 23(7), 1162-1174.

## **Publications**

### **1. Articles in Refereed Scientific Journals**

- Tubbs, K. R., and F. T.-C. Tsai. (2010). GPU Accelerated Lattice Boltzmann Model for Shallow Water Flow and Mass Transport, *International Journal for Numerical Methods in Engineering*, DOI: 10.1002/nme.3066.
- Tsai, F. T.-C. and X. Li. (2010). Reply to Comment on "Inverse Groundwater Modeling for Hydraulic Conductivity Estimation Using Bayesian Model Averaging and Variance Window" by Ye, M., D. Liu, S.P. Neuman, and P.D. Meyer, *Water Resources Research*. doi:10.1029/2009WR008591.
- Servan-Camas, B., and F. T.-C. Tsai. (2010). Two-Relaxation-Time Lattice Boltzmann Method for Anisotropic Dispersive Henry Problem. *Water Resources Research*. doi:10.1029/2009WR007837.
- Tubbs, K. R., and F. T.-C. Tsai (2009). Multilayer Shallow Water Flow using Lattice Boltzmann Model with High Performance Computing. *Advances in Water Resources*, 32(11), 1767-1776.
- Li, X., and F. T.-C. Tsai.(2009). Bayesian Model Averaging for Groundwater Head Prediction and Uncertainty Analysis Using Multimodel and Multimethod. *Water Resources Research*, 45, W09403. doi:10.1029/2008WR007488.
- Tsai, F. T.-C., Bayesian Model Averaging Assessment on Groundwater Management under Model Structure Uncertainty, *Stochastic Environmental Research and Risk Assessment*, 24(6), 845-861, 2010.

### **2. Book Chapter**

- Tsai, F. T.-C. and W. W-G. Yeh. (2010). Chapter 7: Model Calibration and Parameter Structure Identification in Characterization of Ground Water Systems, in *Ground Water Management Manual* (M. Aral and S. Taylor ed.) American Society of Civil Engineers. Accepted.

### **3. Dissertations**

- Kevin R. Tubbs, 2010, Ph.D. Dissertation "Lattice Boltzmann Modeling for Shallow Water Equations Using High Performance Computing, Engineering Science Program, College of Engineering, Louisiana State University, Baton Rouge, Louisiana, 128 pages.

### **4. Water Resources Research Institute Reports**

- Frank Tsai, 2009, Saltwater Intrusion Management with Conjunctive Use of Surface Water and Ground Water, Louisiana Water Resources Research Institute, Louisiana State University, Baton Rouge, Louisiana, 10 pages. (USGS 104G)

- Frank Tsai, 2009, Electrical Resistivity Tomography (ERT) Laboratory Experiments on Saltwater Encroachment Tracking and Modeling in Saturated Heterogeneous Sediment, Louisiana Water Resources Research Institute, Louisiana State University, Baton Rouge, Louisiana, 10 pages. (USGS 104B)

### **5. Conference Proceedings**

- Tsai, F. T.-C. (2010). A Co-Generalized Parameterization Method for Hydraulic Conductivity Estimation, World Water & Environmental Resources Congress, Providence, Rhode Island, May 16-20, 2010.
- Tsai, F. T.-C. (2010). Multimodel Approach for Groundwater Model Calibration, Prediction, and Application, World Water & Environmental Resources Congress, Providence, Rhode Island, May 16-20, 2010. (invited)

### **6. Other Publications (Abstract/Presentations)**

- Tsai, F. T.-C. (2010). Data Fusion using Co-Generalized Parameterization: Hydraulic Conductivity Estimation, 2010 Western Pacific Geophysics Meeting, 22–25 June 2010, Taipei, Taiwan
- Tsai, F. T.-C. (2010). Hierarchical Bayesian Model Averaging for Groundwater Multimodel Prediction and Management under Uncertainty, 2010 Western Pacific Geophysics Meeting, 22–25 June 2010, Taipei, Taiwan
- Tsai, F. T.-C. (2010). A Co-Generalized Parameterization Method for Hydraulic Conductivity Estimation, World Water & Environmental Resources Congress, Providence, Rhode Island, May 16-20, 2010.
- Tsai, F. T.-C. (2010). Multimodel Approach for Groundwater Model Calibration, Prediction, and Application, World Water & Environmental Resources Congress, Providence, Rhode Island, May 16-20, 2010. (invited)

### **7. Student Support**

- Kevin R. Tubbs, PhD, Spring 2010 (Graduated)

# Scale-dependent behavior and modeling of dissolved oxygen in coastal Louisiana rivers

## Basic Information

<b>Title:</b>	Scale-dependent behavior and modeling of dissolved oxygen in coastal Louisiana rivers
<b>Project Number:</b>	2010LA73B
<b>Start Date:</b>	3/1/2010
<b>End Date:</b>	2/28/2011
<b>Funding Source:</b>	104B
<b>Congressional District:</b>	6th
<b>Research Category:</b>	Water Quality
<b>Focus Category:</b>	Water Quantity, Solute Transport, Models
<b>Descriptors:</b>	
<b>Principal Investigators:</b>	Zhi-Qiang Deng

## Publications

1. Deng, Z.-Q., Jung, H.-S., and Ghimire, B. (2010). "Effect of channel size on solute residence time distributions in rivers." *Advances in Water Resources*, 33 (9), 1118–1127, DOI: 10.1016/j.advwatres.2010.06.016.
2. Ghimire, B., and Deng, Z.-Q. (2011). "Event flow hydrograph-based method for shear velocity estimation." *Journal of Hydraulic Research*, 49(2), 272-275.
3. Ghimire, B., and Deng, Z.-Q. (2011). "Event Flow Hydrograph-Based Method for Modeling Sediment Transport." *ASCE Journal of Hydrologic Engineering* (in review).
4. Zahraeifard, V. and Deng, Z. (2011). "VART Model-Based Method for Estimation of Instream Dissolved Oxygen and Reaeration Coefficient." *ASCE Journal of Environmental Engineering* (in review)

# Scale-Dependent Behavior and Modeling of Dissolved Oxygen in Coastal Louisiana Rivers

## BASIC INFORMATION

<b>Title:</b>	Scale-Dependent Behavior and Modeling of Dissolved Oxygen in Coastal Louisiana Rivers
<b>Project Number:</b>	2010LA73B
<b>Start Date:</b>	3/01/2010
<b>End Date:</b>	2/28/2011
<b>Funding Source:</b>	104B
<b>Congressional District:</b>	6th
<b>Research Category:</b>	Water Quality
<b>Focus Category:</b>	Water Quantity, Solute Transport, Models
<b>Descriptors:</b>	Dissolved Oxygen, Scale-dependent Behavior, Streams
<b>Principal Investigators:</b>	Zhi-Qiang Deng

## PUBLICATIONS

1. Deng, Z.-Q., Jung, H.-S., and Ghimire, B. (2010). "Effect of channel size on solute residence time distributions in rivers." *Advances in Water Resources*, 33 (9), 1118–1127, DOI: 10.1016/j.advwatres.2010.06.016.
2. Ghimire, B., and Deng, Z.-Q. (2011). "Event flow hydrograph-based method for shear velocity estimation." *Journal of Hydraulic Research*, 49(2), 272-275.
3. Ghimire, B., and Deng, Z.-Q. (2011). "Event Flow Hydrograph-Based Method for Modeling Sediment Transport." *ASCE Journal of Hydrologic Engineering* (in review).
4. Zahraeifard, V. and Deng, Z. (2011). "VART Model-Based Method for Estimation of Instream Dissolved Oxygen and Reaeration Coefficient." *ASCE Journal of Environmental Engineering* (in review).

## RESEARCH

### Problem and Research Objectives

The dissolved oxygen variation displays a strong scale-dependent behavior. At the seasonal scale, the DO becomes low in summer and high in winter following seasonal temperature change. At event (e.g. floods) scale, DO fluctuation in coastal Louisiana rivers with fine-grained sediment is significantly affected by flood events. The seasonal variation in DO is already well known. However, the DO fluctuation in response to flood events is still poorly understood, making it impossible to quantify the uncertainty and thereby the margin of safety (MOS) involved in the DO TMDL (Total Maximum Daily Load) development. This is a critical regional and state water quality problem needing to be addressed.

The primary goal of this project is to understand the linkage between the episodic sediment resuspension and DO cycling in fine-grained coastal Louisiana rivers. The specific objective of this project is to develop an efficient and effective mathematical model for simulating scale-dependent behavior of dissolved oxygen in coastal Louisiana rivers characterized with fine-grained sediment.

### Methodology

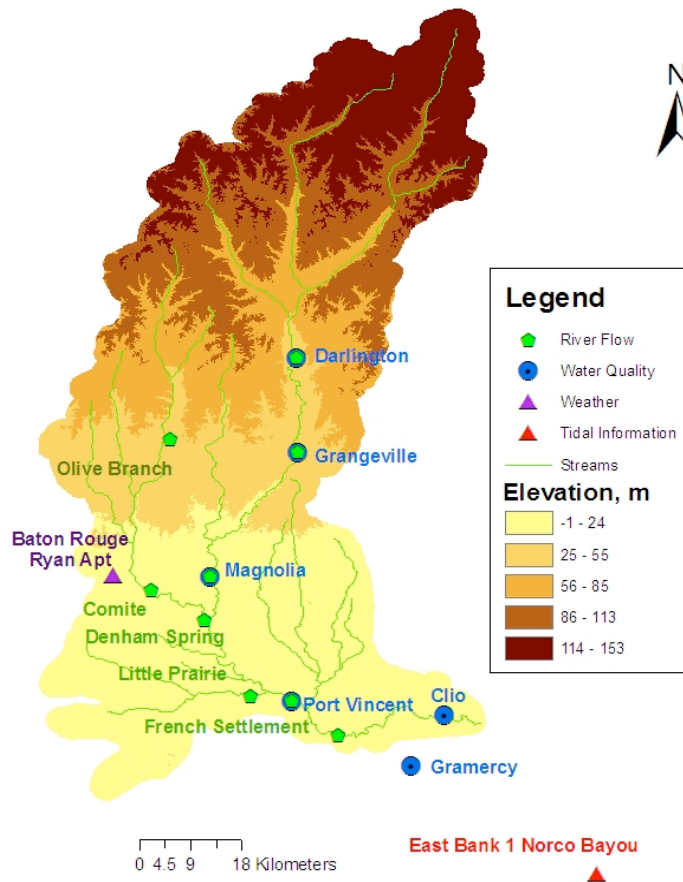


**Figure 1.** Map of the Amite River watershed.

The Lower Amite River at the Port Vincent was selected as the study site, as shown in Figure 1. The Amite River flows generally southwestward to Lake Pontchartrain estuary that is connected to the Gulf of Mexico. Therefore, the Lower Amite River is a typical coastal river with fine-grained sediment. The Lower Amite River (Subsegment 040303) is on US EPA’s 2006 Impaired Water 303(d) List because it was “not supporting” the designated use of Fish and Wildlife Propagation. The Lower Amite River is impaired for dissolved oxygen and some other nutrients such as nitrate/nitrite and total phosphorus. In order to understand the scale-dependent behavior of DO in coastal rivers, a number of mathematical models have been developed, including (1) event flow hydrograph-based method for estimation of shear velocity (see Publication 2), (2) event flow hydrograph-based method for modeling sediment resuspension (see Publication 3), (3) improved variable residence time (VART) model for simulation of instream solute transport (see Publication 1), and (4) VART-DO model for estimation of

instream dissolved oxygen and reaeration coefficient (see Publication 4). The four models are then combined to form a new model for simulation of sediment resuspension-induced scale-dependent behavior of instream DO:

$$\frac{\partial C}{\partial t} + U \frac{\partial C}{\partial x} = \frac{\partial}{\partial x} \left( E \frac{\partial C}{\partial x} \right) + \frac{A_{adv} + A_{diff}}{A} \frac{1}{T_V} (C_s - C) + K_2 (C_{sat} - C) - \Lambda C$$

where  $x$  = distance,  $t$  = time variable,  $C$  = dissolved oxygen concentration in the water column,  $C_s$  = dissolved oxygen concentration in the sediment,  $C_{sat}$  = dissolved oxygen in the saturation condition,  $U$  = flow velocity,  $E$  = dispersion coefficient,  $A_{adv.}$  = advection-dominant area of storage zone,  $A_{diff}$  = diffusion-dominant area of storage zone (defined in Paper 1),  $A$  = channel cross-sectional area,  $T_V$  = actual varying residence time of solute (defined in Paper 1),  $K_2$  = reaeration coefficient,  $\Lambda$  = sediment resuspension coefficient. The parameter  $\Lambda$  was determined using the model presented in Publication 3 while parameter  $K_2$  was determined using the model presented in Publication 4. The parameter values were calibrated using flow and DO data collected at Denham Springs (Figure 1) in 1990 by Louisiana Department of Environmental Quality (LDEQ). The calibrated model was then applied to perform continuous simulation of DO variations at the Port Vincent in January and July of 1990. The two months (January and July) represents the two extreme conditions in terms of the seasonal scale variation in DO. The modeling results are compared with observed DO data from LDEQ.

## PRINCIPAL FINDINGS AND SIGNIFICANCE

### 1. Flow Hydrograph-based Method for Shear Velocity Estimation (Paper 2)

A simple event flow hydrograph-based method is developed for determining the shear velocity during river floods. The method is based on the Saint-Venant equations, simplified for floods in mild-sloping rivers of constant channel width. Applications of the new method using published experimental data and simulated results indicate that the method is comparable with existing more complex methods in terms of accuracy but requires less input data, especially if the channel is prismatic and the flow conditions are similar to those in typical lowland rivers.

This method is particularly applicable to natural floods in relatively straight reaches of lowland rivers where the non-inertia wave approximation to the Saint-Venant equations is theoretically appropriate.

Comparisons between the new method (Equations 9 and 10 in Figure 2) and other methods against measured data are shown in Figure 2 (a - d).

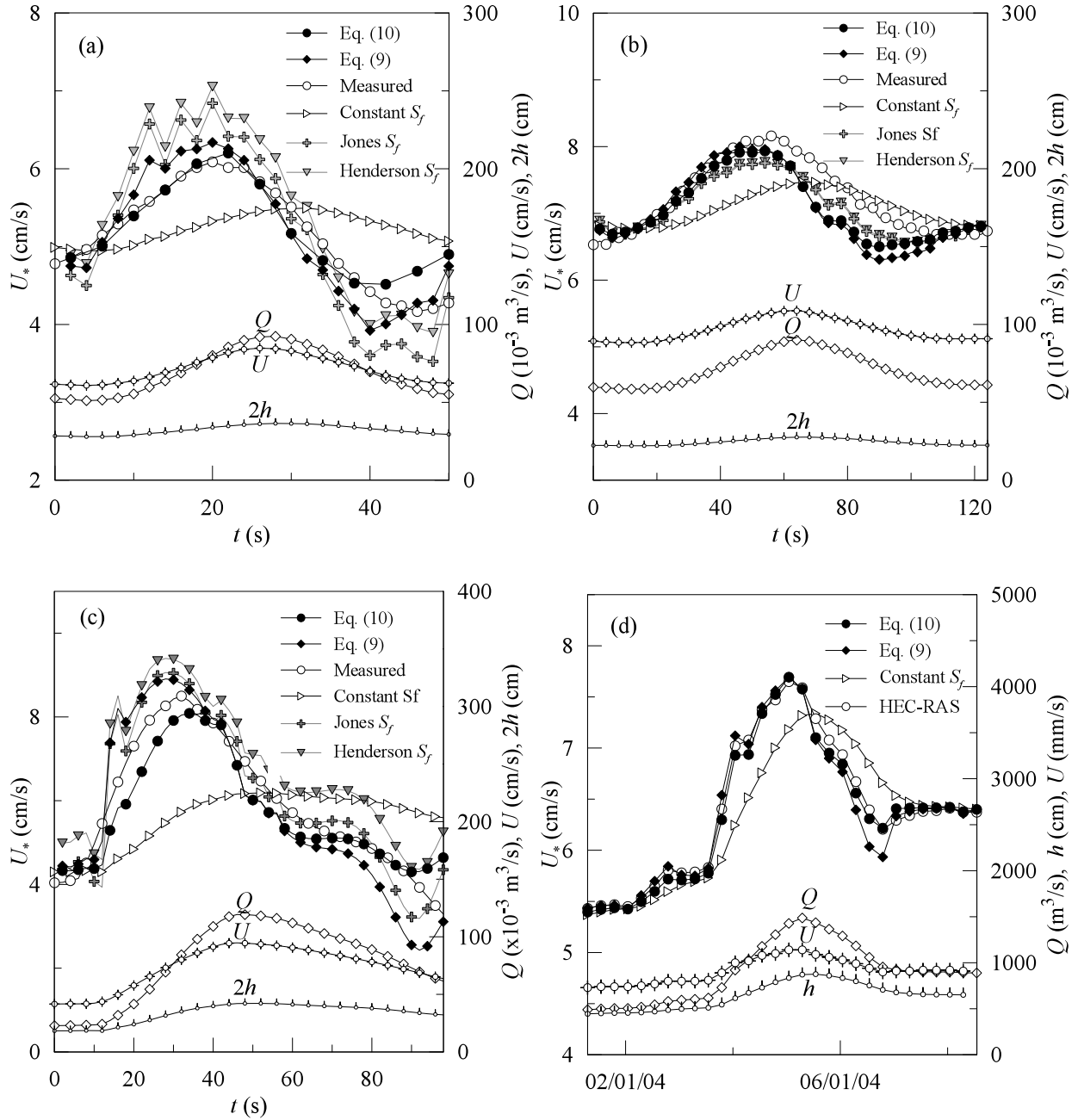


**Figure 2.** Comparison of shear velocities  $U_*$  for (a) Exp. S-15-936, (b) Exp. S30-931, (c) Exp. NS1(1), (d) HEC-RAS results for January 2004 flood of Muskingum River at McConnellsville OH. Measured values for  $Q$ ,  $U$  and  $h$  (or  $2h$ ) are also shown.

## 2. Flow Hydrograph-based Method for Modeling Sediment Resuspension (Paper 3)

- (1) Under the assumptions of equilibrium transport, uniform sediment and prismatic channel, the application of the proposed hydrograph-based method indicates that this method is comparable with more advanced numerical model such as HEC-RAS in terms of overall accuracy and gives relatively better results during rising as well as falling phases of large flood events (Figure 3). This is an encouraging result, especially as the proposed method is much simpler, less data intensive and does not require numerical computation.
- (2) This method is able to reproduce clockwise hysteresis of sediment concentration frequently observed in natural rivers (Figure 4). Obviously, this method assumes that the trends in shear stress explain the trend in sediment transport. When the sediment supply is limited or the trend in the sediment transport is independent of channel hydraulics, this method is not directly applicable.
- (3) Since the better simulation of sediment transport is achieved with improved estimates of hydrodynamic parameters such as bed shear stress or friction slopes, this method may be useful for studying the performance of sediment entrainment relations during flood events when observed data are available.
- (4) The proposed method appears to be a more practical alternative to advanced numerical models that are included in the contaminant transport modelling framework but are costly in terms of input data. With this simple yet effective tool, the need to compromise with the accuracy by resorting to uniform flow formula for simplicity during unsteady flow events is largely eliminated.

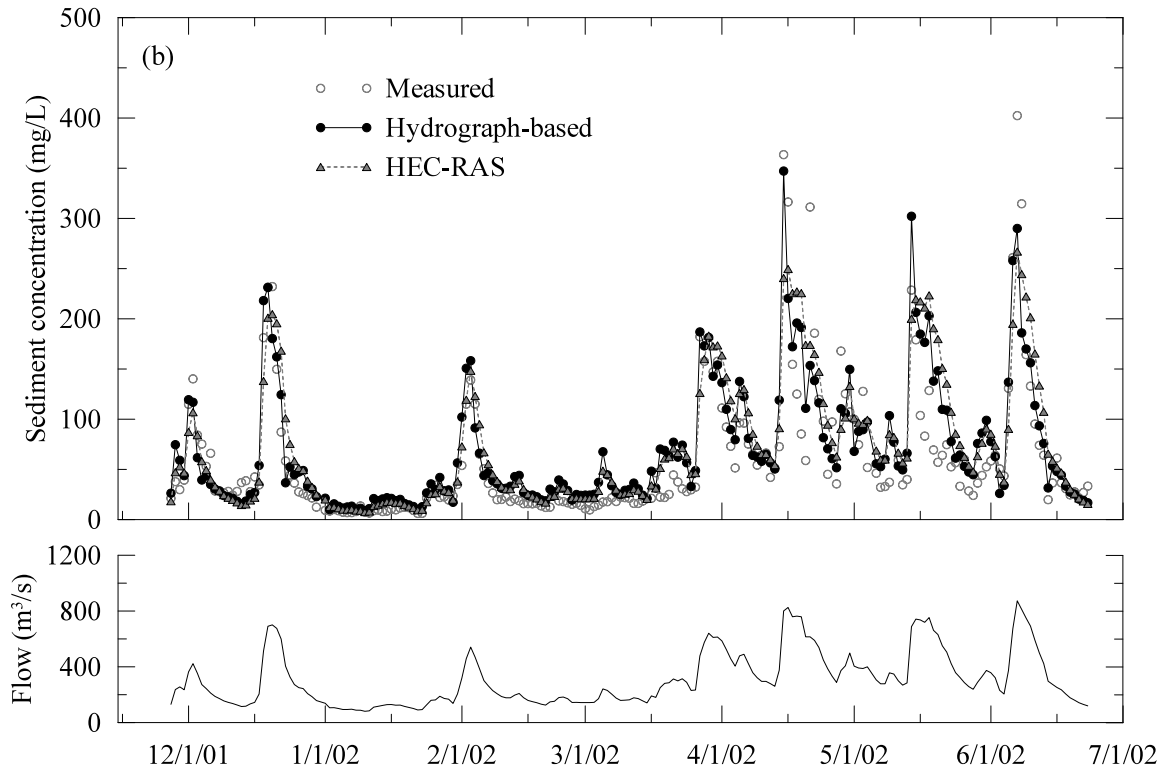


**Figure 3.** Comparison of measured and computed sediment concentrations using hydrograph-based method and HEC-RAS model at McConnelsville, OH during high flow seasons in 2002.

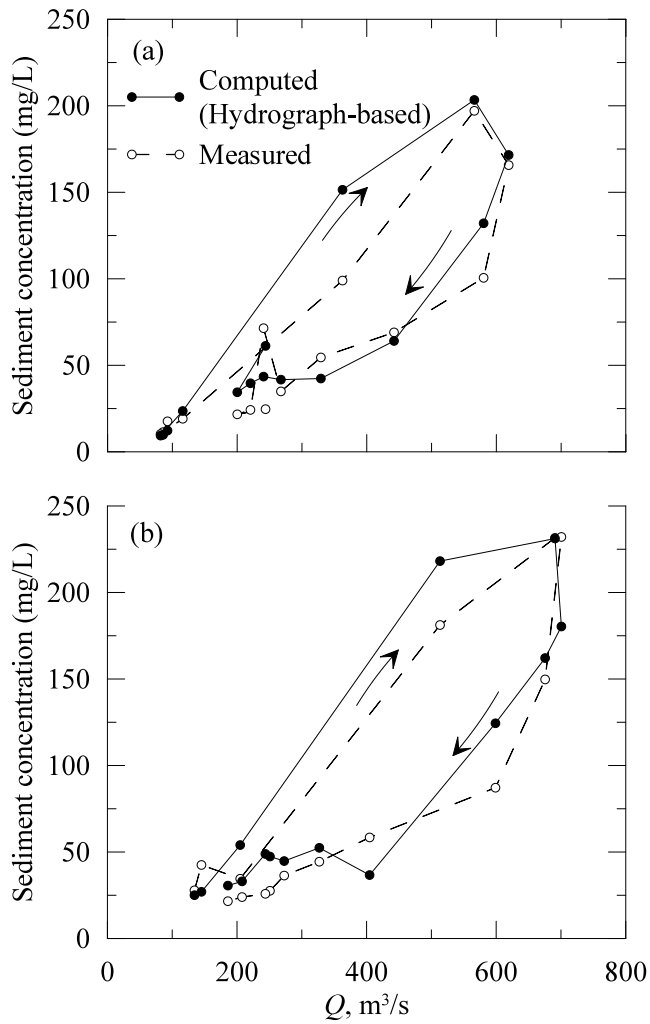


**Figure 4.** Hysteresis of sediment concentration at McConnelsville during two single peak flood events: (a) January 2001 and (b) December 2001.

### 3. VART Model-Based Method for Estimation of Instream Dissolved Oxygen (Papers 1 and 4)

- (1) The transient storage effect may significantly affect the reaeration coefficient  $K_2$  values. Storage zones can reduce  $K_2$  and RMSE (root mean squared error) values by about 30 percent. Therefore, it is important to include their effects in the DO modeling.
- (2) The dispersion mechanism is also important to DO exchange. The study showed that strong longitudinal dispersion can increase  $K_2$  values significantly. According to a sensitivity analysis, the dispersion coefficient may increase  $K_2$  value by about 50 percent and decreases RMSE by about 48 percent.
- (3) The  $K_2$  value computed using the VART-DO model may be up to 6 times greater than those obtained from existing empirical equations. The combined effects of storage zones and dispersion coefficient should be considered in the estimation of the reaeration coefficient.

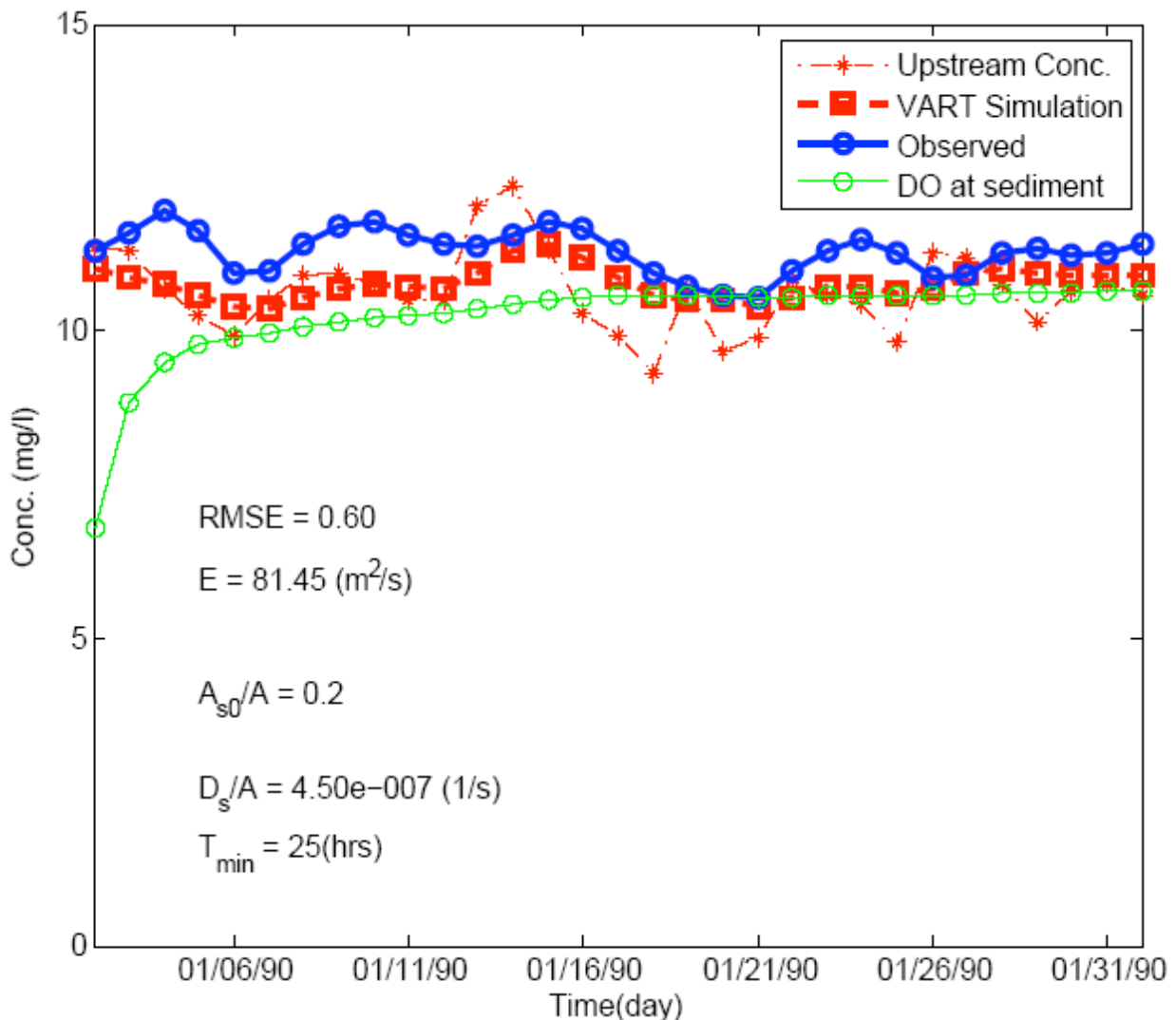


**Figure 5.** Comparison between observed and simulated DO levels in January 1990 at Port Vincent. The simulated DO concentration in bottom sediment at Port Vincent is also shown (the green line). Also included in the figure is the observed DO level at Denham Springs.

(4) The VART-DO model is capable of simulating DO variations in both water column and bottom sediment, as shown in Figures 5 and 6. This feature is particularly appealing for understanding the scale-dependent behavior of dissolved oxygen in fine-grained coastal Louisiana rivers.

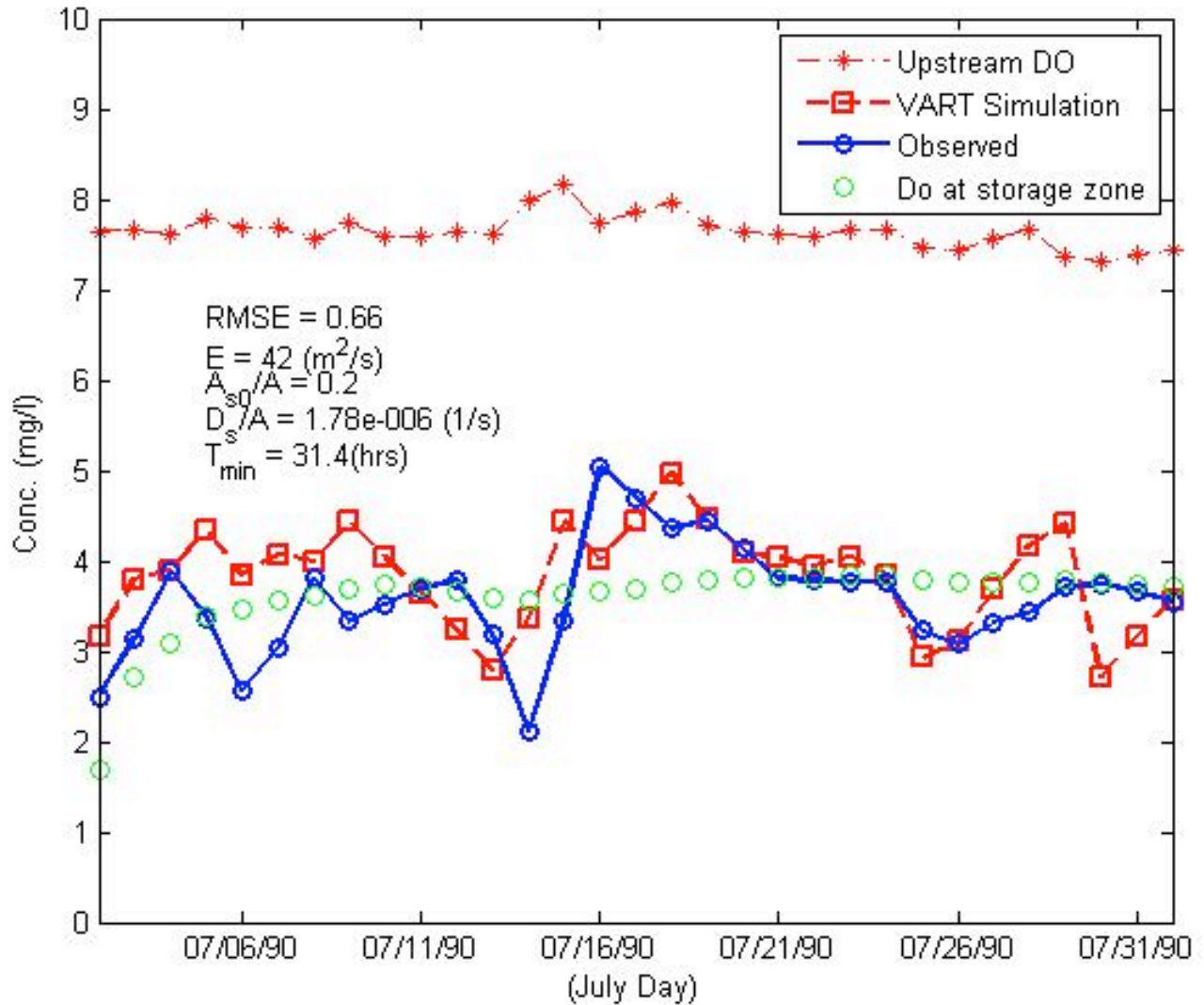


**Figure 6.** Comparison between observed and simulated DO levels in July 1990 at Port Vincent. The simulated DO concentration in bottom sediment at Port Vincent is also shown (the green circle line). Also included in the figure is the observed DO level at Denham Springs.

## **INFORMATION TRANSFER**

The findings and methods for modeling sediment resuspension-induced DO variation will be transferred to the Louisiana Department of Environmental Quality (LDEQ) for applications in TMDL developments and stream restoration.

## **STUDENT SUPPORT**

**Name of supported graduate student:** Bhuban Ghimire (Male)

**Degree Program:** Ph.D. in Water Resources

**Dissertation Title:** Characterization of Cycling-Induced Sediment-Water Interface and Exchange of Solutes in Fine-Grained Streams

**Anticipated Graduation Date:** December, 2011

## **FOLLOW-ON FUNDING**

**Title:** Remote Sensing Detection of Water Quality Indicators for Oyster Norovirus Outbreaks

**PI:** Zhi-Qiang Deng

**Funding Agency:** NASA (National Aeronautics and Space Administration) and LaSPACE (Louisiana Space Consortium)

**Duration:** 10/01/2010 – 09/30/2011

**Amount:** \$74,998

# Hierarchical Multimodel Saltwater Intrusion Remediation and Sampling Designs: A BMA Tree Approach

## Basic Information

<b>Title:</b>	Hierarchical Multimodel Saltwater Intrusion Remediation and Sampling Designs: A BMA Tree Approach
<b>Project Number:</b>	2010LA76G
<b>Start Date:</b>	9/1/2010
<b>End Date:</b>	8/31/2013
<b>Funding Source:</b>	104G
<b>Congressional District:</b>	Louisiana
<b>Research Category:</b>	Ground-water Flow and Transport
<b>Focus Category:</b>	Groundwater, Management and Planning, Methods
<b>Descriptors:</b>	None
<b>Principal Investigators:</b>	Frank Tsai, Jeff Hanor

## Publications

1. Tsai, F.T.-C. (2011). Scavenger Wells Stop Saltwater Intrusion in Baton Rouge, Louisiana, IGWMC MODFLOW and More 2011 Conference: Integrated Hydrologic Modeling, Golden, Colorado, June 5-8, 2011.
2. Tsai, F. T.-C., and Ahmed S. Elshall (2011). A Hierarchical Bayesian Model Averaging Approach to Cope With Sources of Uncertainty in Conceptual Ground Water Models, World Water & Environmental Resources Congress, Palm Springs, California, May 22-26, 2011.
3. Tsai, F. T.-C. (2011). Stop Saltwater Intrusion Toward Water Wells Using Scavenger Wells, World Water & Environmental Resources Congress, Palm Springs, California, May 22-26, 2011.
4. Callie E. Anderson and Jeffrey S. Hanor (2011) Origin of waters causing salinization of the Baton Rouge aquifer system, Louisiana. South-Central Section Geological Society of America 45th Annual Meeting, March 27-29, 2011.
5. Frank T.-C. Tsai (2011). Saltwater Intrusion Simulation in the “1,500-Foot” Sand of the Baton Rouge Area: Pre-Anthropogenic Pumping, Current Situation, Future, Fifth Annual Louisiana Groundwater, Coastal Geology and Subsidence-Land Loss Symposia, Baton Rouge, Louisiana, January 11-12, 2011.
6. Callie E. Anderson and Jeffrey S. Hanor (2011) The St. Gabriel salt dome as a potential source of the salty waters contaminating the Baton Rouge aquifer system. Fifth Annual Louisiana Groundwater, Coastal Geology and Subsidence-Land Loss Symposia, Baton Rouge, Louisiana, January 11-12, 2011.
7. Ahmed Elshall and Frank T.-C. Tsai (2011). Geophysical and geostatistical approaches to subsurface characterization of the Baton Rouge area, Fifth Annual Louisiana Groundwater, Coastal Geology and Subsidence-Land Loss Symposia, Baton Rouge, Louisiana, January 11-12, 2011.
8. Nima Chitsazan and Frank T.-C. Tsai (2011). Bed boundary delineation of “1,500-foot”, “1,700-foot”, and “2,000-foot sands of the Baton Rouge area, Fifth Annual Louisiana Groundwater, Coastal Geology and Subsidence-Land Loss Symposia, Baton Rouge, Louisiana, January 11-12, 2011.
9. Tsai, F. T.-C. (2010). “1,500-Foot” Sand Saltwater Intrusion Simulation and Management Using Scavenger Wells, Baton Rouge Geological Society, Baton Rouge, Louisiana, December 10, 2010. (invited)

## Hierarchical Multimodel Saltwater Intrusion Remediation and Sampling Designs: A BMA Tree Approach

10. Tsai, F.T.-C. (2010), Scavenger Wells Stop Saltwater Intrusion in Baton Rouge, 2010 Louisianan Water Quality Technology Conference, Alexandria and Baton Rouge, Louisiana, December 14-15, 2010. (invited)
11. Tsai, F.T.-C. (2010) Scavenger Well Operation to Stop Saltwater Intrusion Toward BRWC Lula Wells in the Baton Rouge Area, Louisiana Capital Area Ground Water Conservation Commission, September 14, 2010. (invited)

## SYNOPSIS

**Title:** Hierarchical Multimodel Saltwater Intrusion Remediation and Sampling Designs:

A BMA Tree Approach

**Project Number:** G10AP00136

**Start Date:** 9/1/2010

**End Date:** 8/31/2013

**Funding Source:** 104G

**Research Category:** Ground-water Flow and Transport

**Focus Categories:** GW, M&P, MET

**Descriptors:** Remediation Design, Sampling Design, Saltwater Intrusion, Optimization, Uncertainty

**Primary PI:** Frank T.-C. Tsai

**Other PI:** Jeffrey S. Hanor

### Problem and Research Objectives

The water withdrawal in Baton Rouge, Louisiana is approximately 629,000 m<sup>3</sup> per day (166 million gallons per day) out of which 88% is ground water and the rest is surface water (Sargent, 2007). Due to excessive ground water pumping, saltwater is intruding from the saline aquifers in the south part of the Baton Rouge fault. Thus, in the absence of any remediation measure, some of public supply water wells in East Baton Rouge Parish are under the threat of being abandoned in the near future. The project objective is to analyze the uncertainty of the ground water numerical models, which are used for the management and remediation of the ground water resources. The first step in this project is to develop conceptual models that capture the complexity and heterogeneity of the subsurface geology

Subsurface models have a distinctive position since subsurface data are scarce due to economic reasons. For example, this study area is approximately 1005 km<sup>2</sup>. To characterize the subsurface 55 resistivity and self-potential logs are used. Assuming that the radius of influence of the long normal resistivity is 5 m and given a total number of 55 wells, thus the presence or absence of sand lenses is sampled over an area of approximately 0.00043% of the total area. Since this could be a common scenario for many subsurface problems, significant body of the subsurface literature focuses on developing stochastic data analysis techniques that would improve the utility of the scarce subsurface data and thus improve the model prediction and provide an analysis of model uncertainty.

Thus, due to limited amount of data and since model uncertainty always exists, multiple models are usually developed. Model selection, model elimination, model reduction, and model discrimination are commonly used to select the best model. It is clear that modeling uncertainty is always underestimated if only the best model is used. One would ask why only the best model is used afterwards when so many efforts have been devoted to calibrating many models. This certainly wastes valuable resources and important information from other good models. Hierarchical Bayesian model averaging (HBMA) best utilize all possible models for model prediction and application under Bayesian statistical framework. HBMA presents several advantages over model selection: (1) Information from all possible models is used based on their

model importance (model weights). Calibration efforts are not wasted. (2) The model importance is based on the evidence of data, which avoids over-confidence in the best model that does not have a dominant model weight. And (3) model structure uncertainty is increased and is better presented than that by using a single model. Moreover, HBMA is able to distinguish model uncertainty arising from individual models and between models. HBMA is able to identify unfavorable models even though they may present small prediction uncertainty.

In this study, HBMA is used to estimate the sand-clay distribution in the Baton Rouge aquifer system. Indicator geostatistical techniques are used to analyze electrical resistivity logs and reconstruct the subsurface accordingly. The HBMA is applied to analyze the conceptual model structure uncertainty arising from the different sand-clay line cutoff values for the resistivity logs and the different sand-clay cutoff probabilities for the interpolated values.

## METHODOLOGY

### Indicator Kriging

Given the volumetric domain  $D \subset \mathbb{R}^n$ , the indicator function  $\{I(\mathbf{x}, v) : \mathbf{x} \in D\}$  is a random function. The indicator random variable  $v$  describes the spatial extension of a categorical variable  $C$ , which is the sand-clay distribution in aquifers under different sand-clay line cutoff  $\alpha$  as determined from the electrical resistivity logs. The random function of the indicator random variable of class  $C$  is defined as:

$$I(\mathbf{x}, v) = \begin{cases} 1 & v \in C, \quad v(\mathbf{x}) > \alpha \\ 0 & v \notin C, \quad v(\mathbf{x}) < \alpha \end{cases}$$

The indicator function  $I(\mathbf{x}, v)$  is a random function of two variables in which  $v$  is an outcome of random variable at location  $\mathbf{x}$  in which the one and zero indicates the presence of sand and clay, respectively.

The indicator variogram has the same definition as the normal variogram except that the real random function is replaced by the indicator random function  $I(\mathbf{x})$  as follows

$$\gamma_I(h) = \frac{1}{2N(h)} \sum_{i=1}^{N(h)} [I(x_i) - I(x_i + h)]^2$$

where  $N(h)$  is the number of pairs within the lag interval  $h$ . In this case study, 55 observation boreholes are used in which 42 are located north of the fault Baton Rouge fault and 13 wells are located at the south. The main source of the sample data, which are used to generate the IK variograms, is from the electrical resistivity logs that are provided by the Baton Rouge Water Company. For each foot and for every resistivity log location, the resistivity values indicate either sand or clay depending on the sand-clay line cutoff as determined from the clay line in the resistivity curves. Another source of data is from the study of Wendeborn and Hanor (2008), in which they analyzed spontaneous potential (SP) curves to identify the sand-clay distribution along the Baton Rouge fault. The interpretation of these logs in terms of sand-clay sequences are amended to the main data to provide more sampling locations. All observation points are

amended together through linear interpolation over each foot. The number of samples in each observation point varies from 800 to 3000 depending on the depth of each borehole. Thus, over a depth  $z$  with an increment of 1 foot, an experimental variogram is generated. A pseudo 3D horizontal experimental variogram is obtained by averaging all the 2D experimental variograms for all depths.

The exponential model fits well with the geological process under study since it is an indicative of a sharp transition occurring between blocks of different values (Rubin, 2003). The exponential model is formulated as:

$$\gamma_{Exp}(h) = X_1 + X_2 \cdot \left( 1 - \exp \left( -3 \cdot \frac{h}{X_3} \right) \right)$$

where the correlation parameters are the nugget effect  $X_1$  and the sill  $X_2$ , which the variance approaches at an effective range  $X_3$ . The theoretical variogram is fitted to the experimental variogram automatically through using the pattern search method of Hooke and Jeeves (1961), which performs a direct directional search for the values of  $X_1, X_2$  and  $X_3$ , which would minimize the weighted squared root difference between the experimental and the theoretical variograms.

Under the basic assumption that the sample domain is stationary, ergodic and sufficient to reliably reproduce the statistics, the obtained theoretical variogram is used for the indicator kriging interpolation as a method for constructing the subsurface stratigraphy. The aim of kriging is to estimate the value of a random variable at unsampled points. Over larger defined grid size, which is  $500 \text{ m} \times 500 \text{ m}$  in this case, kriging uses weighted average of the neighboring sample data points to estimate the value in each grid using the following equation:

$$A\lambda = b$$

such as

$$\begin{bmatrix} \gamma(x_1, x_1) & \gamma(x_1, x_2) & \cdots & \gamma(x_1, x_N) & 1 \\ \gamma(x_2, x_1) & \gamma(x_2, x_2) & \cdots & \gamma(x_2, x_N) & 1 \\ \vdots & \vdots & \cdots & \vdots & \vdots \\ \gamma(x_N, x_1) & \gamma(x_N, x_2) & \cdots & \gamma(x_N, x_N) & 1 \\ 1 & 1 & \cdots & 1 & 0 \end{bmatrix} \begin{bmatrix} \lambda_1 \\ \lambda_2 \\ \vdots \\ \lambda_N \\ L \end{bmatrix} = \begin{bmatrix} \gamma(x_1, x_0) \\ \gamma(x_2, x_0) \\ \vdots \\ \gamma(x_N, x_0) \\ 1 \end{bmatrix}$$

in which  $\gamma(x_i, x_j)$  is the variogram of  $v$  between the data points  $x_i$  and  $x_j$ , and the  $\gamma(x_i, x_0)$  is the variogram between the data point  $x_i$  and the target point  $x_0$ . To guarantee that the estimates are unbiased, the sum of the weights  $\lambda_i$  is one. The unbiased constrained is imbedded to the minimization problem through the use of the Lagrange multiplier  $L$ . By multiplying the inverse of the matrix  $A$  with the vector  $b$ , we obtain the weight for each data point. The last step is to calculate the expected value and the kriging variance by solving the following equations.

$$\mathbf{v}^*(x_0) = \sum_{i=1}^N \lambda_i I(x_i) \quad \text{and} \quad \sigma_{IK}^2 = b^T \boldsymbol{\lambda}$$

The estimated values could be viewed as the conditional probability that a value is less than a certain sand-clay cutoff.

### Hierarchical Bayesian Model Averaging (HBMA)

To cope with sources of uncertainty in ground water conceptual models a hierarchical Bayesian model averaging is adopted. An early study by Elshall and Tsai (2011) conducted a sensitivity analysis on different methods and parameters. First, the use by of 2D variogram model for each layer is compared to a pseudo 3D variogram model, which is a weighted average of all the 2D variograms. Also, different sand-clay line cutoff and sand-clay cutoff probabilities are investigated. The results are much more sensitive to the cutoff of the sand-clay line and sand-clay cutoff probabilities in comparison with the selection of different variogram models. Four sand-clay line cutoffs of 10, 11, 12 and 13 ohm-m are considered. For each of these four models a sand-clay cutoff of probabilities 0.4, 0.5 and 0.6 is considered.

The key issue of HBMA is the determination of the posterior model probability. Given a number of conceptual models  $\mathbf{M} = \{M^{(p)}; p = 1 \dots 4\}$  for determining the sand-clay distribution  $\mathbf{v}$  over the model domain with different cutoff probabilities  $\Theta^{(p)} = \{\theta_q^{(p)}; q = 1 \dots 3\}$ , the posterior probability of predicted sand-clay distribution is obtained by using the twelve conceptual models through HBMA given a set of data  $\mathbf{D}$ , which is the boreholes data from the USGS indicating the sand lenses at different depths at 65 different locations. An HBMA method after Li and Tsai (2009) is adopted in this study. In HBMA in which multi-parameter uncertainty is considered, the posterior probability for the given data  $\mathbf{D}$ , sand-clay line cutoff  $\mathbf{M}$  and sand-clay cutoff probability  $\Theta^{(p)}$  is given as

$$\begin{aligned} \Pr(\mathbf{v}|\mathbf{D}) &= E_{\mathbf{M}} \left[ E_{\Theta} \left[ \Pr(\mathbf{v}|M^{(p)}, \theta_q^{(p)}, \mathbf{D}) \right] \right] \\ &= \sum_p \sum_q \Pr(\mathbf{v}|M^{(p)}, \theta_q^{(p)}, \mathbf{D}) \Pr(\theta_q^{(p)}|M^{(p)}, \mathbf{D}) \Pr(M^{(p)}|\mathbf{D}) \end{aligned}$$

where  $\Pr(\mathbf{v}|M^{(p)}, \theta_q^{(p)}, \mathbf{D})$  is the posterior probability of the sand-clay distribution for a given data set  $\mathbf{D}$  and sand-clay line cutoff  $M^{(p)}$  and sand-clay probability cutoff  $\theta_q^{(p)}$ .  $E_{\Theta}$  and  $E_{\mathbf{M}}$  are the expectations. The joint posterior probability (model weight) according to the Bayes' rule is:

$$\Pr(\theta_q^{(p)}, M^{(p)}|\mathbf{D}) = \Pr(\theta_q^{(p)}|M^{(p)}, \mathbf{D}) \Pr(M^{(p)}|\mathbf{D}) = \frac{\Pr(\mathbf{D}|M^{(p)}, \theta_q^{(p)})}{\sum_p \sum_q \Pr(\mathbf{D}|M^{(p)}, \theta_q^{(p)})}$$

where  $\Pr(\theta_q^{(p)}|M^{(p)}, \mathbf{D})$  is the marginal model likelihood function for a given sand-clay line cutoff  $M^{(p)}$ , and sand-clay cutoff probability  $\theta_q^{(p)}$ . The total weight is  $\Pr(\theta_q^{(p)}, M^{(p)}|\mathbf{D}) = 1$ .

The marginal likelihood function  $\Pr(\mathbf{D} | M^{(p)}, \theta_q^{(p)})$  is commonly approximated using the Laplace approximation with the Bayesian information criterion (BIC)

$$BIC_q^{(p)} = -2 \ln \Pr(\mathbf{D} | M^{(p)}, \theta_q^{(p)}, \hat{\mathbf{B}}_q^{(p)}) + m_q^{(p)} \ln n$$

where  $\hat{\mathbf{B}}_q^{(p)}$  are the maximum likelihood estimated parameters in a model structure given  $\theta_q^{(p)}$  and  $M^{(p)}$ ,  $m_q^{(p)}$  is the number of the parameters  $\hat{\mathbf{B}}_q^{(p)}$  and  $n$  is the number of data  $\mathbf{D}$ .  $\Pr(\mathbf{D} | M^{(p)}, \theta_q^{(p)}, \hat{\mathbf{B}}_q^{(p)})$  is the likelihood function value. The parameters  $\hat{\mathbf{B}}_q^{(p)}$  are the variogram model parameters in this study. One can obtain the means of the sand-clay distribution using the law of total expectation:

$$\begin{aligned} E(\mathbf{v} | \mathbf{D}) &= E_M \left[ E_\theta \left[ E(\mathbf{v} | M^{(p)}, \theta_q^{(p)}, \mathbf{D}) \right] \right] \\ &= \sum_p \sum_q E(\mathbf{v} | M^{(p)}, \theta_q^{(p)}, \mathbf{D}) \Pr(\mathbf{D} | M^{(p)}, \mathbf{D}) \cdot \Pr(M^{(p)} | \mathbf{D}) \end{aligned}$$

with variance matrix of the predicated sand-clay distribution as:

$$\begin{aligned} Var(\mathbf{v} | \mathbf{D}) &= E_M E_\theta \left[ Var[\mathbf{v} | M^{(p)}, \theta_q^{(p)}, \mathbf{D}] \right] + E_M Var_\theta \left[ E[\mathbf{v} | M^{(p)}, \theta_q^{(p)}, \mathbf{D}] \right] \\ &\quad + Var_M E_\theta \left[ E[\mathbf{v} | M^{(p)}, \theta_q^{(p)}, \mathbf{D}] \right] \end{aligned}$$

The first term of the right side of the above equation is the within-model variance, which relates to the uncertainty of the predicated sand-clay distribution using combination of different sand-clay line cutoff  $M^{(p)}$  and sand-clay cutoff probability  $\theta_q^{(p)}$ . The second term is the between-model variance, which relates to the uncertainty using different sand-clay probability cutoffs. The third term is between-model variance, which relates to the uncertainty of using different sand-clay line cutoffs.

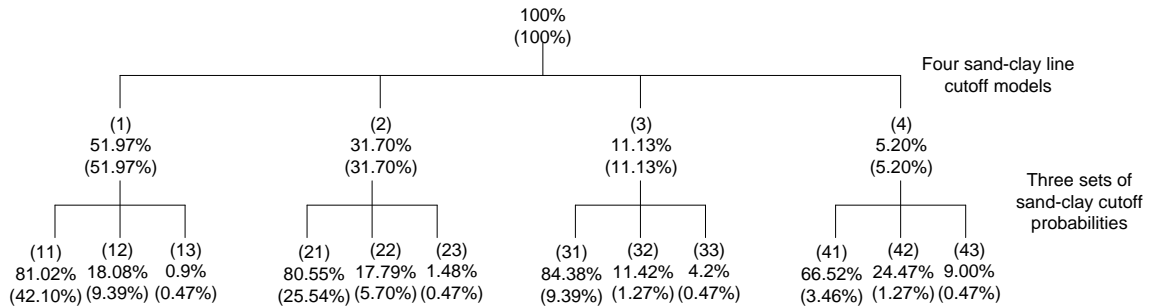


**Figure 1.** BMA tree of model weights in HMBA. The model weights in parentheses are  $\Pr(\theta_q^{(p)}, M^{(p)} | \mathbf{D})$ . The model weights without parentheses are  $\Pr(\theta_q^{(p)} | M^{(p)}, \mathbf{D})$ .

## Principal Findings and Significance

This section presents the results of studying the sand-clay distribution based on different sand-clay lines of 10, 11, 12 and 13 ohm-m and sand-clay cutoff probability of 0.4, 0.5 and 0.6. Model weights are calculated according to the BIC, which is more skewed to the best models as shown in Figure 1.

The models for different probability values are the third level models, which are 12 models corresponding to the three cutoff probabilities for each for the four sand-clay line cutoffs. When the third level models are averaged with their weights, they form the second level models, which are 4 models corresponding to the four different sand-clay lines as shown in Figure 2. Although the weights are calculated based on the results of 190 layers from a depth of 1460 to 1650 feet below msl, the results are only shown for a 2D plan at a depth of 1551 feet below msl.

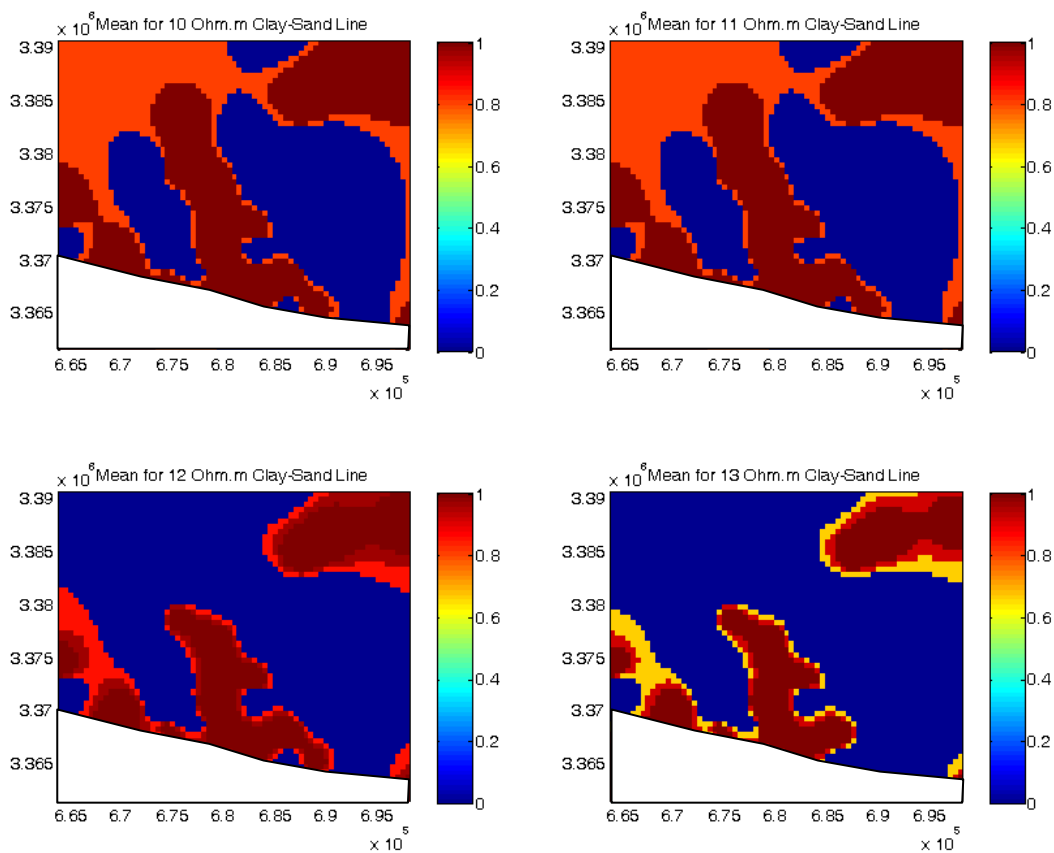


**Figure 2.** Sand-clay distribution for the second level models for different sand-clay line cutoffs.

The BMA prediction variance includes the within-model variance and between-model variance with the total variance being the summation of these two components. Although the calculated sand-clay distribution can be significantly different when using different sand-clay lines and cutoff probabilities, yet the within-model variance is larger than the between-model variance.

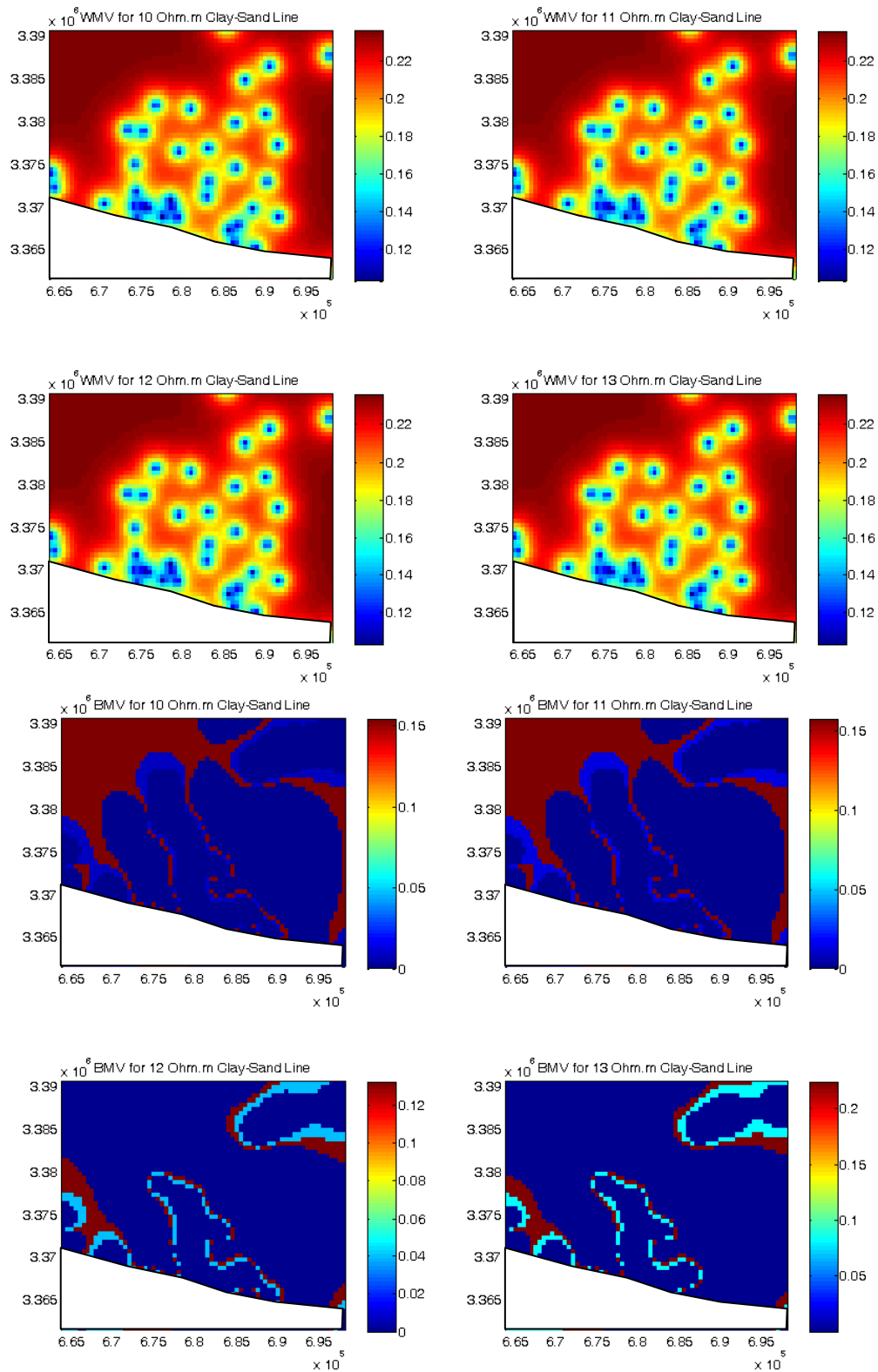


**Figure 3.** Within-model variance (WMV) and between-model variance (BMV) for different sand-clay line cutoffs.

Similarly, one can obtain the first level model, which is a weighted average of the second level models as shown in Figure 4. For the between-model variance being smaller than the within-model variance does not suggest the unimportance of the sand-clay line. Rather it simply suggests that good models produce similar predictions close to the expectation of the BMA predictions. Bad models have little influence on the sand-clay distribution because their model weight is very small and thus their predictions are further apart from the BMA prediction.

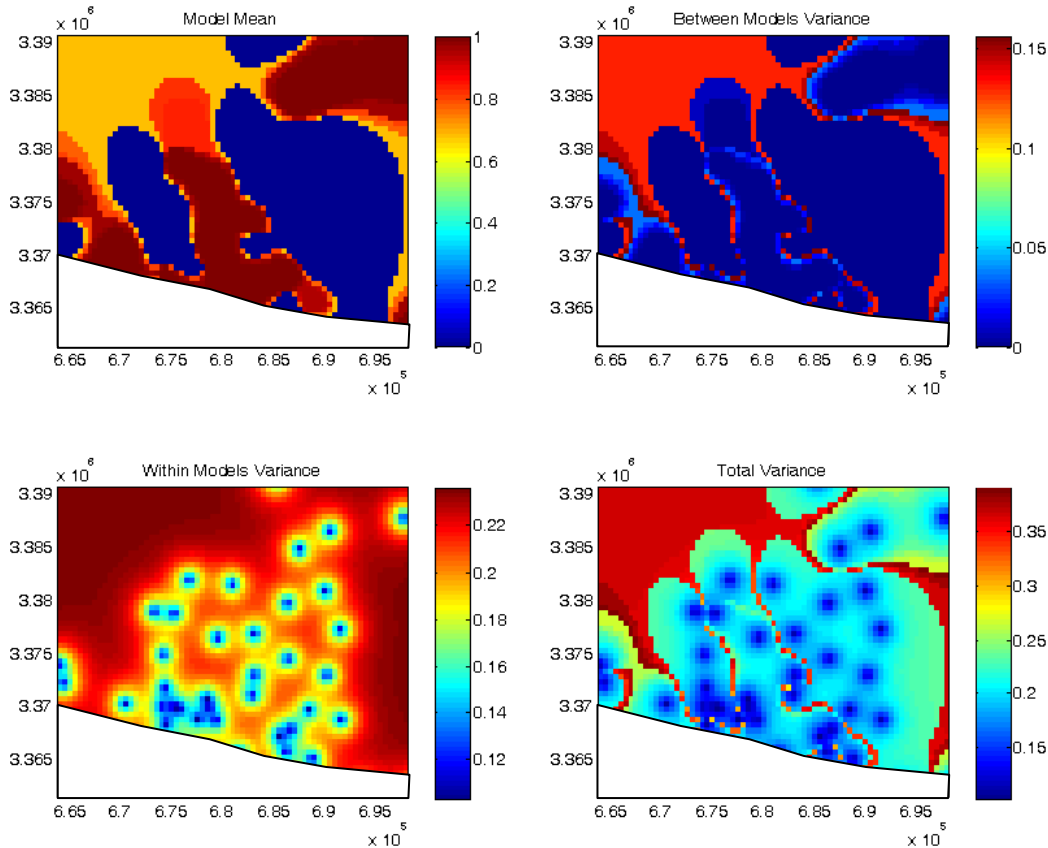


**Figure 4.** Sand-clay distribution, within-model variance, between-model variance and total variance for the first level model.

## CONCLUSION

This study focuses on model structure uncertainty. Using a single model will ignore the uncertainty arising from different model parameters. The HBMA applies a Bayesian statistical approach to quantify the overall sand-clay distribution uncertainty. In general, HBMA is successfully applied to study the uncertainty of stratigraphic models. Accordingly, the method can be readily extended to include other sources of structural uncertainty such as the morphology and dipping angle of Baton Rouge fault and borehole elevation uncertainty.

## REFERENCES

Elshall A. S., and Tsai, F. T.-C. (2011). "Subsurface characterization of Baton Rouge area using geophysics and geostatistics." 5<sup>th</sup> Annual Louisiana Groundwater, Coastal Geology and Subsidence-Land Loss Symposia January 11-12, 2011, Baton Rouge Geological Society & Louisiana Geological Survey.

- Hooke R., and Jeeves, T. A. (1961). "Direct search solution of numerical and statistical problems." *Journal of the Association for Computing Machinery* 8 (2): 212–229.
- Li, X., and Tsai, F. T.-C. (2009). "Bayesian model averaging for groundwater head predication and uncertainty analysis using multimodal and multimethod." *Water Resources Research*, 45, W09403.
- Rubin, Y. (2003). "Applied stochastic hydrogeology." Oxford University Press, Oxford.
- Sargent, B. P. (2007). "Water use in Louisiana, 2005." Louisiana Department of Transportation and Development Water Resources Special Report no. 16, p.133.
- Wendeborn, F. C., and Hanor, J. S. (2008). "The Baton Rouge fault, South Louisiana: a barrier and/or conduit for vertical and/or lateral ground water flow?" GSA Annual Meeting Abstracts, Houston.

## **PUBLICATION**

### **1. Articles in Refereed Scientific Journals**

N/A

### **2. Book Chapters**

N/A

### **3. Theses and Dissertations**

N/A

### **4. Water Resources Research Institute Reports**

- Frank Tsai, 2011, Multimodel Uncertainty Analysis for Chance-Constrained Saltwater Intrusion Management, Louisiana State University, Baton Rouge, Louisiana, 10 pages. (USGS 104B)

### **5. Conference Proceedings**

- Tsai, F.T.-C. (2011). Scavenger Wells Stop Saltwater Intrusion in Baton Rouge, Louisiana, IGWMC MODFLOW and More 2011 Conference: Integrated Hydrologic Modeling, Golden, Colorado, June 5-8, 2011.
- Tsai, F. T.-C., and Ahmed S. Elshall (2011). A Hierarchical Bayesian Model Averaging Approach to Cope With Sources of Uncertainty in Conceptual Ground Water Models, *World Water & Environmental Resources Congress*, Palm Springs, California, May 22-26, 2011.
- Tsai, F. T.-C. (2011). Stop Saltwater Intrusion Toward Water Wells Using Scavenger Wells, *World Water & Environmental Resources Congress*, Palm Springs, California, May 22-26, 2011.
- Callie E. Anderson and Jeffrey S. Hanor (2011) Origin of waters causing salinization of the Baton Rouge aquifer system, Louisiana. South-Central Section Geological Society of America 45<sup>th</sup> Annual Meeting, March 27-29, 2011.

### **6. Other Publications (Presentations)**

- Frank T.-C. Tsai (2011). Saltwater Intrusion Simulation in the "1,500-Foot" Sand of the Baton Rouge Area: Pre-Anthropogenic Pumping, Current Situation, Future, Fifth Annual Louisiana Groundwater, Coastal Geology and Subsidence-Land Loss Symposia, Baton Rouge, Louisiana, January 11-12, 2011.

- Callie E. Anderson and Jeffrey S. Hanor (2011) The St. Gabriel salt dome as a potential source of the salty waters contaminating the Baton Rouge aquifer system. Fifth Annual Louisiana Groundwater, Coastal Geology and Subsidence-Land Loss Symposia, Baton Rouge, Louisiana, January 11-12, 2011.
- Ahmed Elshall and Frank T.-C. Tsai (2011). Geophysical and geostatistical approaches to subsurface characterization of the Baton Rouge area, Fifth Annual Louisiana Groundwater, Coastal Geology and Subsidence-Land Loss Symposia, Baton Rouge, Louisiana, January 11-12, 2011.
- Nima Chitsazan and Frank T.-C. Tsai (2011). Bed boundary delineation of “1,500-foot”, “1,700-foot”, and “2,000-foot sands of the Baton Rouge area, Fifth Annual Louisiana Groundwater, Coastal Geology and Subsidence-Land Loss Symposia, Baton Rouge, Louisiana, January 11-12, 2011.
- Tsai, F. T.-C. (2010). “1,500-Foot” Sand Saltwater Intrusion Simulation and Management Using Scavenger Wells, Baton Rouge Geological Society, Baton Rouge, Louisiana, December 10, 2010. (invited)
- Tsai, F.T.-C. (2010), Scavenger Wells Stop Saltwater Intrusion in Baton Rouge, 2010 Louisianan Water Quality Technology Conference, Alexandria and Baton Rouge, Louisiana, December 14-15, 2010. (invited)
- Tsai, F.T.-C. (2010) Scavenger Well Operation to Stop Saltwater Intrusion Toward BRWC Lula Wells in the Baton Rouge Area, Louisiana Capital Area Ground Water Conservation Commission, September 14, 2010. (invited)

### **7. Student Support**

- Nima Chitsazan, PhD student
- Elizabeth L. Chamberlain, MS student

## Information Transfer Program Introduction

Because of the Deep Horizon oil spill, our efforts for information transfer were dominated by that activity in FY 2010. Full details are provided in the “Notable Achievements” section of the report. Highlights of our activities are listed below:

- LWRRI built and managed a collaborative web review process for the Deep Water Horizon Science and Engineering Review Team immediately after the spill. This allowed for rapid review of dozens of documents and storage of GB's of information for review by statewide academic members of the team
- LWRRI participated in the organization of SETAC's focused oil spill conference held in April 2011.
- LWRRI was the chief sponsor of the LSU Environmental Film Series in March and April 2009 at LSU. The following films with a sustainability theme were screened: Garbage Dreams, A Convenient Truth, and Manufactured Landscapes. These were followed by discussions with students and faculty organized by LWRRI. Attendance averaged 120 per night.

## Information Transfer Symposia: Mitigation of Storm Surge using Vegetation (Spring, 2007) and Resilient Environmental Infrastructure for Coastal Communities (Fall, 2007)

### Basic Information

<b>Title:</b>	Information Transfer Symposia: Mitigation of Storm Surge using Vegetation (Spring, 2007) and Resilient Environmental Infrastructure for Coastal Communities (Fall, 2007)
<b>Project Number:</b>	2007LA52B
<b>Start Date:</b>	3/1/2007
<b>End Date:</b>	2/28/2011
<b>Funding Source:</b>	104B
<b>Congressional District:</b>	06
<b>Research Category:</b>	Not Applicable
<b>Focus Category:</b>	Education, Management and Planning, Methods
<b>Descriptors:</b>	
<b>Principal Investigators:</b>	John Pardue, Nedra Davis Korevec

### Publications

There are no publications.

## SYNOPSIS

Title: Information Transfer Symposia: Mitigation of Storm Surge using Vegetation (Spring, 2007) and Resilient Environmental Infrastructure for Coastal Communities (Fall, 2007)

Project Number: 2007LA52B

Start Date: 3/1/2007

End Date: 2/28/2010

Funding Source: 104B

Congressional District: 6

Research Category: NA

Focus Category: Education, Management and Planning; Methods

Primary PI: John Pardue

### Problem and Research Objectives

The Louisiana Water Resources Research Institute made a concerted effort in recent funding cycles to improve and expand outreach efforts to increase visibility in the Louisiana water/environmental community. In Louisiana, limited opportunities exist for exchange between university water scientists, state and federal agencies over water issues. A state “water” conference or summit has not been organized and only the state environmental agency, the Louisiana Department of Environmental Quality, sponsors a scientific/policy conference on environmental issues, some of which involve water. After discussions with the advisory board, the Institute thought this could best be accomplished by sponsoring shorter symposia/workshops to focus on a specific science/engineering issue important to the state.

Two symposia have already been supported by this project: *Mitigating Storm Surge with Vegetation* (2007) and *Water: Friend or Foe*, a transatlantic symposium held jointly with ConRuhr (2008). Originally, a workshop on *Resilient Environmental Infrastructure for Coastal Communities* was proposed for Fall 2007. This was particularly relevant after Hurricane Katrina and Rita where many utilities were damaged after the storm. After several attempts to determine interest among utilities in our coastal communities, it was apparent that other organizations such as the American Water Works Association were meeting the immediate needs of information exchange for these groups. In conjunction with our advisory board, we decided, and received approval from USGS, to utilize the remaining funds to partner with other agencies to assist other educational efforts.

In this reporting cycle LSU cosponsored with the American Society of Civil Engineers (ASCE) the 2008 Louisiana Coastal Engineering Symposium. Over the past century, river management, coastal erosion, and subsidence have had a profound impact on river deltas worldwide, and the Mississippi River delta and the Louisiana coast are no exceptions. The 2005 hurricane season exacerbated these problems in Louisiana and put new focus on the consequences of increased risks to both the natural and built environments in the coastal zone. Sustaining the coastal deltaic landscape represents a major scientific and engineering challenge and is a problem that is fundamentally interdisciplinary. It is clear that discovering real, lasting solutions to these problems will require researchers to interweave a number of core disciplines including coastal and ecological engineering, restoration ecology, coastal, wetland and estuarine science, advanced

mathematical modeling and computational science. There is a great need in the state to begin developing capacity in the areas of coastal and ecological engineering in the existing water resources engineering community in the state. This symposium was directed at that goal.

### Principal Findings and Significance

The objective the 2008 Louisiana Coastal Engineering conference was to continue to build capacity of the current Louisiana engineering and water resource community in the state. The conference was held in Baton Rouge at the Capitol City Hilton May 29 and 30<sup>th</sup>, 2008. The conference attracted over 100 engineering and water resources professionals for two days of invited and submitted talks. The two keynote speakers, Dr. David Basco from Old Dominion and Dr. David Randall from Texas A&M were joined by the head of Louisiana's Governor's Office of Coastal Affairs, Garrett Graves. The conference was another effort by LWRRI to contribute to the efforts related to understanding storm surge, the water implications for coastal restoration and protection and how to mitigate impacts from storm events. The full presentations are available on the LWRRI website ([www.lwrri.lsu.edu](http://www.lwrri.lsu.edu)).

### **2008 Louisiana Coastal Engineering Conference**

#### **Hilton Baton Rouge Capitol Center-Baton Rouge, Louisiana - Technical Transfer**

#### **Keynote Speakers:**

**Dr. David R. Basco**, P.E., Ph.D

Old Dominion University, Department of Civil and Environmental Engineering

**Dr. Robert E. Randall**, Ph.D

Texas A&M University, Center for Dredging Studies

#### **Agenda:2008 Louisiana Coastal Engineering Conference**

**Location:** Hilton Baton Rouge Capitol Center Hotel, May 29-30, 2008, 7:00 AM-5:30 PM

#### **Technical Transfer from Conference:**

Keynote Speaker,Dr. David R. Basco, P.E., Ph.D

Old Dominion University, Department of Civil and Environmental Engineering

Coastal Processes

- Keynote Speaker,Dr. Robert E. Randall, Ph.D  
Texas A&M University, Center for Dredging Studies  
Dredging Equipment and Costs
- Dr. Q. Jim Chen, Ph.D  
Louisiana State University, Department of Civil and Environmental Engineering  
Fundamentals of Wave Theory and Tides

- Keynote Speaker: Garret Graves  
Director of the Governor's Office of Coastal Affairs
- Geotechnical Engineering Applications in Coastal Design  
Charles L. Eustis, P.E. - Capozzoli/GeoEngineers
- Dr. Guoping Zhang, Ph.D - Louisiana State University,  
Dept. of Civil and Environmental Engineering- Settlement Analysis for Marsh Creation
- Computer Modeling Capabilities in Coastal Design  
Santiago Alfageme, P.E. and Rafael Canizares, P.E., Ph.D  
Moffat & Nichol
- Erosion Control and Sediment Budget Analysis: Grand Isle Barrier Shoreline  
Stabilization Study  
Josh Carter, P.E.  
Coast & Harbor Engineering
- The Future of Coastal Engineering Efforts at the Louisiana Department of Natural  
Resources  
Christopher P. Knotts, P.E.  
Louisiana Department of Natural Resources, Coastal Engineering Division
- Case Study on Barrier Island Design: Barataria Barrier Island Complex Project  
Gordon G. Thomson, P.E. and Tom Campbell, P.E., Ph.D  
Coastal Planning & Engineering, Inc.
- Case Study on Shoreline Protection Design: Lake Borgne Shoreline Protection  
Shannon Haynes, P.E.  
Louisiana Department of Natural Resources, Coastal Engineering Division
- Case Study on Marsh Creation Design: Little Lake Dedicated Dredging/Marsh Creation  
Luke E. Le Bas, P.E.  
Louisiana Department of Natural Resources, Coastal Engineering Division
- The Mississippi River and its Role in Restoration Efforts  
Dr. Clinton S. Willson, P.E., Ph.D  
Louisiana State University, Department of Civil and Environmental Engineering

## 2008 Louisiana Water Symposia

### Basic Information

<b>Title:</b>	2008 Louisiana Water Symposia
<b>Project Number:</b>	2008LA56B
<b>Start Date:</b>	3/1/2008
<b>End Date:</b>	2/28/2011
<b>Funding Source:</b>	104B
<b>Congressional District:</b>	6
<b>Research Category:</b>	Water Quality
<b>Focus Category:</b>	Education, Management and Planning, Methods
<b>Descriptors:</b>	
<b>Principal Investigators:</b>	John Pardue, Nedra Davis Korevec

### Publications

There are no publications.

## SYNOPSIS

Title: Information Transfer Symposia: Louisiana Water Conference  
Project Number: 2008LA56B  
Start Date: 3/1/2008  
End Date: 2/28/2011  
Funding Source: 104B  
Congressional District: 6  
Research Category: NA  
Focus Category: Education, Management and Planning; Methods  
Primary PI: John Pardue

### Problem and Research Objectives

The Louisiana Water Resources Research Institute made a concerted effort in recent funding cycles to improve and expand outreach efforts to increase visibility in the Louisiana water/environmental community. In Louisiana, limited opportunities exist for exchange between university water scientists, state and federal agencies over water issues. A state “water” conference or summit has not been organized and only the state environmental agency, the Louisiana Department of Environmental Quality, sponsors a scientific/policy conference on environmental issues, some of which involve water. After discussions with the advisory board, the Institute thought this could best be accomplished by sponsoring shorter symposia/workshops to focus on a specific science/engineering issue important to the state.

Three symposia have already been supported by this project: *Mitigating Storm Surge with Vegetation* (2007) and *Water: Friend or Foe*, a transatlantic symposium held jointly with ConRuhr (2008) and the *Louisiana Coastal Engineering Conference*, jointly supported by LWRRI in summer 2008. This project was initiated to plan and execute a statewide water conference to bring focus to the state’s water problems.

### Principal Findings and Significance

The project has made progress in support for a statewide water conference. At the point of scheduling the conference for late 2009 we lost our long-serving staff conference coordinator and a state hiring freeze has prevented filling the position. We anticipate holding the conference in 2010 and will report the results of the conference in the next cycle. The project is currently on a no-cost extension.

## 2009 Louisiana Water Symposia

### Basic Information

<b>Title:</b>	2009 Louisiana Water Symposia
<b>Project Number:</b>	2009LA63B
<b>Start Date:</b>	3/1/2009
<b>End Date:</b>	2/28/2011
<b>Funding Source:</b>	104B
<b>Congressional District:</b>	6th
<b>Research Category:</b>	Not Applicable
<b>Focus Category:</b>	Water Supply, Water Quality, Management and Planning
<b>Descriptors:</b>	
<b>Principal Investigators:</b>	John Pardue

### Publications

There are no publications.

## SYNOPSIS

Title: Information Transfer Symposia: Louisiana Water Conference  
Project Number: 2008LA56B  
Start Date: 3/1/2008  
End Date: 2/28/2011  
Funding Source: 104B  
Congressional District: 6  
Research Category: NA  
Focus Category: Education, Management and Planning; Methods  
Primary PI: John Pardue

### Problem and Research Objectives

The Louisiana Water Resources Research Institute made a concerted effort in recent funding cycles to improve and expand outreach efforts to increase visibility in the Louisiana water/environmental community. In Louisiana, limited opportunities exist for exchange between university water scientists, state and federal agencies over water issues. A state “water” conference or summit has not been organized and only the state environmental agency, the Louisiana Department of Environmental Quality, sponsors a scientific/policy conference on environmental issues, some of which involve water. After discussions with the advisory board, the Institute thought this could best be accomplished by sponsoring shorter symposia/workshops to focus on a specific science/engineering issue important to the state.

Three symposia have already been supported by this project: *Mitigating Storm Surge with Vegetation* (2007) and *Water: Friend or Foe*, a transatlantic symposium held jointly with ConRuhr (2008) and the *Louisiana Coastal Engineering Conference*, jointly supported by LWRRI in summer 2008. This project was initiated to plan and execute a statewide water conference to bring focus to the state’s water problems.

### Principal Findings and Significance

The project has made progress in support for a statewide water conference. At the point of scheduling the conference for late 2009 we lost our long-serving staff conference coordinator and a state hiring freeze has prevented filling the position. We anticipate holding the conference in late 2010 and will report the results of the conference in the next cycle. The project is currently on a no-cost extension.

# USGS Summer Intern Program

None.

<b>Student Support</b>					
<b>Category</b>	<b>Section 104 Base Grant</b>	<b>Section 104 NCGP Award</b>	<b>NIWR-USGS Internship</b>	<b>Supplemental Awards</b>	<b>Total</b>
<b>Undergraduate</b>	3	0	0	0	3
<b>Masters</b>	1	1	0	0	2
<b>Ph.D.</b>	3	1	0	0	4
<b>Post-Doc.</b>	1	0	0	0	1
<b>Total</b>	8	2	0	0	10

# Notable Awards and Achievements

Of note in FY2010 was LWRRI's participation in response to the Deep Horizon Oil Spill, the largest spill in US history. Parallel to our previous efforts with Hurricane Katrina and Rita, LWRRI was able to respond quickly to the opportunity. Details are presented below.

LWRRI advised response agencies

- Advised the state through the Horizon Science and Engineering Review Team (H-SERT), a group of academic experts who worked with state trustees on the response. LWRRI Director Pardue led one of the standing committees in H-SERT and participated by reviewing and commenting on dozens of documents and plans. LWRRI set up a collaborative web review process for H-SERT which allowed participating by academics across the state. Pardue also participated in helicopter tours with the lead trustee agency, the Office of Coastal Protection and Restoration.
- In addition at the state level, Dr. Pardue advised the Governor's Office of Homeland Security and Emergency Preparedness (GOHSEP) and the National Guard on spill impacts.
- Dr. Pardue also advised EPA on response and participated in meetings at LSU with Lisa Jackson, Head of EPA and Jane Lubchenko, Head of NOAA

LWRRI Conducted Research on the Spill

- LWRRI Director Pardue is coordinating research and damage assessment for the Wisner Donation property in Lafourche Parish, one of the 10 largest landowners in the state. The Wisner Donation property includes 35,000 acres including Fourchon Beach. Dr. Pardue has travelled to Wisner areas to conduct research an average of once per week since October 2010.
- Received research funding from LSU GOMA BP fund and Wisner Donation

LWRRI organized conferences and presented research results

- Participating in conferences and presentation opportunities related to the spill :Scott Bioremediation Workshop, August 31, 2010, Pensacola, FL; Hurricane Ike Conference at Rice University, Houston Texas, September, 2010 (Hurricanes and Oil Spills: Lessons from Deep Horizon, Katrina and Ike); LSU Honors College Presentation. September 2010; Board of Regents Oil Spill Symposium, November 2010)
- Organizing scientific conferences and symposia related to DH Spill (Steering committee of SETAC Focused Oil Spill Conference to be held in Pensacola, FL in April 2011; chairing session at Battelle Bioremediation Conference in Reno, NV in June 2011